WA School of Mines: Minerals, Energy and Chemical Engineering

Pyrolysis of Biomass, Model Compounds and Biomass-Derived Products in a Wire Mesh Reactor

Jinxiu Cao

0000-0001-7054-7130

This thesis is presented for the Degree of

Doctor of Philosophy

of

Curtin University

December 2021

Declaration

To the best of my knowledge and belief this thesis contains no material previously published by any other person except where due acknowledgement has been made.

This thesis contains no material which has been accepted for the award of any other degree or diploma in any university.

Signature:

Date:

To my beloved family

Abstract

Pyrolysis of lignocellulose biomass is proposed as a feasible method to substitute traditional fossil fuels. The thermal degradation behaviours of biomass vary from feedstock types, depending on the physical properties, such as particle size and chemical compositions, including the proportion of cellulose, lignin, and hemicellulose. The extractives and ash components also play significant catalytic effects during the thermal utilisation of biomass feedstock. To alter the product distribution for the desired chemical and bio-products with improved quality, some pre-treatment methods, including acid impregnation, AAEM loading and torrefaction, have been proposed. As a result, the biomass-derived products are obtained before further thermal utilisation. During the pyrolysis process, biomass experiences a molten intermediate phase before further evolving. Upon elevated heating flux, gas bubbles will be generated inside the intermediates. Those gas bubbles will either eject out as droplets or evaporate into the gas phase as vapours if the surface tension is breached out. Meanwhile, secondary reactions, including repolymerisation and interaction reactions, will occur with the gas bubbles remaining in the liquid intermediates. Those secondary reactions need to be minimised for the interpretation of primary pyrolytic behaviours and pyrolysis mechanisms of individual biomass components and biomass-derived products.

This PhD study reports the thermal behaviours and proposes reaction mechanisms during the pyrolysis of biomass components and the biomass-derived products using a wire mesh reactor. Due to the employment of a wire mesh reactor, the secondary reactions can be minimised and therefore, the primary products can be collected and analysed for investigation of the unknown primary pyrolysis mechanisms during the

pyrolysis of biomass components and biomass-derived products. The four research objectives achieved in this study include: (1) to determine the contributions of thermal ejection and evaporation to primary tar formation during cellulose pyrolysis at various heating rates; (2) to investigate the formation of reaction intermediates and primary volatiles during acid-catalysed fast pyrolysis of cellulose (3) to understand the release and transformation of organic and inorganic sodium during the fast pyrolysis of sodium impregnated lignin; (4) to study the effect of carbon dioxide assisted torrefaction and the subsequent pyrolysis of lignin. Among these objectives, the significance of liquid intermediates, especially the ejection and evaporation of the liquid and gaseous products during the pyrolysis process is addressed.

Firstly, the ejected aerosols and the evaporated vapours from cellulose fast pyrolysis at 600 °C and various heating rates of 1 – 1000 K/s have been successfully collected and characterised. The results indicate that some non-volatile compounds (i.e., cellotriosan, cellotetraosan and cellopentaosan) are only present in the ejected aerosols with similar collection efficiencies, while volatile compounds such as 5-hydroxymethylfurfural are only present in the evaporated vapours with high collection efficiencies (>90%). Those key compounds can be considered as the “tracers” to estimate the average collection efficiencies of the ejected aerosol and the evaporated vapours, which are critical to determining the true yields of the ejected aerosols and the evaporated vapours. Based on this novel method, it can be estimated that the true yield of the ejected aerosols from cellulose pyrolysis continuously increases with the heating rate from 29% at 1 K/s to 57% at 1000 K/s, accompanied by the continuous decrease in the yield of the evaporated vapours from 43% at 1 K/s to 28% at 1000 K/s. The total tar yield of cellulose pyrolysis still increases with the heating rate (from 72% at 1 K/s to 86% at 1000 K/s), with the contribution of the ejected aerosols increasing

from 40% at 1 K/s to 67% at 1000 K/s. The data clearly demonstrate the key role of thermal ejection in the formation of primary volatiles from cellulose fast pyrolysis, greatly influencing the yields and compositions of the generated volatiles (and the condensed bio-oil). Overall, the results of this study significantly enhance the understanding of the formation of primary volatiles from cellulose fast pyrolysis via thermal ejection and evaporation.

Secondly, the fundamental reaction mechanisms during fast pyrolysis of the acid-impregnated cellulose in a wire-mesh reactor are obtained. The key compounds in the reaction intermediates and primary volatiles were quantified. The results indicate that acid impregnation reduces the onset reaction temperature of cellulose pyrolysis. At temperatures <100 °C, acid catalyses hydrolysis reactions to produce glucose, which is further dehydrated to 1,6-Anhydro-beta-D-glucofuranose (AGF) at 120 °C. At temperatures >160 °C, acid enhances the dehydration of glucose, levoglucosan and AGF to produce 5-HMF and levoglucosenone (LGO) as major primary products. Once produced, those products can be easily released into the vapour phase, as either aerosols via thermal ejection or vapours via evaporation. As the pyrolysis temperature increases to 240 °C, aromatic compounds can be identified in the primary volatiles, indicating condensation reactions also play important roles during acid-catalysed cellulose pyrolysis under the conditions. As a result, char formation becomes the favoured pathway during acid-catalysed cellulose pyrolysis at temperatures >300 °C.

Thirdly, acid-washed lignin, organic and inorganic sodium loaded lignin were pyrolysed at 300-800 °C. The collected primary tar and char were characterised and quantitatively analysed to reveal the effect of sodium loading. The results suggest that various sodium occurrences display different catalytic effects and distinguishing transformation properties during lignin pyrolysis. Sodium impregnation catalyses the

formation of aromatic structures during fast pyrolysis. While inorganic sodium yields more aromatics with more fused rings, organic sodium loaded lignin tends to release more low-molecule-weight compounds with sodium at low temperatures (e.g., 300 °C). The transformation between various sodium occurrences occurs in an early pyrolysis stage, and sodium within molten intermediates is mainly released to tar by ejection, especially inorganic sodium. Also, inorganic sodium is more stable than organic sodium, with more than 70% of the total sodium retained in char residues.

Fourthly, the effect of CO_2 addition and temperature on the torrefaction of lignin and the subsequent pyrolysis were investigated in this study. Torrefaction of lignin experiences breakage of β-O-4 bonds demethoxylation reactions to release methoxyl and methyl groups and polycondensation reactions. Those reactions result in the reduction of oxygen content and higher heating value. The addition of CO_2 leads to more weight loss with densified lignin structure by releasing more aromatics with more fused rings into the gaseous products. For the subsequent pyrolysis, higher torrefaction temperature leads to significantly higher char yield. At torrefaction temperature 200 ºC and 250 ºC, CO_2 enhances the release of aromatic volatiles. However, the addition of 15% CO_2 tends to reserve more aromatics in the char residues at 300 ºC. The dense structure inhibits the generation of gaseous products, and therefore the release of volatile is largely reduced.

Acknowledgements

I would like to acknowledge the Curtin International Postgraduate Research Scholarship (CIPRS) and Curtin Strategic International Research Scholarship (CSIRS), Curtin University HDR Mobility Grant (2019), HDR Completion Scholarship, CIPRS and Research Stipend Scholarship from Curtin University to support my PhD study.

I would like to express my sincere gratitude to my supervisor, Professor Hongwei Wu. With his extensive knowledge and broad experience, I learned so much to become a well-trained researcher, from generating innovative ideas, initiating feasible proposals, conducting convincing experiments, suggesting reasonable explanations, to establishing comprehensive mechanisms. I would like to thank Dr Yun Yu and Sui Boon Liaw. As my co-supervisors, they not only corrected my wrongs when conducting experiments but also straightened my thoughts. Without their generous help, my PhD study will be much more difficult.

In addition, I appreciate the help from Professor Yu Qiao and Erwei Leng from Huazhong University of Science and Technology for the establishment of a wire mesh reactor. I also would like to acknowledge the group members: Mingming Zhang, Yu Long, Bing Song, Xujun Chen, Wenran Gao, Changya Deng, Zhiliang Wu, Fanhui Guo, Yanshan Yin, Yee Wen Chua, Rashedul Khondakar, Mingyang li, Qiqing Shen, Victor Olet, and Md Rahman. I would also thank the lab technical supports from Andrew Chan, Melina Miralles, Xiao Hua, Roshanak Doroushi and Jennifer Wang.

Most importantly, I would like to express the utmost gratitude to my beloved family for backing me up, shielding me from harm, and cheering me up.

List of Publications

Paper(s) Published in Refereed International Journals

[1] **Jinxiu Cao**, Sui Boon Liaw, Yu Long, Yun Yu, and Hongwei Wu. Formation of reaction intermediates and primary volatiles during acid-catalysed fast pyrolysis of cellulose in a wire-mesh reactor. Proceedings of the Combustion Institute, 2021, 38, (3), 4301-4308.

Papers Submitted to Energy Fuels

[2] **Jinxiu Cao**, Yun Yu, and Hongwei Wu. Contributions of Thermal Ejection and Evaporation to the Formation of Primary Volatiles during Cellulose Fast Pyrolysis.

Papers to Be Submitted to Refereed International Journals

[3] **Jinxiu Cao**, Yun Yu, and Hongwei Wu. The release and transformation of organic and inorganic sodium during the fast pyrolysis of sodium impregnated lignin.

[4] **Jinxiu Cao**, Yun Yu, and Hongwei Wu. Effect of carbon dioxide torrefaction on the fast pyrolysis of lignin in a wire-mesh reactor.

Table of Contents

Abstract III

Acknowledgements VII

List of Publications VIII

Table of Contents IX

List of Tables XV

List of Figures XVI

CHAPTER 1 Introduction 1

1.1 Background and motive 1

1.2 Scope and objectives 3

1.3 Thesis outline 3

CHAPTER 2 Literature Review 6

2.1 Introduction 6

2.2 Lignocellulosic biomass compositions 6

2.3 Pyrolysis of biomass 7

2.3.1 Pyrolysis process 7

2.3.2 Pyrolysis products 9

2.3.3 Aerosols generation and thermal ejection 12

2.4 Pyrolysis of biomass model compounds 15

2.4.1 Pyrolysis of cellulose 15

2.4.2 Pyrolysis of lignin 18

2.4.3 Pyrolysis of hemicellulose 19

2.5 Pyrolysis of biomass-derived products 20

2.6.1 Acid impregnated biomass samples 21

2.6.2 AAEM loaded biomass samples 24

2.6.3 Torrefied biomass samples 28

2.6 Pyrolysis reactors 33

2.7 Conclusions and research gaps 35

2.8 Research objectives 35

CHAPTER 3 Research Methodologies and Analytical Techniques 36

3.1 Introduction 36

3.2 Methodology 36

3.2.1 A method for quantifying ejected aerosols and evaporated vapours during cellulose pyrolysis 38

3.2.2 Effect of acid-impregnation during cellulose pyrolysis 38

3.2.3 Effect of AAEM and the release and transformation during lignin pyrolysis 39

3.2.4 Effect of carbon dioxide assisted torrefaction and the subsequent pyrolysis of lignin 39

3.3 Experimental 40

3.3.1 Raw chemicals and sample preparation 40

3.3.2 Reactor configurations 41

3.3.3 Pyrolysis experiments 46

3.3.4 Torrefaction experiments 46

3.4 Instruments and Analytical Techniques 47

3.4.1 Quantification of sugars 47

3.4.2 Conversion, yield and selectivity 47

3.4.3 Quantification of inorganic species 48

3.4.4 UV fluorescence spectra and FTIR spectra 49

3.4.5 Optical imaging and SEM 49

3.4.6 Ultimate and proximate analysis 49

3.4.7 Higher heating value and energy yield 49

3.5 Summary 50

CHAPTER 4 Contributions of Thermal Ejection and Evaporation to the Formation of Condensable Volatiles during Cellulose Pyrolysis 51

4.1 Introduction 51

4.2 The yields of the ejected aerosols and the evaporated vapours collected from cellulose pyrolysis at different heating rates 53

4.3 Characterisation of the ejected aerosols and the evaporated vapours collected from cellulose pyrolysis at different heating rates 55

4.3.1 Particle size distribution of the ejected aerosols droplets 55

4.3.2 Yields of key compounds in the ejected aerosols and the evaporated vapours 56

4.3.3 Collection efficiencies of key compounds in the ejected aerosols and evaporated vapours 58

4.4 Estimation of the true yields of the ejected aerosols and the evaporated vapours from cellulose pyrolysis at different heating rates 62

4.5 Further discussion on the formation mechanism of primary volatiles during cellulose fast pyrolysis 68

4.6 Conclusions 70

CHAPTER 5 Formation of Reaction Intermediates and Primary Volatiles during Acid-catalysed Fast Pyrolysis of Cellulose 72

5.1 Introduction 72

5.2 Cellulose conversion during the pyrolysis of the raw and acid-impregnated cellulose 73

5.3 Yields of the water-soluble products in the solid residue and tar during the pyrolysis of the raw and acid-impregnated cellulose 75

5.4 Characterisation of the water-soluble products in the solid residue and tar produced from the pyrolysis of the raw and acid-impregnated cellulose 76

5.5 Discussion on the acid-catalysed cellulose pyrolysis mechanism 83

5.6 Conclusions 84

CHAPTER 6 `The Release and Transformation of Organic and Inorganic Sodium during Fast Pyrolysis of the Sodium Impregnated Lignin 86

6.1 Introduction..... 86

6.2 Product distribution during the pyrolysis of different types of lignin 88

6.3 Characterization of tar and char products during the pyrolysis of organic and inorganic sodium loaded lignin 90

6.3.1 FT-IR analysis of lignin samples and the char residues..... 90

6.3.2 UV fluorescence analysis of tar samples 93

6.4 Sodium distribution and transformation in the tar and char residues during the pyrolysis of organic and inorganic sodium loaded lignin 94

6.4.1 Sodium retention 94

6.4.2 Organic and inorganic sodium distribution in the tar and char residues 95

6.4.3 Sodium transformation in the tar and char residues..... 99

6.5 Discussion on the release and transformation of different sodium during lignin pyrolysis 102

6.6 Conclusions 103

CHAPTER 7 Effect of Carbon Dioxide Assisted Torrefaction on the Fast Pyrolysis of Lignin 105

7.1 Introduction..... 105

7.2 Characterisation of organosolv lignin torrefied under various temperatures and atmospheres 107

7.2.1 Conversion of the torrefied organosolv lignin 107

7.2.2 Elementary composition of the torrefied organosolv lignin 108

7.2.3 Morphological changes of the torrefied organosolv lignin 110

7.2.4 FTIR spectrum of the torrefied organosolv lignin 113

7.2.5 UV-fluorescence spectrum of the solvent-soluble torrefied organosolv lignin and its generated volatiles 115

7.3 Effect of torrefaction on pyrolysis 116

7.3.1 Conversion of the torrefied organosolv lignin after pyrolysis 116

7.3.2 UV-fluorescence spectrum of the pyrolysis of torrefied organosolv lignin 118

7.4 Conclusions 120

CHAPTER 8 Conclusions and Recommendations 121

8.1 Introduction 121

8.2 Conclusions 121

8.2.1 Contributions of thermal ejection and evaporation to primary tar formation during cellulose pyrolysis in a wire mesh reactor at various heating rates 121

8.2.2 Formation of reaction intermediates and primary volatiles during acid-catalysed fast pyrolysis of cellulose in a wire-mesh reactor 122

8.2.3 The release and transformation of organic and inorganic sodium during the fast pyrolysis of sodium impregnated lignin 122

8.2.4 Effect of carbon dioxide assisted torrefaction on the fast pyrolysis of lignin in a wire-mesh reactor 123

8.3 Recommendations 124

REFERENCES 125

APPENDIX 1: Copyright Permission Statements 166

APPENDIX 2: Attribution Tables 167

List of Tables

Table 2-1 Recent studies on the pyrolysis of acid-treated biomass samples 23

Table 2-2 Recent studies on pyrolysis of AAEM loaded biomass samples..... 27

Table 2-3 Recent studies on the pyrolysis of torrefied biomass samples 31

Table 2-4 Recent studies on torrefaction of biomass samples under non-inert atmospheres..... 32

Table 2-5 Characteristics of biomass pyrolysis reactors 34

Table 6-1 proximate, ultimate and ash compositional analysis of three lignin samples 88

Table 6-2 Product yields during the pyrolysis of the lignin samples at different temperatures 90

Table 6-3 Peak assignments for FT-IR spectra 92

Table 7-1 Ultimate, proximate analysis, estimated HHV and EY of torrefied lignin 109

Table 7-2 FTIR peak assignment of torrefied lignin samples[326-330] 114

List of Figures

Figure 1.1 Thesis map 5

Figure 2.1 Structures of biomass with cellulose, hemicellulose and lignin 7

Figure 2.2 Thermal utilisation of biomass 9

Figure 2.3 Schematic illustration of biomass pyrolysis products 10

Figure 2.4 Structure of cellulose[3, 117] 16

Figure 2.5 Summarised pyrolysis pathways of cellulose 17

Figure 2.6 Chemical structure of lignin 19

Figure 2.7 Chemical structure of hemicellulose[48] 20

Figure 3.1 Research methodology and the linkages to the research objectives in this PhD study 37

Figure 3.2 Schematic diagram of wire mesh reactor 42

Figure 3.3 Experimental set up of wire mesh reactor: a) collection of total tar, b) collection of ejected aerosols, and c) collection of evaporated vapours 44

Figure 3.4 Experimental set up of tube furnace for torrefaction of lignin samples ... 46

Figure 4.1 The yields of the ejected aerosols and the evaporated vapours collected from cellulose pyrolysis at 600 °C with a particle size at 106-150μm and a holding time of 10s at different heating rates of 1–1000 °C/s 55

Figure 4.2 Particle size distribution of the ejected aerosols droplets during cellulose pyrolysis at 600 °C with a particle size at 106-150μm and a holding time of 10s at different heating rates 56

Figure 4.3 The yields of key compounds in the total tar, the ejected aerosols and the evaporated vapours during cellulose pyrolysis at 600 °C with a particle size at 106-150μm and a holding time of 10s at 1–1000 K/s. (a) Total tar; (b) Ejected aerosols; (c) Evaporated vapours. 58

Figure 4.4 The collection efficiencies of the key compounds in the ejected aerosols and the evaporated vapours during cellulose pyrolysis at 600 °C with a particle size at 106-150μm and a holding time of 10s at 1–1000 K/s. (a) AC3-AC5 in the ejected aerosols; (b) AC1-AC2 in the ejected aerosols; (c) 5-HMF in the evaporated vapours; (d) AC1-AC2 in the evaporated vapours. 61

Figure 4.5 The estimated yields of the ejected aerosols and the evaporated vapours during cellulose pyrolysis at 600 °C with a particle size at 106-150μm and a holding time of 10s at 1–1000 K/s. Note: the yields of the ejected aerosols and the evaporated vapours collected from experiments (hatched) are also presented for comparisons.. 64

Figure 4.6 Distribution of ejected and evaporated products in the total tar during cellulose pyrolysis at 600 °C with a particle size at 106-150μm and a holding time of 10s at 1–1000 K/s. 64

Figure 4.7 The estimated yields of the ejected and evaporated AC1 (panel a) and AC2 (panel b) during cellulose pyrolysis at 600 °C with a particle size at 106-150μm and a holding time of 10s at different heating rates. 66

Figure 4.8 Distribution of the ejected and evaporated AC1 (panel a) and AC2 (panel b) in the total tar during cellulose pyrolysis at 600 °C with a particle size at 106-150μm and a holding time of 10s at 1–1000 K/s. 67

Figure 5.1 Cellulose conversions based on weight, carbon and sugar during the pyrolysis of the raw (solid symbol) and acid-impregnated (open symbol) cellulose at different temperatures 74

Figure 5.2 Yields of the water-soluble products in the solid residue and tar produced from the pyrolysis of the raw (solid symbol) and acid-impregnated cellulose (open symbol) at different temperatures 76

Figure 5.3 Yields (Panel a and c) and selectivities (Panel b and d) of the major compounds in the water-soluble intermediates from the pyrolysis of the raw (solid symbol) and acid-impregnated cellulose (open symbol) at different temperatures ... 78

Figure 5.4 Yields (Panel a) and selectivities (Panel b) of the major compounds in the water-soluble tar from the pyrolysis of the raw (solid symbol) and acid-impregnated cellulose (open symbol) at different temperatures 79

Figure 5.5 Distribution of the major compounds in the reaction intermediates (hatched) and primary volatiles (empty) as a function of temperature 81

Figure 5.6 Constant energy (-2800 cm^{-1}) synchronous spectra of the solvent-soluble tars produced from the pyrolysis of acid-impregnated cellulose at 240 and 320 °C . 82

Figure 5.7 Proposed acid-catalysed cellulose pyrolysis mechanism 84

Figure 6.1 FT-IR spectra of lignin char samples from different pyrolysis temperatures in the region of 700–2000 cm^{-1} 92

Figure 6.2 Constant energy (-2800 cm^{-1}) synchronous spectra of the solvent-soluble tar produced from the pyrolysis of lignin samples at different temperatures 94

Figure 6.3 Sodium retention during the pyrolysis of sodium loaded lignin samples at different temperatures 95

Figure 6.4 Sodium distribution during the pyrolysis of In-Na-lignin 98

Figure 6.5 Sodium distribution during the pyrolysis of Or-Na-lignin 98

Figure 6.6 Inorganic and organic sodium distribution during the pyrolysis of lignin samples 100

Figure 6.7 Organic and inorganic sodium distribution in char and tar during the pyrolysis of lignin samples 101

Figure 6.8 Proposed release and transformation of various sodium during lignin pyrolysis 103

Figure 7.1 Solid yield of torrefied organosolv lignin under different atmospheres and temperatures 107

Figure 7.2 Van Krevelen plot of torrefied lignin under various temperatures and atmospheres 110

Figure 7.3 SEM photos of organosolv lignin samples before and after torrefaction 112

Figure 7.4 FT-IR spectra of lignin char samples from different pyrolysis temperatures in the region of 700–2000 cm^{-1} 114

Figure 7.5 Constant energy (-2800 cm^{-1}) synchronous spectra of the solvent-soluble volatiles from the torrefaction of lignin at different temperatures and atmospheres 115

Figure 7.6 Constant energy (-2800 cm^{-1}) synchronous spectra of the solvent-soluble residues from the torrefaction of lignin at different temperatures and atmospheres 116

Figure 7.7 Pyrolysis product yields of torrefied organosolv lignin samples at 500 ºC 117

Figure 7.8 Constant energy (-2800 cm^{-1}) synchronous spectra of the solvent-soluble volatiles from the pyrolysis of torrefied lignin at different temperatures and atmospheres 119

Figure 7.9 Constant energy (-2800 cm^{-1}) synchronous spectra of the soluble solid residues from the pyrolysis of torrefied lignin at different temperatures and atmospheres 119

CHAPTER 1 Introduction

1.1 Background and motive

Lignocellulosic biomass has attracted massive attention in recent decades for its capability to serve as a potential renewable energy source.[1] Thermal treatment of biomass to produce value-added bio-fuel and bio-chemicals is one of the most promising and feasible ways.[2-4] As the intimal process of the three most fundamental thermal processing- pyrolysis, combustion and gasification,[5] fast pyrolysis is widely recognised as an efficient method to produce liquid bio-fuel as well as platform chemicals[6].

Cellulose, lignin and hemicellulose are the three major compositions in lignocellulosic biomass, accounting for ~40- 60%, 20- 40% and 10- 25% of biomass, respectively, together with some inorganic metal species in the biomass matrix.[7, 8] It is reported that the pyrolysis of lignocellulosic biomass experience a molten phase (so-called intermediates),[9-11] before evolving into final solid, liquid and gaseous products. Those intermediates will either evaporate into vapours and thermal eject[12, 13] into aerosols, or undergo secondary reactions[13] to form secondary products. It is reported that the large oligomers with high molecule weight in bio-oil and the non-volatile inorganic species are likely to originate from the aerosols[14, 15], since it is not possible to be evaporated because of high boiling points. Many researchers have studied the ejection and evaporation phenomenon during the pyrolysis of lignocellulosic biomass, but a quantitative method for the determination of ejection and evaporation yields is not available yet. Besides, understanding the properties of those intermediates and the primary volatiles is of significant importance for the subsequent production of bio-fuel and bio-chemicals. Because of the short-lived nature of the liquid intermediates[16], it is

challenging for the characterisation. Therefore, a wire mesh reactor[17-20] is introduced because of the unique features of rapid heating and swiftly sweeping of the generated volatiles. As a result, it is possible to minimise the secondary reaction and collect the primary products, and further understand the reaction mechanism of the pyrolysis of biomass and its model compounds.

Despite the considerate potential of biomass utilisation, its commercialisation is hindered by poor properties of bio-products, such as high moisture content, high acidity, low energy density and poor stability.[21, 22] Therefore, some pre-treatment methods, for instance, acid loading[23-28], alkali and alkaline earth metals (AAEM) impregnation[29-33], torrefaction[34-36] have been proposed and studied. It is reported that the AAEM in biomass matrix results in the increase of char yield and decrease of organic volatile yield.[29, 37] Also, organically bonded intraparticles and inorganic extraparticles have distinct catalytic effects on lignin pyrolysis.[3,31] Acid treatment is often employed to remove the majority of metals in biomass in order to promote the production of liquid fuel. However, the addition of acid not only removes the metals, but also alters the organic structure of biomass, further influencing the reaction mechanisms and product distribution.[38-40] Previous studies[24, 38-40] primarily investigated the product distribution, ignoring the effect on the condensed-phase chemistry[28]. Torrefaction is another promising method to improve the grindability and high heating value of the raw biomass material.[35, 41] These pre-treatment methods significantly alters the reaction mechanism, especially the formation of primary products. Understanding the effect of these pre-treatment methods on the production of primary volatiles is of great importance to understand the fundamental reaction chemistry and the yield of valuable bio-fuel and bio-chemicals.

1.2 Scope and objectives

This thesis attempts to study the fundamental reaction mechanism and the effect of pre-treatment methods during the pyrolysis of cellulose and lignin with the following specific objectives:

- to characterise the ejected aerosols and evaporated vapours during cellulose pyrolysis under various heating rates using a wire mesh reactor;
- to investigate the formation of reaction intermediates and primary volatiles during acid-catalysed fast pyrolysis of cellulose using a wire mesh reactor;
- to study the release and transformation of organic and inorganic sodium during the fast pyrolysis of sodium impregnated lignin using a wire mesh reactor;
- to understand the effect of carbon dioxide assisted torrefaction and the following fast pyrolysis of lignin using a wire mesh reactor.

1.3 Thesis outline

This thesis contains eight chapters with detailed descriptions of each chapter listed below and a schematical structure diagram is presented in Figure 1.1.

- Chapter 1 gives the background and objectives of this research;
- Chapter 2 summarises a thorough range of literature in terms of fast pyrolysis of cellulose and lignin and the effects of various pre-treatment methods, including acid-loading, AAEM impregnation, and torrefaction. Subsequently, the research gaps and objectives are specified in current research;
- Chapter 3 introduces the methodologies and techniques adopted in this research to accomplish the listing objectives in current study with a detailed

description of the employed samples, reactor configurations, analytical equipment and procedures;

- Chapter 4 characterises and further proposes a quantitative method to determine the yield of ejected aerosols and evaporated vapours during cellulose pyrolysis under various heating rates;
- Chapter 5 aims at the fundamental reaction mechanism, especially the formation of reaction intermediates during the pyrolysis of acid-loaded cellulose;
- Chapter 6 reports the release and transformation of organic and inorganic sodium during the fast pyrolysis of sodium-loaded lignin;
- Chapter 7 investigates the effect of carbon dioxide assisted torrefaction and the subsequent pyrolysis of lignin;
- Chapter 8 concludes the major findings and lists our future research works.

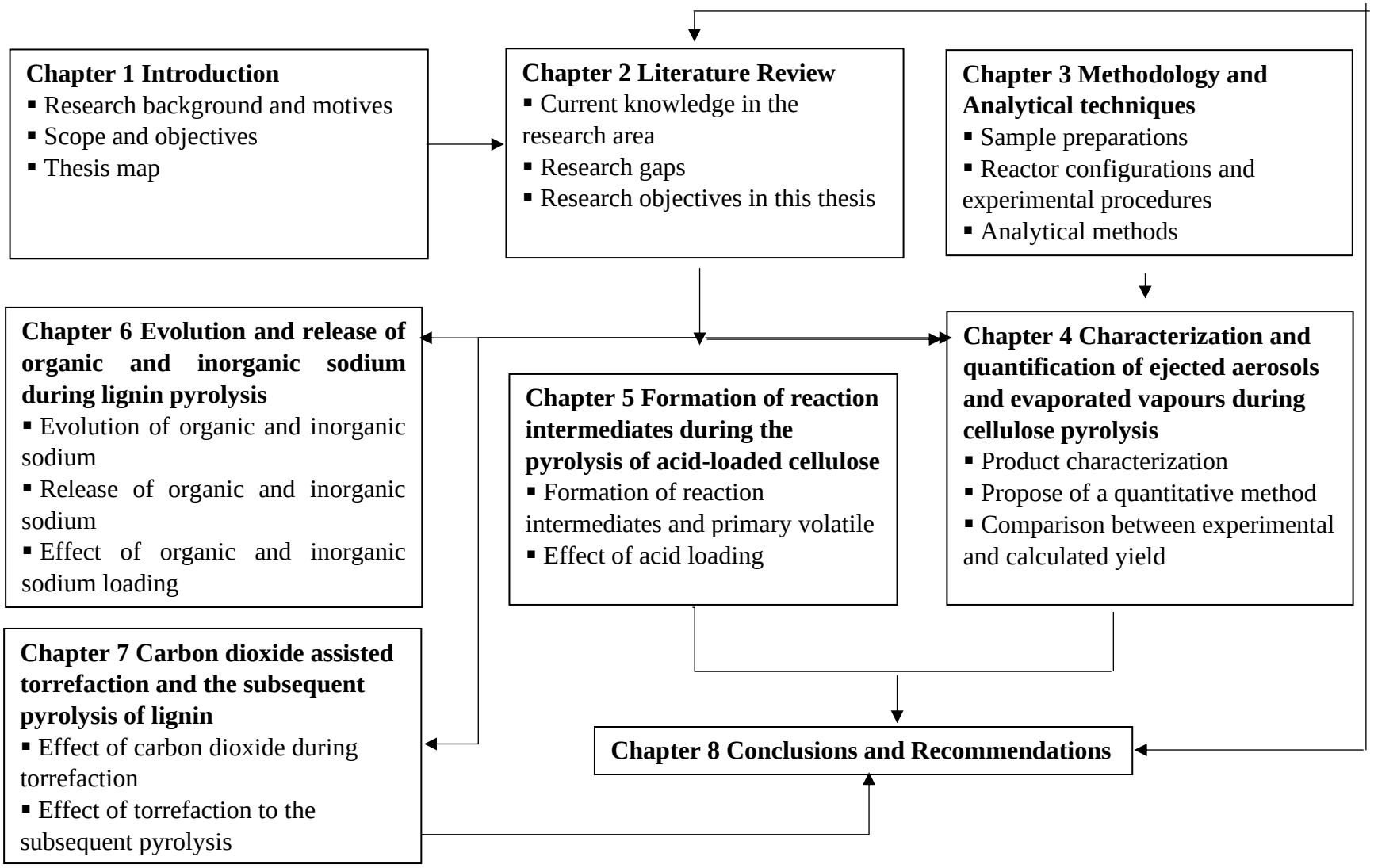

Figure 1.1 Thesis map

CHAPTER 2 Literature Review

2.1 Introduction

Thermal conversion of biomass to produce solid, liquid and gaseous bio-fuels and chemicals is a feasible way to substitute fossil fuel.[42] And fast pyrolysis of lignocellulose biomass is one of the most practical approaches to producing renewable and sustainable liquid fuel in a performance-competitive way.[5] As the original poor properties of generated bio-liquid[4, 22, 43-45] hinder its further utilisation, various pre-treatment methods were proposed to improve the quality and alter the product distribution for more value-added chemicals. This chapter targets to provide a thorough review of the comprehensive and up-to-date research of the pyrolysis of biomass model compounds and biomass-derived products. The reaction process, mechanism and product distribution of biomass pyrolysis are outlined. In addition, the effects of various pre-treatment methods of biomass to yield more value-added or desirable bio-fuel and bio-chemicals are summarised. According to available knowledge and advancement of biomass pyrolysis, the research gaps are laid out, and the objectives of this thesis are accordingly put forward.

2.2 Lignocellulosic biomass compositions

Biomass is composed of cellulose, hemicellulose, lignin, organic extractives and inorganic metal species.[46] The composition percentage varies by types of biomass, and the difference in composition significantly alters the following utilisation process and the ultimate product distribution.[47] The structure of typical biomass is shown in Figure 2.1. Cellulose associates with hemicellulose and lignin to form a heteromatrix structure to various extents, based on the species of biomass[48]. Lignin provides structural

support, elasticity, and strength to plant wall,[49, 50] while hemicellulose entangles cellulose-fibrils[48]. Understanding the reaction mechanism of the individual compositions of biomass is fundamental to escalate to the overall biomass thermal utilisation. In addition, the natural occurrence of the organic extractives or inorganic AAEM species show catalytic effects during the thermal treatments of biomass and the model components.[51]

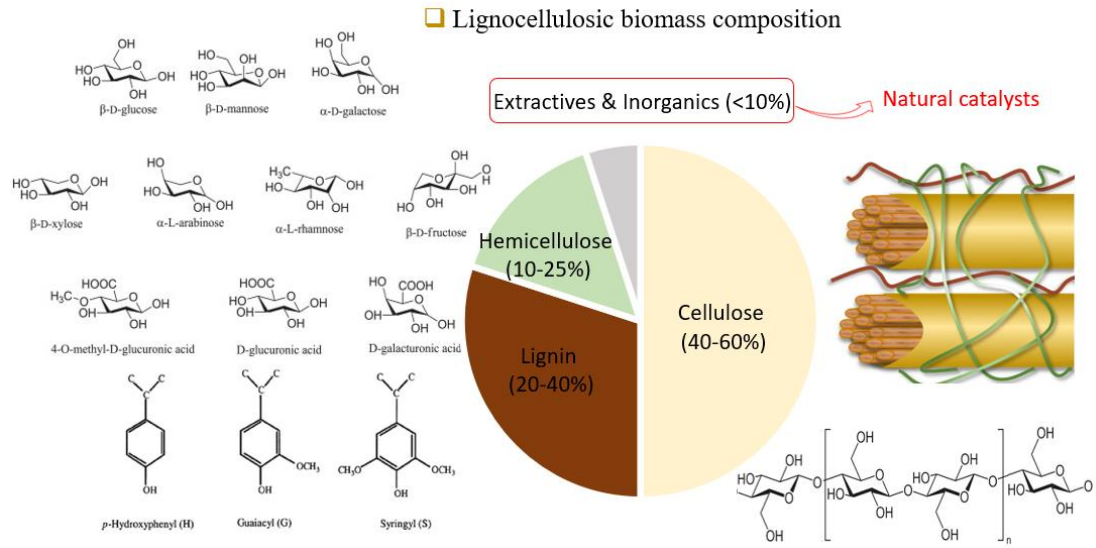

Figure 2.1 Structures of biomass with cellulose, hemicellulose and lignin

2.3 Pyrolysis of biomass

2.3.1 Pyrolysis process

The fast pyrolysis of biomass has arisen broad interest considering its potentiality to produce a high yield of bio-oil to ease the depletion of fossil fuel.[52, 53] And recent research of biomass pyrolysis set emphasis on increasing the yield of bio-oil as well as upgrading the quality of the bio-products. The thermal utilisation of biomass is

demonstrated in Figure 2.2. The pyrolysis of biomass under different heating conditions leads to various yields and properties of char, tar and gas, as well as distinct product distributions. It is reported that the pyrolysis of biomass produces 60−75 % of bio-oil, 15−25 % of char, and 10−20 % of gases, depending on the feedstock types.[54] Biomass pyrolysis also has the potential to produce clean and renewable bio-chemicals, such as ethanol[55, 56], levoglucosan and 5-hydroxymethylfurfural.[6, 10, 57-60] The degradation of biomass under fast heating conditions evolves with the occurrences of liquid intermediate, depolymerisation, and the subsequent repolymerisation reactions.[11, 61] The gaseous products evolve from the evaporation or ejection effect of the liquid intermediate phase, while the char is generated from the repolymerisation reactions between different phases. Due to the so-called "reactive boiling effect"[13], the composition in bio-oil is composed of ejected aerosols, evaporated vapours, and some inorganic species. A recent investigation demonstrated that biomass and biomass components experience a combination of melting, ejection, evaporation process under 100 °C/s.[62] While the intermediate phase plays a vital role during biomass pyrolysis, a wide range of reaction parameters, including temperature, heating rate, and pre-treatment methods, influences the biomass pyrolysis pathways and the subsequent production yield and distribution.[63] Generally, high heating rates facilitate volatile generation[64, 65] because of the shorter residence time of the generated vapours. In addition, the interactions[66] between the different phases and the catalytic effect of inorganic species within the biomass matrix make significant differences. Previous research found that the pyrolytic lignin, as the heavy product in biomass pyrolysis oil, presents a similar and expected structure as the original lignin.[67]

The process of breaking of chemical bonds during biomass pyrolysis is concluded as depolymerization[68-70], fragmentation[71], and char formation[72-74] to define the

pathways.[75] Many review papers summarised the potential pyrolysis mechanism of biomass pyrolysis, such as, the reaction evolution,[63, 76, 77] reaction chemistry,[75, 78] roles and reaction mechanisms of the individual component[60, 75, 79] and effect of pre-treatments[35, 80]. Owing to the complexity of biomass structure and composition, the achievement of the above mentioned objectives requires a more comprehensive understanding of the fundamental reaction mechanism and the corresponding detailed reviews are described in the following sections.

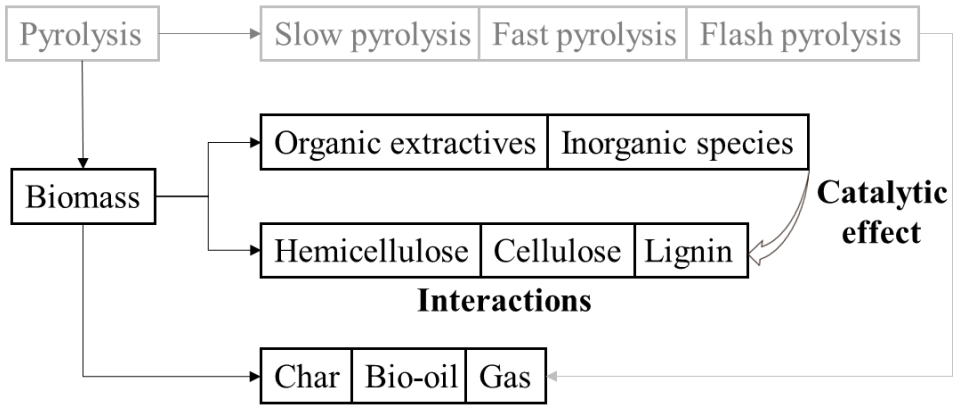

Figure 2.2 Thermal utilisation of biomass

2.3.2 Pyrolysis products

Biomass pyrolysis leads to the formation of liquid, gaseous and solid products in general. However, before thermal conversion of biomass samples, pre-treatments are conducted to improve the quality and properties of those products. And the thermal process of biomass and biomass-derived products often undergoes a liquid intermediate phase, where the ejection and evaporation occur. Those ejected and evaporated products are referred to as primary volatiles. Meanwhile, if the liquid intermediates remain in the heating zone, considerable secondary reactions take place,

including the interaction between different phases and repolymerisation reactions. Overall, those secondary products and primary volatiles consist the ultimate products of biomass pyrolysis.

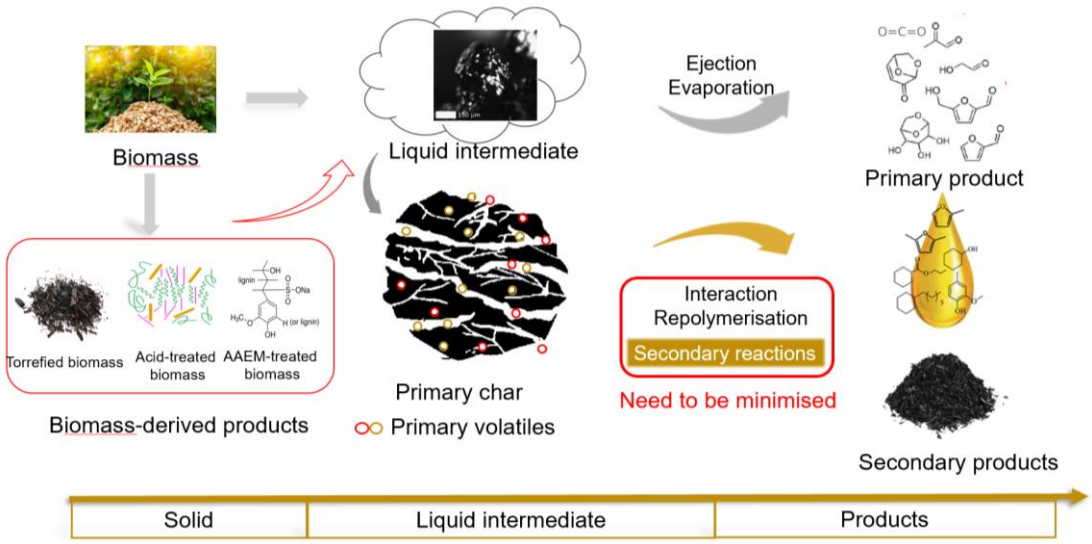

Figure 2.3 Schematic illustration of biomass pyrolysis products

2.3.2.1 Char

The pyrolysis of lignocellulose biomass leads to the generation of a carbonaceous product, and often with porous and aromatic structures.[81, 82] It is worth pointing that the carbonaceous product, namely char, originates from the intra- and intermolecular cross-linking reactions to facilitate the formation of benzene rings, benefiting the thermal stability of the residue[83]. Those processes are often influenced by the original feedstock and the peak temperature, significantly changing char composition. High pyrolysis temperatures result in a higher carbon content in char residues and produce a melted phase of biomass[84, 85], thus completely changing the original structure. On the contrary, slow heating rates promote the char formation process with the reservation of the initial internal structure of the biomass matrix.

Inorganic species are present and often accumulate in char residues, mainly depending on the initial inorganic biomass composition. Because of the high boiling points and the non-volatile nature, some inorganic, such as Ca, Si, are almost completely retained. However, some other elements, such as K, Na, can be released to the liquid or gas phase. For example, alkali metals in water-soluble or ion-exchangeable forms have an outstanding potential for release[86, 87]. However, their release is usually quite low[88].

2.3.2.2 Volatiles

The fast pyrolysis of biomass produces a large number of volatile compounds, including condensable liquid products and permanent gases. Permanent gases only contribute to ~20 wt % of total product, mainly CO, CO_2, CH_4, H_2 and some other light molecule weight compounds. Meanwhile, the production of bio-oil is the top priority of biomass utilisation, with a typical yield higher than 75% under fast and flash pyrolysis conditions[89]. The condensable liquid products are utilised as a clean and sustainable new source of energy considering its environmental advantages over fossil fuels, such as CO_2/ GHG neutral.

Chemically, bio-oil fraction comprises hundreds of compounds, including water, acids, sugars, phenols, furans, ketones and other high molecular weight compounds with larger degrees of polymerisation.[90] The oligomeric species in bio-oil, especially those with high degree of depolymerisations, are derived mainly from lignin and cellulose. As the boiling point of those large molecules are reported to be very high, most of those compounds are originated from the aerosols. And the compounds derived from lignin are known as pyrolytic lignin with various mass distributions.[91] Also, the complexity and diversity of bio-oil composition complicate and hinder the subsequent

utilisation or upgrading for commercial application as commodity chemicals and fuels [92]. For example, the pyrolytic lignin will polymerise during storage, forming the heaviest lignin-rich fraction.[93] Moreover, the acid and water in bio-oil and other thermal unstable compounds show the signs of reactions between different compounds during storage or handling. Those reactions can change the quality and properties of bio-oil, often increasing viscosity and water content while decreasing the volatility.

To optimise the bio-oil quality, pre-treatment of biomass feedstock at the upward stream can couple with upgrading the bio-oil at the downward stream. Therefore, research has been done to improve the quality and properties of bio-oil by modifying the raw material with the addition of chemicals or catalysts and optimising the experimental conditions. For example, acid treatment promotes the dehydration reactions during biomass pyrolysis. Also, the removal of AAEM species dramatically influences the properties of bio-oil, e.g., viscosity, while hardly shows effects on the yields of bio-oil.

2.3.3 Aerosols generation and thermal ejection

The thermal utilisation of biomass undergoes a molten intermediate liquid phase. With the increasing heat flux, gas bubbles within the intermediate are produced. Once the bubbles breach the surface tension of the intermediate, the bursting with liquid jets starts to occur.[9] Those gas bubbles and liquid jets contain generated vaporised products and melted intermediates. As a result, the aerosols generated from the thermal ejection effect contain the non-volatile biomass-derived products or partly decomposed oligomers with original linkages. Several studies have been conducted to visualise the generation and ejection effect during the pyrolysis of cellulose and other biomass

compounds using high speed photography.[12, 13, 94]. These observations confirmed the formation of liquid intermediates phase and gas bubbles and the process depended on the experimental conditions. For example, the crystallinity of cellulose [95], fast and slow heating of lignin[96] influence the formation of liquid intermediates. It was suspected that the aerosols were originated from the collapse of gas bubbles during lignocellulose biomass pyrolysis due to the aerosol compositions.[13, 61, 97, 98] Furthermore, the small-angle neutron scattering (SANS) results supported the thermal ejection mechanism.[99] The aerosol size distributions were measured during the pyrolysis of sucrose and organosolv lignin in several different reactor systems, including a fluidised bed reactor and a cyclone pyrolyser.[97] The results indicated that the collected bubble size follows a log-normal distribution, which changes in viscosity over the time frame resulting from the solidification process.

During reactive boiling ejections, the aerosols contain the primary vapours and the non-volatile compounds, including the organic high molecule weight compounds and the inorganic species within the liquid intermediates. Those aerosols contribute to a large proportion of the liquid products from the lignocellulose biomass pyrolysis process.[100-102] Previous studies indicated that 20- 42 wt% of bio-oil originates from aerosols and particulates from different collection reactors or accounts for 8– 30wt% of the original feedstock.[14, 100, 101, 103-105] Moreover, the chemical composition of various oil fractions seems to be remarkably distinct.[14, 100, 103, 106, 107] For example, ejected aerosols typically contain some non-volatile organic polysaccharides, heavy pyrolytic lignin fractions as well as inorganic compounds[103, 106]. Those compounds with higher boiling points are unlikely to be produced from evaporation. The ejected aerosols also contain some low molecular weight compound, primary cellulose derived oxygenates, but with much lower concentrations than the evaporated vapours. It is

reported that high heating rates favour the thermal ejection effect to produce aerosols.[108] Furthermore, the particle size and temperature affect the bubbling process and the subsequent aerosol ejection. For example, previous work achieved an aerosol yield of 25 wt% with the condition of 1000 W/m^2 °C with a 1 mm particle, and 10–15 wt% with a lower heating rate at 50 W/m^2 °C.[98] Due to the higher fraction of lignin-derived products,[107] the aerosols own lower H/C and O/C ratios and higher heating values, compared with condensable oils. Also, the aerosol is more viscous and unstable because of the significant portion of energy-rich compounds.[106, 109]

There were also differences in the distribution of inorganics between the ejected aerosols and evaporated vapours. A recent study suggests that more than 60 wt% of the inorganic species out of total liquid product existing in the aerosols.[104] Differently from coal pyrolysis or combustion, biomass pyrolysis tends to yield high concentrations of volatile alkali and chorine[110, 111]. The existence of those inorganics was observed in the boiler walls and heat-exchange surfaces due to the deposition of the aerosols.[112] There are several different interpretations for this phenomenon: (1) volatilisation of part of the inorganics and the nucleation/condensation reactions after the flue gas starting to cool down; (2) aerosols with melted inorganics (including ion-free and organic bounded) are thermally ejected out; (3) some char particles with inorganics in the matrix, are transported with the evolution of aerosols; and (4) char particles served as condensation nuclei for the generated volatiles.[105] Even though the significance of aerosols have been properly addressed for the transportation of non-volatile organic and inorganic compounds, their yields and sizes are vital for downstream processes and further upgrading or utilisation. The characterisation and difference in separated ejected aerosols and evaporated vapours lack a comprehensive interpretation and require further investigation.

2.4 Pyrolysis of biomass model compounds

2.4.1 Pyrolysis of cellulose

Cellulose is a semicrystalline linear polymer with the replications of glucose monomer in a β glucosidic linkage[113, 114], and hydrogen bonding to stabilise and support cellulose structure[115]. Three hydroxyl groups in glucose units can form hydrogen bonds,[116] which play an important role in the crystalline structures of cellulose microfibers.[117] [118] The amorphous region of cellulose experiences a glass transition phase at a temperature ~243 °C[119], while the pyrolysis of cellulose initiates at a temperature between 325 and 400 °C[46, 120]. The breakage of glycosidic bonds tends to occur under acidic or high-temperature conditions. The pyrolysis process of cellulose experiences an active intermediate phase,[121-123] with the photographic observations[12, 13, 94] confirming the existence of the liquid phase and the active ejection phenomenon. Extensive studies have investigated the product composition from the pyrolysis of cellulose,[124, 125] which is mainly levoglucosan. Other dehydrated and decomposed products might originate from levoglucosan (LG), including levoglucosenone (LGO), 1,6-anhydro-β-d-glucofuranose (AGF), and 5-hydroxymethylfurfural (5-HMF)[126]. The formation of levoglucosan is either produced from unzipping reactions[127] or heterolytic glycosidic cleavage[128, 129]. The furan products, including 5-HMF, were mainly produced from the subsequent dehydration of monosaccharide units. And the degree of polymerisation (DP) of cellulose samples alters the final product distribution, mainly changing the product yield to other species. A previous study[129] showed that the pyrolysis of glucose-based carbohydrates generates almost identical products, including LG, 5-HMF, furfural, methylglyoxal, hydroxyacetaldehyde (HAA) and acetic acid. The formation of those pyran products was significantly related to the DP, with higher DPs favouring the generation of pyrans.

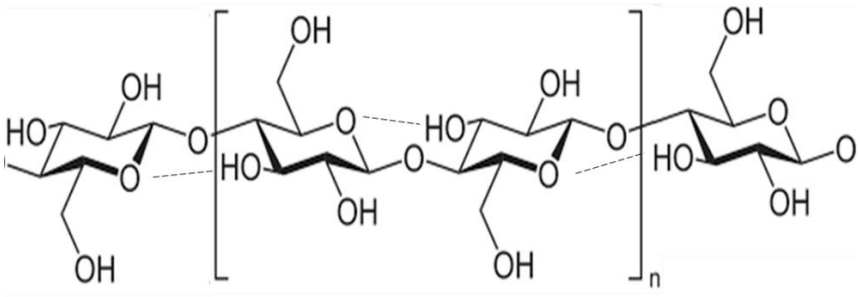

Figure 2.4 Structure of cellulose[3, 117]

Several cellulose pyrolysis mechanisms were proposed, including Broido–Shafizadeh scheme[127, 130] Piskorz scheme[131] Banyasz scheme[132, 133], and summarised in Figure 2.5. The Broido–Shafizadeh (B–S) model was first proposed for cellulose pyrolysis based on the product formation.[134] Before 300 °C, there is only minimal mass loss, mainly due to the loss of moisture from the cleavage of intermolecular and intramolecular hydrogen bonds[135, 136]. There also are some gaseous products, including CO, CO_2 and organic compounds.[137] However, different reactions already occur with the formation of the liquid intermediary phase, also called active cellulose.[83, 132] As the temperature increases to higher than 300 °C, an intermediate phase gradually forms when the glycosidic bond becomes very reactive, leading to the fast depolymerisation process. As a result, as the most kinetically favoured products, levoglucosan and other condensable volatiles are generated. Meanwhile, the dehydration of some sugar polymers to form other anhydro-saccharides contributes to the product distribution[71]. 5-HMF and furfural also exist in the volatiles due to the depolymerisation reactions[95, 138]. The liquid products generated from the pyrolysis of cellulose can be divided into two parts, aerosols and vapours. Aerosols are composed of oligomers with high molecule weight, while the vapours are principally the volatilisable monomers and small molecules.[61]

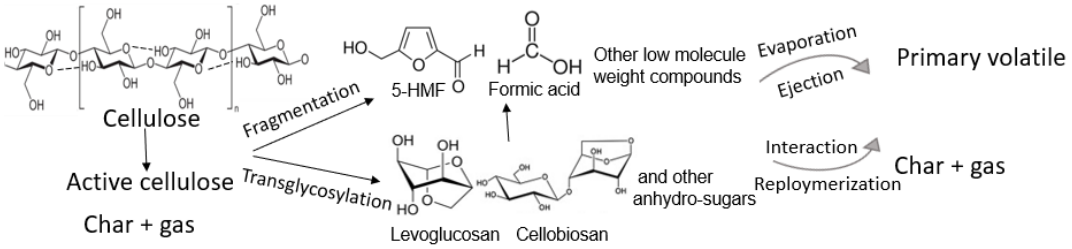

Figure 2.5 Summarised pyrolysis pathways of cellulose

It is reported that the occurrence of secondary reaction of cellulose pyrolysis largely depends on the vapour residence time,[139] which will significantly alter the optimal product distribution. The secondary reactions mainly involve the thermal degradation of volatiles to generate light volatiles and repolymerisation reactions within the vapour–solid phase to form char. For instance, primary volatiles can crack at high temperatures if remaining in the heating zone once generated. The char yield depends on a variety of parameters, including heating rate, final temperature, retention time of the volatiles, pressure, presence of inorganics, and atmosphere.[78] Low heating rates lead to a high char yield[140] and the long retention time of the volatiles in the solid matrix also promotes char yield[141]. It has been[142] claimed that the reactions between the pyrolytic vapours, with furans being probable intermediates[143], maybe the only source of cellulose char. However, if the heating rate is dramatically increased and volatile residence time is greatly decreased, the char yield of cellulose could be ignored as widely reported.

2.4.2 Pyrolysis of lignin

Lignin is phenolic polymer consisting of monolignols with three different polymerisations, including p-hydroxyphenyl (H type), guaiacyl (G type), and syringyl (S type).[144-146] The main structure of lignin is presented in Figure 2.6. The high degree of cross linking[147, 148] in lignin structure results in high thermally stablility[149], leading to a higher decompose temperature between 300 and 550 °C.[150] The linkages of basic lignin units are complex and can be divided into three classes: ether bonds, carbon-carbon bonds and ester bonds, depending on the types of biomass lignin. The various oxygenated functional groups in lignin structure, including methoxyl, hydroxyl, significantly affect the reactivity of lignin and the subsequent formation of char residues. The evolution of methoxyl groups[145] during lignin pyrolysis affected the product distribution[151, 152]. Also, methoxyl groups can undergo degradation reactions to form small molecular radicals, such as methane and methanol,[153, 154] which are reported to stabilise the large-molecule fragments other than undergoing the repolymerisation for char formation. Thereafter, the lignin samples with high methoxyl group contents tend to generate less pyrolysis char. The hydroxyl groups, which varies from the different biomass types, also play important roles in lignin pyrolysis, affecting the final phenolic product distribution[152, 155]. And the hydroxyl groups mainly include aliphatic, guaiacyl phenolic, syringyl phenolic and p-hydroxyphenyl hydroxyl groups. During the lignin pyrolysis process, the aliphatic hydroxyl group can be easily removed from the side chains via dehydration reactions at low temperatures, resulting in an unsaturated side-chain structure. Other oxygenated groups, including carboxyl and carbonyl groups, also exist in the lignin structure. Those oxygenated groups undergo depolymerisation reactions to form small-molecule

chemicals with low boiling points. Meanwhile, they could also be retained in the side chains of phenols.[156, 157]

Pyrolysis of lignin[158] experiences several stages over a wide temperature range[75, 159], compared with cellulose pyrolysis. Generally, lignin starts to melt at 160–190 °C[160] to form a mobile glass transitions phase, and the occurrence of dehydration reactions happens at ~200 °C when the mass starts to lose. The cleavage of various linkage gradually involves increasing temperature. To be specific, the breakage of alkylether linkages, aliphatic side chains and methoxyl groups occurs at 150 to 300 °C, 300 °C, 310 to 340 °C, respectively.[96] Therefore, it is critical to investigate the product distribution and the mechanism of lignin pyrolysis.

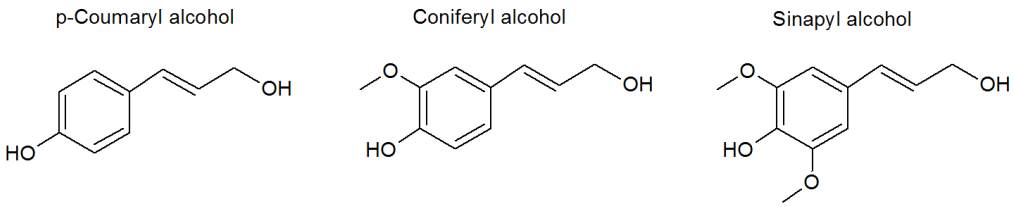

Figure 2.6 Chemical structure of lignin

2.4.3 Pyrolysis of hemicellulose

Hemicellulose consists of a bunch of short-chain heteropolysaccharides, including mainly glucose, mannose, galactose, xylose and arabinose. There are also some uronic and acetyl groups existing in the hemicellulose structure. Because of the complexity of hemicellulose compositions, the pyrolysis behaviour of hemicellulose is often studied by investigating the individual monosaccharide units. Xylose[161, 162] as well as arabinose[163] are mostly investigated. The product distributions from the pyrolysis of

those individual components were similar in species but with different product yields.[164] Typically, the thermal decomposition of xylan starts at a temperature between 250 and 350 °C, generating furans, furfural, ketones and anhydrosugars as major products.[162] The results suggested that those components in hemicellulose easily experience the ring-opening and cracking process, generating some small molecular compounds.[162]

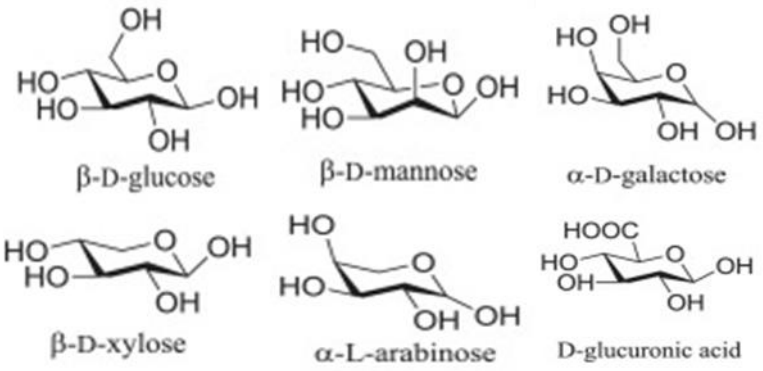

Figure 2.7 Chemical structure of hemicellulose[48]

2.5 Pyrolysis of biomass-derived products

Biomass-derived products[56, 165-168] has attracted extensive research interests to overcome the obstacles in liquefaction of biomass. Those biomass-derived products are often obtained from various pre-treatment methods. Those pre-treatments alter the structure for more efficient and accessible conversions, including reducing the particle size, improving the high heating value, and enhancing the grindability. The pre-treatments enhance properties of biomass-derived products, tune the reaction pathways and eventually influence the chemical characteristics of final products after thermal

conversion.[169] The detailed review papers of biomass-derived products and the pyrolysis of biomass-derived products can be found elsewhere[116, 170, 171].

2.6.1 Acid impregnated biomass samples

Dilute acid pre-treatment has been proposed as one of the most promising methods for the commercial production of ethanol and other valuable chemicals from biomass products.[168, 172] The acid treatment of biomass materials changes the physical as well as the chemical structure of biomass components. For example, acid presence leads to the loosened hydrogen bonding in cellulose structure, which plays an essential role in the crystalline structure. As a result, the acid-treated cellulose tends to contain lower DP but higher crystallinity,[173] due to the loss of amorphous cellulose. In addition, acid is capable of dissolving some acid-soluble lignin fractions.[116, 174] Acid also cleaves glycosidic bonds in hemicelluloses structures and glucuronosyl linkages in polyuronides,[175] with the formation of inhibitor compounds, such as furfural, 5- HMF, and some organic acids[116, 176].

Different acids have been utilised for the acid treatment of biomass, including sulphuric acid, hydrochloric acid, and phosphoric acid. Sulfuric acid is widely investigated for the biomass pre-treatment[177-181], leading to the damage of microstructures[182]. The addition of sulfuric acid was reported to promote the hydrolysis of cellulose into partly decomposed cellulose and glucose[183] and remove some hemicellulose heteropolysaccharides. The introduction of sulphuric acid in biomass pre-treatment not only changes the structure of biomass matrix, but also the subsequent pyrolysis products. According to previous research, sulfuric acid addition was adopted for the manufacturing of commercial furfural.[184] Also, it is reported that

it led to lower proportions of aromatics at pyrolysis temperature of 450 to 500 °C.[185] Hydrochloric acid[186-188], and phosphoric acid [23, 176, 188, 189] have also been studied. Phosphoric acid was added for cellulose samples to obtain higher yields of levoglucosan and levoglucosenone in the liquid products.[23] With the presence of phosphoric acid and water, the acid-catalysed ring contraction reaction and dehydration reactions, the cellulose samples with lower crystallinity tend to generate HMF, 5-methylfurfural, and furfural. By altering the concentration of phosphoric acid, the optimum active carbon yield[189] and anhydro-sugar yield[23] can be achieved from the pyrolysis of microcrystalline cellulose.

Table 2-1 Recent studies on the pyrolysis of acid-treated biomass samples

Raw material	Acid	Reactor	Conditions	Results	References
Mallee Eucalyptus loxophleba	Dilute nitric acid	Fluidized bed reactor	500 °C	Increases phenolic concentration and decreases pyrolytic sugar concentration	Mourant et al.[190]
Douglas fir and hybrid poplar	H_2SO_4 and $NH_4H_2PO_4$	Thermogravimetry	600 °C	Bestows thermal stability in biomass	Das et al.[191]
Rice straw	Dilute hydrochloric acid	Fixed bed reactor	550 °C	Influences on the pyrolysis process	Cen et al.[192]
Corn stover, rice straw and bamboo	Sulfuric acid	Py/GC–MS	900 °C	Mitigates AAEMs effect, improves the pyrolysis performance.	Zhou et al.[193]
Rice husk	H_2SO_4, HCl	Furnace	1078 °C	Effects the pyrolysis products distribution	Dan et al.[182]

2.6.2 AAEM loaded biomass samples

A small amount of inorganic species, including potassium, calcium, sodium, magnesium, silicon, phosphorus, sulfur, chlorine, and some trace elements, is present in biomass.[194, 195] The presence of those inorganic species, especially the alkali and alkaline-earth metal salts, shows a catalytic effect during the thermal utilisation of lignocellulose biomass.[196-198] For example, the occurrence of potassium in biomass results in decreased decomposition temperatures and the corresponding activation energy.[199] These cations lead to the fragmentation of the monomers, compared with the predominant depolymerisation reactions of polymers in the absence of inorganics, favouring the formation of char residues while hindering the generation of liquid products. [200-202] As a result, it suppresses the formation of levoglucosan, but promotes the generation of some lower molecular weight compounds during cellulose pyrolysis.[203]

The AAEM species have a negligible effect on the yields of bio-products; however, they dramatically change the product distribution and properties.[204] For instance, with the removal of AAEM, the yields of sugars and lignin-derived oligomers in the bio-oil are promoted, while the char yield, water and light organic compounds content are supressed.[190, 205] Also, the presence of AAEM oxalates promoted the generation of ketones. On the other hand, NaOH has been used for alkaline treatment in lignocellulosic biomass.[116, 206] Soaking in alkaline solutions, the lignin content in biomass samples will be greatly obliterated.[166] During the alkaline treatment, the diffusion of cations enhances the polyionic character. As a result, the lignocellulosic materials start to swell, causing higher digestibility. For the subsequent thermal treatment, AAEM species were reported to decrease the onset gasification temperature,

but increase the peak gasification value, due to the interaction between AAEM–cellulose/lignin.[207]

As AAEM plays an essential role in the catalytic effect during lignin pyrolysis, their existence in the bio-products also influences the stability and quality. Therefore, knowing the release and transformation of those inorganics is of great importance for the downstream utilisation of those products. A previous study observed the release of 15−20% of AAEM species at 1000 °C/ s and 800 °C during the pyrolysis of pine.[208] The release of those AAEM species is partly due to the evaporation with the decomposition of lignin, hemicellulose and cellulose of biomass, while the other proportion is related to the char and volatile interactions.[209, 210] In the low-temperature range (180−500 °C), a small amount of the alkali is released with the organic structures,[218] while the release of the major part is connected with the chlorine content at the high-temperatures, during the pyrolysis of wheat straw.[86, 211] It is also observed that K release took place at temperatures above 700 °C, leading to the loss of 25% K at 1050 °C, mainly in the form of KCl, KOH and/or elemental K during the pyrolysis of a fixed bed of wheat straw.[212] The retentions of AAEM species in biomass char are less than 50% during the pyrolysis of mallee in a drop tube furnace.[213] Davidsson et al.[214, 215] studied the alkali (K and Na) release during the pyrolysis of biomass, suggesting the release of AAEM is caused by the surface ionisation techniques. It is found that more than 60% of released AAEM species were connected with liquid products and existing in the form of both water-soluble and water-insoluble tar.[216, 217] The recent studies AAEM-loaded biomass pyrolysis are presented in Table 2-2. In view of the above, the effect of AAEM species during the pyrolysis of biomass and biomass-derived product is vital for further utilisation. And the primary evolution and

release of those organic or inorganic AAEM species should be investigated to understand their migration properties.

Table 2-2 Recent studies on pyrolysis of AAEM loaded biomass samples

Raw material	Conditions	Results	References
Cypress wood sawdust	1g sample/ 10ml AAEM (5-100g/L)	Affects char morphology and pyrolysis product distribution	Haddad et al.[204]
Cellulose	With the addition AAEM oxalates	The Ea of cellulose pyrolysis is decreased	Wang et al.[218]
Glucose	0.35 mmol metal salt per g of glucose	The catalytic effect of AAEMs could be attributed to the interaction of metal within the transition state	Arora et al. [219]
Microcrystalline cellulose	1g sample/ 10ml AAEM salt	Enhances cracking and dehydration reactions	Wang et al.[220]
Southern pine	0.1, 0.5, 1, and 2 wt of metals % of biomass	Changes the thermal decomposition behavior of biomass	Mahadevan et al.[191]

2.6.3 Torrefied biomass samples

Torrefaction of biomass is considered a promising method to boost the energy efficiency of biomass pyrolysis and improve bio-oil quality. It has been widely approved that torrefaction of biomass results in the elimination of moisture and reduction of oxygen content, thus increasing the higher heating value and improving the grindability of the biomass.[221] It can also reduce the power consumption required for size reduction[222], making the treated materials more attractive for transportation and more efficient for following gasification[223]. Some researches proved that the pyrolysis of torrefied biomass generates a bio-oil with lower acid content and higher quality.[34, 224, 225] A review paper[226] demonstrated the torrefaction process, products distribution, the physical properties and chemical composition of the solid torrefied products. The recent studies of biomass torrefaction are listed in Table 2-3 Recent studies on the pyrolysis of torrefied biomass samples

Torrefaction is the thermal treatment of feedstock under various atmospheric conditions in the temperature range of 200 to 300 °C.[80] Briefly, biomass starts to lose water at temperatures of 50 to 100 °C. While at 120 to 200 °C, the lignin begins to soften and become a molten phase, and the thermal degradation commences to produce products including water, carbon dioxide, formic acid, and acetic acid. Further increasing of the temperature to 200–320 °C leads to carbonisation and devolatilisation of the biomass, particularly hemicellulose.[226] The breakage of inter- and intra-molecular hydrogen, C–C and C–O bonds during this temperature range will generate acids, alcohols, aldehydes, and light gases. The moisture loss of torrefied biomass is comparative to the continuous dehydration reactions during the torrefaction process. In addition, the generated non-polar unsaturated structures provide the torrefied biomass with hydrophobicity.[227]

Thermal pre-treatment also impacts the following pyrolysis process. For instance, high pre-treatment temperatures resulted in increased char production and decreased oxygen content in the pyrolysed liquid products.[228] A research has been conducted to understand the torrefaction effects on fast pyrolysis with torrefaction temperatures of 240 to 320 °C and a pyrolysis temperature of 520 °C.[229] The results showed that the yield of water and acetic acid in volatiles decreased with increasing torrefaction temperature, while the total liquid yield was significantly suppressed. Kasparbauer[230] found the product yields and properties were less affected by the different particle size and moisture content from torrefaction, but were majorly influenced by the pyrolysis temperature.

Some researchers also employ CO_2, flue gas or oxidising environment for biomass torrefaction to improve the economic feasibility, with the detailed information presented in Table 2-3. Adopting CO_2 as the torrefaction medium resulted in the increased weight loss, as well as improved grindability of the biomass due to the formation of pores and increased surface area.[231, 232] The proximate and heating value analysis also showed that the heating value of the torrefied samples increases with escalated temperatures. CO_2 wet torrefaction was also investigated and confirmed to present a faster torrefaction process and produced less solid product, compared with wet torrefaction in N_2. It is also reported that CO_2 enhances the capacity of wet torrefaction to remove ash compounds, promote reactivity during torrefaction, thus producing hydrochar with improved physical properties.[233-237] Torrefaction with fuel gas, [238-240] and the difference of inert and non-inert gas [231, 235] air conditions[241-244] were also investigated. Torrefaction of various biomass in those non-inert atmospheres resulted in increased energy density and carbon content with the hollow porous

structure. Those improved properties prove that the utilisation of non-inert atmospheres is a feasible way for biomass torrefaction.

Table 2-3 Recent studies on the pyrolysis of torrefied biomass samples

Raw material	Torrefied conditions	Pyrolysis conditions	Results	References
Woody biomass	Nitrogen; 200, 225, 250 and 275 °C	Thermobalance; 800 °C	Increases char yield and decrease tar yield	Wannapeera et al.[245]
Cotton stalk and corn stalk	Nitrogen; 200, 230, 260 or 290 °C	Fixed bed reactor; 550–650 °C	Improves the grindability; liquid oil is upgraded	Chen et al.[246]
Poplar	Nitrogen; 200, 225, 250, 275, and 300 °C	TA-Q500; 800 °C	Increases the high heating value and the mass energy density	Ru et al.[247]
Pine, ash wood, miscanthus, wheat straw	Nitrogen; 280 °C	Fixed-bed reactor; 500 °C	Affects the yield and composition of tar	Konsomboon et al.[248]
Pine chips	Nitrogen; 240, 260, 280, 300, or 320 °C	Bubbling fluidised bed; 520 °C	Decreases the yield of total liquid because of the cross-linking and carbonisation	Zheng et al.[229]

Table 2-4 Recent studies on torrefaction of biomass samples under non-inert atmospheres

Raw material	Atmosphere	Torrefaction conditions	Results
Woody biomass	Carbon dioxide	240 °C	Increases weight loss and improves grindability[231]
		200−300 °C	Increases internal surface area[232]
Bamboo, pine and poplar		220–340°C	Decomposes carbohydrates,[236] increases hydrophobicity[237]
Oil palm kernel shell		250 °C	Increases gas yield and decrease energy yield[235, 249]
Empty fruit bunches	Combustion gas	200–300 °C	Decreases yield of solid, with hollow porous structure[239, 240]
Patula pine	Air	180–240 °C	Increases the specific surface area and reactivity[241]
Oil palm empty fruit bunches	Oxygen	220–350 °C	Decreases mass yield and energy yield [242-244, 250]

2.6 Pyrolysis reactors

A wide range of techniques and reactors have been employed to investigate the pyrolysis mechanism, kinetics and product distribution of biomass and the model components.[3] The employment of various kinds of reactors greatly influences the reaction pathways and the ultimate product distribution of biomass pyrolysis. Briefly, fixed bed reactors involve the slow pyrolysis process, with the heating rate ranging from 1 °C /min to 20 °C /min, while the fluidised bed reactor represents fast pyrolysis with a heating rate more than 1000 °C/s. TG[54] and Py-GC-MS analysis were also widely employed for the investigation of pyrolysis kinetics and pyrolysis product distribution. However, many of those reactors cannot avoid the secondary reactions. Therefore, some flash pyrolysis reactors, such as ablative reactor and wire mesh reactor, are designed with minimised secondary reactions and able to provide fast heating over 100 °C/s. As presented in previous sections, the pyrolysis of biomass materials involves reactions in different phases, and the understanding of primary reaction in the liquid intermediate phase is critical for the biomass pyrolysis fundamental reaction mechanism and the subsequent utilisation. Therefore, it is vital to understand the advantages and disadvantages of various reactors. The features of various reactors are summarised in Characteristics of biomass pyrolysis reactors.

Table 2-5 Characteristics of biomass pyrolysis reactors

Reactor type	Samples	Temperature	Heating rate	Oil yield	Advantages	Disadvantages
Fixed bed	Safflower seed[251]	500°C	5, 40 or 80 °C/ min	44%	Large scale	Slow heating; Secondary reactions
	Cotton stalk[252]	400°C to 700 °C	7 °C/min	23%		
Fluidised bed	Waste wood[253]	400°C to 550 °C	1000–10000 °C/s	67.8%	Efficient heat transfer; Large scale	Secondary reactions
	Switchgrass[254]	480 °C		60%		
Ablative	Pine wood[255]	450°C to 600 °C	>1000°C/s	67.7%	Fast or flash heating	Small scale
Vacuum	Sugarcane bagasse[256]	500 °C	12 °C/ min	62%	Avoided side reactions	Small scale
Wire mesh reactor	Cellulose[16]	300°C to 600 °C	100°C/s	80%	Primary reactions	Small scale
	Pine wood[257]	500 °C	7000 °C/s	84%		

2.7 Conclusions and research gaps

Basing on previous literature review, the conclusions and research gaps are concluded as follows:

1) The properties of liquid intermediates during biomass pyrolysis are unclear; the proportions of ejection and evaporation need further exploration;
2) The properties and characterisation of primary products during biomass-derived products pyrolysis need to be investigated.

2.8 Research objectives

As mentioned in the previous section, the research gaps need to be fulfilled. Due to the limited time frame in this PhD study, several research objectives were achieved which are listed as:

1) to propose a quantification method for the proportions of ejection and evaporation during biomass pyrolysis.
2) to investigate the formation of reaction intermediates and primary volatiles during acid-catalysed fast pyrolysis of cellulose;
3) to study the release and transformation of organic and inorganic sodium during the fast pyrolysis of sodium impregnated lignin;
4) to understand the effect of carbon dioxide assisted torrefaction and the subsequent fast pyrolysis of lignin.

CHAPTER 3 Research Methodologies and Analytical Techniques

3.1 Introduction

This chapter introduces the research methodologies and techniques to achieve the current research objectives. The detailed experimental configurations and analytical methods are described below.

3.2 Methodology

Two main model compounds of biomass (cellulose and lignin) were employed in this study with various pre-treatment methods. Several sets of experiments were conducted to achieve the research objectives, including:

- Pyrolysis of cellulose in a wire mesh reactor to collect and characterise the ejected aerosols and evaporated vapours at various heating rates;
- Pyrolysis of acid-impregnated cellulose and raw cellulose;
- Pyrolysis of inorganic and organic sodium loaded lignin at elevated temperatures;
- Carbon dioxide assisted torrefaction at various concentrations and temperatures and the subsequent pyrolysis.

The overall research methodology map is illustrated in Figure 3.1. All experiments and analysis were at least duplicated. Also, the employed reactors with different configurations are detailed in section 3.2.1-3.2-5.

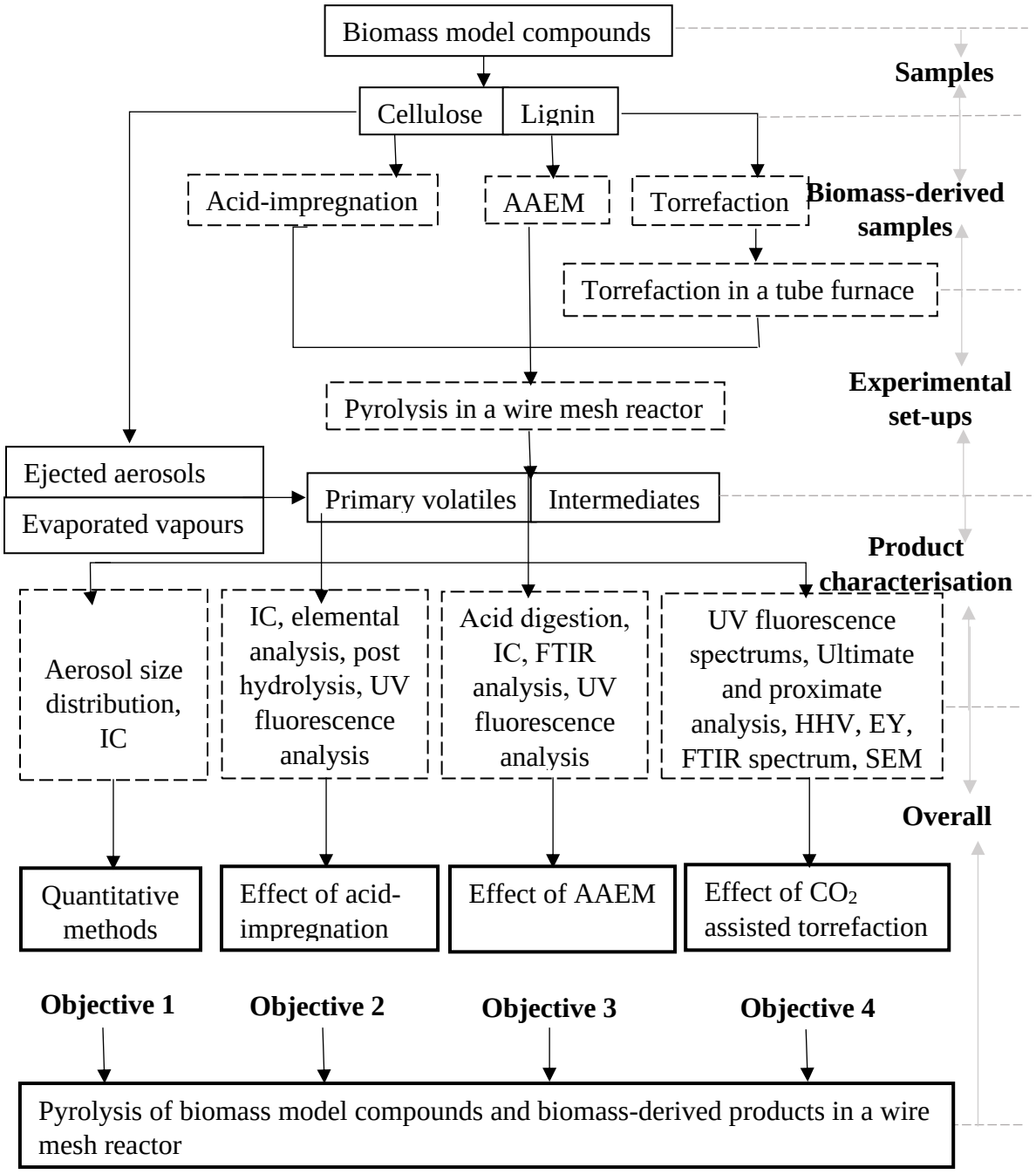

Figure 3.1 Research methodology and the linkages to the research objectives in this PhD study

3.2.1 A method for quantifying ejected aerosols and evaporated vapours during cellulose pyrolysis

Raw cellulose samples (Avicel PH-101) with a particle size of 150– 200 μm, were pyrolysed in a wire mesh reactor at various heating rates from 1°C/s to 1000°C/s. The generated bio-oil contains both ejected aerosols and evaporated vapours with different properties, which influence the downstream storage and utilisation. Therefore, in this objective, the ejected aerosols, evaporated vapours, and the total volatiles were separately collected using various reactor set-ups. The detailed description of the reactor configurations and experimental set-ups are presented in Section 3.3.2. The generated liquids were characterised using an IC-3000 compacted with HPAEC–PAD for their yields using commercially available standards. A quantitative method to calculate the ejection and evaporation yields in the total volatiles during the pyrolysis of cellulose was proposed. The results and discussion are laid out in Chapter 4.

3.2.2 Effect of acid-impregnation during cellulose pyrolysis

Acid-impregnated cellulose (see section 3.3.1) and raw cellulose were pyrolysed in a wire mesh reactor to investigate the effect of acid-loading at evaluated temperatures. The volatiles and intermediates (section 3.3.3) were collected, and the water-soluble parts were subjected to a total carbon analyser and post-hydrolysis. The conversions based on weight, sugar and carbon were calculated (section 3.4.2). Furthermore, the characterisation and comparison of the generated products from acid-loaded samples and raw samples were made (see section 3.4.1 for details). The generated volatiles were also subjected to a UV fluorescence spectroscopy analysis (section 3.4.4).

Eventually, a reaction mechanism of acid-impregnated cellulose pyrolysis was proposed, with detailed information presented in Chapter 5.

3.2.3 Effect of AAEM and the release and transformation during lignin pyrolysis

The alkali lignin was washed with acid and dried before loading with sodium sulfate and sodium acetate (section 3.3.1). The pyrolysis experiments were performed in a wire mesh reactor at various temperatures and a heating rate of 100 °C/s. The residues were subjected to an FTIR analyser, and generated volatiles were dissolved in a solvent and subjected to a UV-florescence analysis (section 3.4.4). The products were processed using acid digestion for the determination of total sodium. Another set of products with identical experimental conditions was dissolved with ultra-pure water to obtain the yield of water-soluble sodium. The liquid samples were subjected to a cation IC to measure sodium distribution during lignin pyrolysis. Based on the above result, the evolution and release of sodium within lignin pyrolysis were proposed. The detailed results and conclusions were summarised in Chapter 6.

3.2.4 Effect of carbon dioxide assisted torrefaction and the subsequent pyrolysis of lignin

The organosolv lignin was torrefied under various temperatures and different concentrations of carbon dioxide in a tube furnace. Before and after torrefaction, the physical and chemical properties of lignin were characterised for the ultimate and proximate analysis (section 3.4.6). Various characterisation techniques, such as HHV, EY, UV Fluorescence spectrum, FTIR spectra, and SEM, were conducted in this

research (see section 3.4 for details). The torrefied lignin samples were further pyrolysed in a wire mesh reactor. The yields and UV spectrum of generated volatile and intermediates from the pyrolysis of torrefied lignin under various experimental conditions were also obtained with detailed information presented in Section 3.3.

3.3 Experimental

3.3.1 Raw chemicals and sample preparation

Objective 1. Raw cellulose (Avicel PH-101) was purchased from Sigma-Aldrich and seveied to a particle size at 106-150μm and used in Chapter 4. The filter (Teflo 2um) was from Pall Corporation and the glass slide (microscope slide) was from Rowe Scientific.

Objective 2. The Avicel PH-101 cellulose at a particle size of 75-106μm was used. Sulphuric acid with a concentration of 0.5 mmol/g cellulose was used to prepare the acid acid-impregnated cellulose, according to our previous method[25]. Then the treated samples were dried using a freeze dryer (Alpha 2-4 L Dplus, Martin Christ) to remove the remaining moisture, and the dry samples were stored in a freezer at –20 ˚C.

Objective 3. Alkali lignin samples were sieved to yield a particle size of 90-150 μm and washed with a diluted acid solution multiple times to prepare the acid-washed AAEM free lignin. The mixture was then washed with ultra-pure water to remove excess acid and dried in an oven at 105 °C overnight. The sodium sulphate and sodium acetate were dissolved in ultra-pure water with a concentration of 0.15 mmol Na/g lignin and added to the dry acid-washed lignin. Sodium acetate is able to organically bond with the carboxylic and phenolic groups in lignin structure, therefore can be employed as the organic sodium source. And it was further washed with ultra-pure

water to remove excess sodium to ensure completely organic sodium bonded lignin samples. The pre-treated samples with sodium sulphate and sodium acetate were referred to as In-Na-lignin and Or-Na-lignin, separately. Then the residues were dried and stored for further pyrolysis experiments.

Objective 4. Organosolv lignin was placed in an oven at 40 ºC until no weight loss. The dried organosolv lignin was stored in the desiccator for further use in Chapter 7.

Solvents. Chloroform and methanol solution (80:20 in volume) was used to collect the volatile generated in the wire mesh reactor, and a THF solution was employed to collect the torrefied lignin gaseous products.

Analytical chemical standards. A series of anhydro-sugar and sugar compound standards with the degree of depolymerisation up to 5 were purchased from Sigma-Aldrich and Synthose, with the abbreviations are given below: levoglucosan, cellobiosan, cellotriosan, cellotetraosan and cellopentaosan (AC1 to AC5 respectively), glucose, cellobiose, cellotriose, cellotetrase and cellopentaose (C1 to C5 respectively). 5-hydroxymethylfurfural (5-HMF), levoglucosenone (LGO), were also employed for identification and quantification. The standards of 1,6-anhydro-β-D-glucofuranose (AGF) and 1,4:3,6-Dianhydro-α-d-glucopyranose (DHGP) were purchased from Synthose.

3.3.2 Reactor configurations

The pyrolysis experiments were conducted in a wire mesh reactor with various set-ups, and the torrefaction experiments were carried out in a tube furnace. The wire mesh reactor was used for the pyrolysis of cellulose and lignin samples, while the tube

furnace was employed for the torrefaction of lignin samples under various experimental conditions.

Wire mesh reactor configurations

Wire mesh reactor is designed to minimise the secondary reactions in order to obtain the primary volatiles from the pyrolysis experiments under various heating rates. The first wire mesh reactor was invented by Loison and Chauvin[258], then extensively modified by Howard and Anthony[17, 18]. Afterwards, Hamilton[259] improved the electrical design with a PID temperature control feedback system for precise temperature control, which is integrated by Kandiyoti[19, 20]. Other organisations also contributed to the development of wire mesh reactor, such as Niksa[260], Stangeby[261], Sathe[208, 262, 263], and Zhou[264, 265].

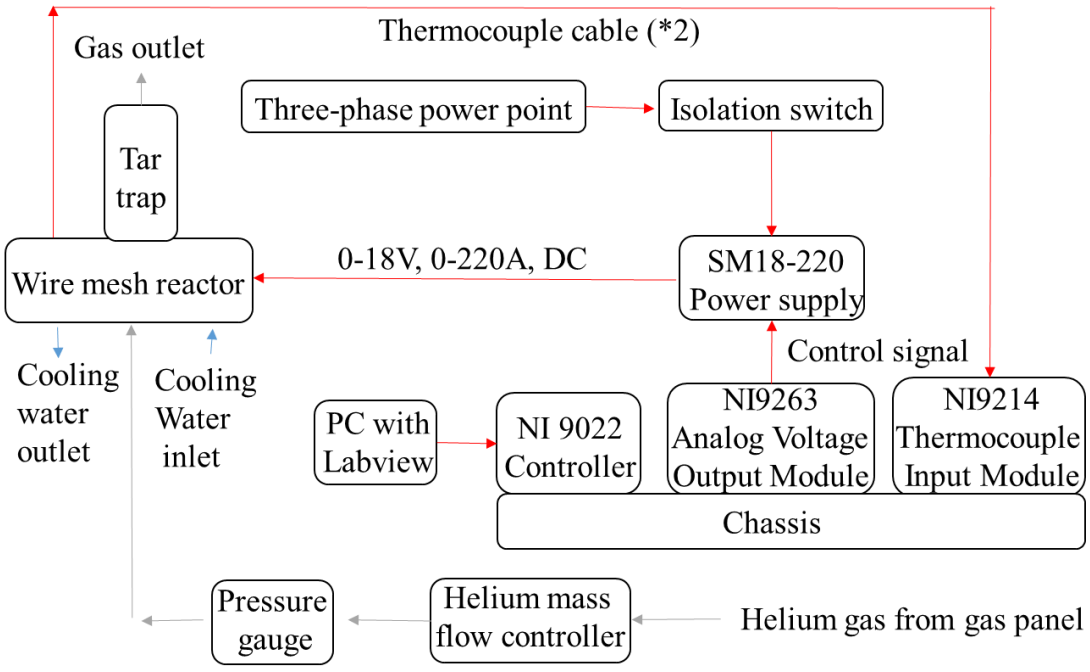

Figure 3.2 Schematic diagram of wire mesh reactor

In this PhD study, the wire mesh reactor is adopted from Huazhong University of Science and Technology with the mechanical design and modified the electrical configuration. The schematic diagram of the wire mesh reactor is presented in Figure 3.2 Schematic diagram of wire mesh reactor. The temperature control system includes the Labview based temperature measurement in PC and a Compact RIO integrated heating control system. The temperature of the samples on wire mesh is collected by two pairs of thermocouples, then fed to the PID controller. The actual temperature will be compared with the programmed temperature with a specific heating rate and peak temperature. Then the PID controller will produce an analog voltage signal accordingly and send it to the connected power supply to adjust the output voltage. The precise temperature control can be achieved by altering the PID parameter and maintaining the heating cycle period within 20 ms.

The main mechanical drawing of the wire mesh reactor is presented in Figure 3.3. The main structure contains the base, which also connects to the negative electrode. The wire mesh is clamped between the positive and negative electrodes with the mica insulation to separate the mesh and the water-cooled plate holder. A liquid nitrogen cooled tar trap is tightly mounted above the sampling area of the wire mesh with a glass chamber. The glass chamber is fixed to the base of the wire mesh reactor to provide a separate environment from the atmosphere. During the experiments, a pulsed voltage will be applied to the electrodes to heat the sandwiched samples in the layered wire mesh. Two pairs of thermocouples will be connected to the thermocouple connection wire located at the base to provide temperature feedback. After the complement of the experiments, the generated volatiles was swiped by a stream of helium gas upwards.

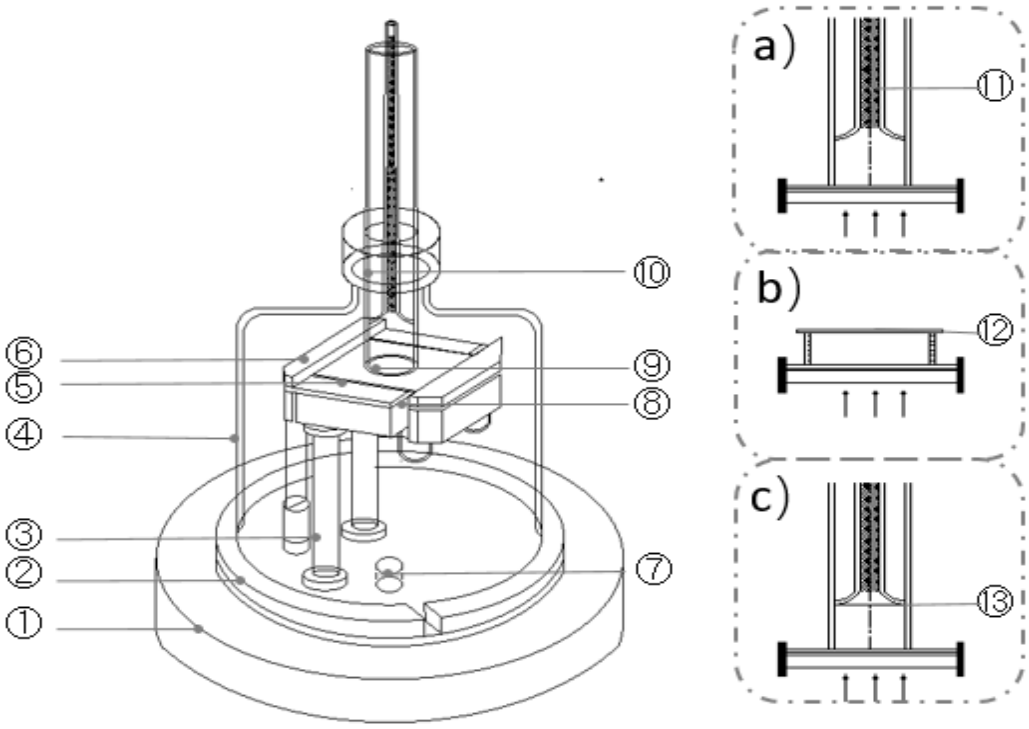

Figure 3.3 Experimental set up of wire mesh reactor: a) collection of total tar, b) collection of ejected aerosols, and c) collection of evaporated vapours

1) Reactor base 2) Hoop 3) Cooling water inlet/outlet 4) Glass chamber 5) Wire mesh 6) Positive electrode 7) Helium gas inlet 8) Negative electrode 9) Sample holding area 10) Tar trap 11) Teflon shredding 12) Glass slide 13) Filter

The configurations of wire mesh reactor employed in this study for separate collection of volatile products were diagrammed in Figure 3.3. As shown, the configuration of wire mesh varies for three types of volatile collection: a) collection of total tar, b) collection of ejected aerosols and c) collection of evaporated vapours. The collection of total tar utilised a liquid nitrogen cooled tar trap, while the collection of evaporated vapours employed a filter at the bottom of the tar trap to block the ejected aerosols. Although the combination methods of total tar and aerosol collection could lead to the calculation of evaporated vapours, only a small amount of evaporated vapours can be

collected in a tar trap due to the loss of vapours inside of the glass chamber. To obtain the majority of vapours, the filter was placed at the bottom of the tar trap where all volatile stream goes through. A glass slide was placed over the mesh to collect the ejected aerosols. The height of the glass slide is adjusted to maintain the temperature at ~ 200 °C to minimise the secondary reactions and the condensation of vapours. With such configurations, the separate collection of those primarily released volatiles can be achieved. However, it should be pointed out that although the total liquid can be collected in the tar trap, those configurations are not capable of recovering the ejected aerosols and evaporated vapours. For the ejected aerosols, they not only can be adhered to the glass slide, but also can be carried away with the helium gas stream sideways, causing the loss in the experiments. Meanwhile, some evaporated vapours can also be captured on the surface of the filter, resulting in the incomplete collection of vapours. Despite the shortage of those set-ups, the separate collection of various volatiles is achieved, and the composition of those collected products is identical to their original formation.

Tube furnace configurations

The schematic system of the tube furnace is shown in Figure 3.4. The lignin samples were torrefied in the quartz reactor in a tube furnace. The nitrogen and carbon dioxide gas streams were applied, and the temperature was calibrated with a thermocouple. The condensable generated gaseous products were collected in the bubbler bottle.

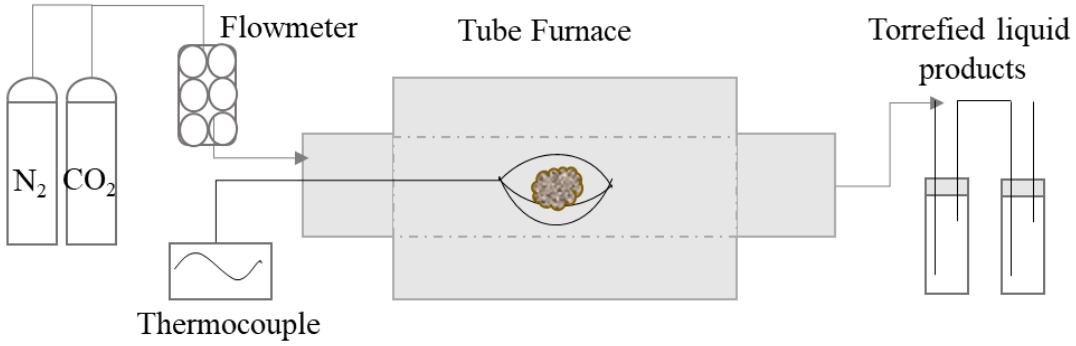

Figure 3.4 Experimental set up of tube furnace for torrefaction of lignin samples

3.3.3 Pyrolysis experiments

Pyrolysis experiments in a wire mesh reactor were conducted in various conditions according to different objectives. In objectives 1, a series of pyrolysis experiments in a wire mesh reactor was conducted at 600 °C with four different heating rates: 1, 10, 100 and 1000 °C/s and a holding time of 10s. During the pyrolysis experiments, a helium gas stream from the gas distributor with a flow rate of 2L /min was employed. In objectives 2, ~ 15 mg samples were sandwiched between the wire mesh. Then the mesh was heated up at a heating rate of 20 °C/s and temperature 40 – 320 °C using helium gas at 4L/min. Meanwhile, a temperature range of 300- 800 °C with a heating rate of 100 °C/s and a holding time 10s was employed in objective 3. Moreover, objective 4 adopted a temperature of 500 ºC at a heating rate of 100 °C/s.

3.3.4 Torrefaction experiments

Around 2 g dried organosolv lignin was loaded in the porcelain boat, thereby placed in the tube furnace. Nitrogen or carbon dioxide concentrations of 5% and 15% co-feed stream with a total flow rate of 500 ml/min was employed. The lignin samples were

heated with a heating rate of 10 °C /min to the desired temperatures of 200, 250 and 300 ºC, respectively. After holding at the peak temperature for 30 min, the furnace was turned off while the gas flow was maintained until the temperature of the samples is under 40 ºC. The torrefied samples were stored in a desiccator for further analysis and experiments.

3.4 Instruments and Analytical Techniques

3.4.1 Quantification of sugars

The quantification of the total sugar content of treated cellulose samples was obtained according to the NREL post-hydrolysis method[266]. And the filtered water-soluble cellulose samples were subjected to an HPAEC–PAD system in Dionex ICS-3000 and ICS-5000-MS for the identification and determination of sugar and anhydro-sugars compounds. The detailed methodology for quantitation of those compounds in this study followed a previous research[267]. In order to adequately separate the various components of cellulose pyrolysis, a CarbonPac PA20 analytical column was employed. Two different programs were used using 25% or 100% 100 mM NaOH as eluent with a flow rate of 0.5 mL/min. LGO, AGF and DHGP were analysed with ICS-5000 coupling with MS.

3.4.2 Conversion, yield and selectivity

The weight before and after pyrolysis experiments was calculated for the weight conversion. The carbon content in the solution after post-hydrolysis was determined by a TOC. The sugar content was obtained according to section 3.4.1. After

quantification of the weight, carbon and sugar content, their conversions are calculated by the following equations:

$$\mathbf{C}(\boldsymbol{weight}) = \frac{\mathbf{W(cellulose)} - \mathbf{W(char)}}{\mathbf{W(cellulose)}} \quad (3\text{-}1)$$

$$\mathbf{C}(\boldsymbol{carbon}) = \frac{\mathbf{W(cellulose)} * \mathbf{c(cellulose)} - \mathbf{W(char)} * \mathbf{c(char)}}{\mathbf{W(cellulose)} * \mathbf{c(cellulose)}} \quad (3\text{-}2)$$

$$\mathbf{C}(\boldsymbol{sugar}) = \frac{\mathbf{W(cellulose)} * \mathbf{s(cellulose)} - \mathbf{W(char)} * \mathbf{s(char)}}{\mathbf{W(cellulose)} * \mathbf{s(cellulose)}} \quad (3\text{-}3)$$

where W, c and s refer to the weight (daf), carbon and sugar contents of samples, respectively.

The sugar content (s) of the samples is calculated by the following equation:

$$\mathbf{s}(\boldsymbol{sample}) = \frac{\mathbf{W(sugar)}}{\mathbf{W(sample)}} \quad (3\text{-}4)$$

3.4.3 Quantification of inorganic species

Lignin samples loaded with sodium were acid digested following a previous method[268], and the remaining was dissolved in diluted methanesulfonic acid solution. Another set of samples was also dissolved in water to obtain the water-soluble sodium. The solution was filtered via a 0.45 um polyvinylidene difluoride (PVDF) syringe filter for further analysis. Subsequently, the solutions were subjected to an ion chromatography (IC, model DIONEX ICS-3000) following a previous method[269] to determine sodium content.

3.4.4 UV fluorescence spectra and FTIR spectra

Both liquid and solid samples were dissolved in the solvent and subjected to a fluorescence spectrometer (Perkin-Elmer LS 55 at a constant energy difference of 2800 cm^{-1}), with the detailed setting detailed elsewheres[270]. And the functional groups of solid samples were analysed with a Fourier transform infrared spectra (Perkin Elmer Spectrum 100).

3.4.5 Optical imaging and SEM

The optical images of ejected aerosols of cellulose pyrolysis experiments were acquired using an optical microscope. The obtained photos are processed in ImageJ for particle size distribution with a method described elsewhere[13, 108].

3.4.6 Ultimate and proximate analysis

The ultimate analysis of solid samples was conducted in an elemental analyser (PerkinElmer 2400 series II CHN/O). The proximate analysis was carried out in a thermogravimetric analyser (TGA, Mettler TGA/DSC 1 STAR model).

3.4.7 Higher heating value and energy yield

The higher heating rate (HHV) and energy yield (EY) of torrefied lignin samples were calculated using the following equation, which is used in the previous studies[271]:

$$\mathbf{HHV\ (MJ/kg)} = \mathbf{0.3383C} + \mathbf{1.422}\left(\mathbf{H} - \frac{\boldsymbol{O}}{\mathbf{8}}\right) \quad (3\text{-}5)$$

$$\mathbf{EY}(\%) = \mathbf{Y_{mass}} * \frac{\mathbf{HHV\ product}}{\mathbf{HHV\ feed}} * \mathbf{100} \quad (3\text{-}6)$$

3.5 Summary

Primary volatiles and intermediates can be produced from the pyrolysis of cellulose, acid-impregnated cellulose, sodium loaded lignin and torrefied lignin samples. The volatiles, including ejected aerosols and evaporated vapours, were separately collected and analysed in an IC. Then a quantitative method for the yield determination was proposed. Also, the effects of pre-treatment methods were analysed by utilising various ranges of techniques. In addition, the evolution and release of sodium during lignin pyrolysis were investigated. The effect of torrefaction under different atmospheres was explored by studying the physical and chemical properties of the treated materials. More importantly, the fundamental pyrolysis mechanism of the pyrolysis of biomass model compounds and biomass-derived products were suggested in this research.

CHAPTER 4 Contributions of Thermal Ejection and Evaporation to the Formation of Condensable Volatiles during Cellulose Pyrolysis

4.1 Introduction

Biomass fast pyrolysis, as a promising process for producing renewable bio-oil and biochemicals, has received tremendous attention over the past decades.[1, 272] Despite a high yield (60–70 wt.%) of bio-oil from biomass fast pyrolysis, it suffers from poor quality including high water content, high acidity, high viscosity, and phase instability, which has largely hindered the commercialisation of bio-oil production. [273-275] It is known that the bio-oil quality is largely determined by the composition of condensable volatiles generated during biomass pyrolysis. To develop novel technologies to produce a high-quality bio-oil, it is of critical importance to understand the formation mechanism of volatiles from biomass fast pyrolysis.

The evaporation of volatile compounds in the pyrolysing biomass is key to the formation of volatiles from biomass pyrolysis. However, recent studies have reported the formation of a liquid intermediate phase during biomass pyrolysis. [276] [10, 11, 277] As the volatile products are formed in the liquid intermediate phase, the bubbles need to diffuse through the liquid intermediate phase to the gas/liquid interface before evaporation. Eventually, the bubbles burst at the gas/liquid interface, generating the primary aerosols via thermal ejection, as captured by a high-speed camera.[277] While the primary aerosols originate from the molten liquid intermediates, secondary aerosols can be also formed from the condensation of the primary products such as levoglucosan[276]. As a result, both the ejected aerosols and the evaporated vapours

contribute to the formation of condensable volatiles during biomass pyrolysis, thus affecting the composition and quality of condensable volatiles produced from biomass pyrolysis. Particularly, the ejection mechanism can explain the release of some non-volatile species (i.e., such as cellobiosan[278, 286] and inorganic species[278]) from biomass pyrolysis. It is known that the heating rate is an important factor influencing the ejection and evaporation behaviour of species in the liquid intermediate phase during biomass pyrolysis, thus greatly affecting the pyrolysis kinetics [279, 280] and char yield[281-283].

Over the last several decades, considerable effort has been devoted to understanding the composition and properties of the liquid intermediates and the volatiles produced during the pyrolysis of biomass and its model compounds.[16, 121, 123, 284, 285] Particularly, several important studies have been conducted to understand the release of aerosols from biomass pyrolysis, including the collection and characterisation of aerosol formation by thermal ejection[108, 278] and the modelling of bubble formation dynamics and aerosol formation by thermal ejection. Unfortunately, the role of ejected aerosols and evaporated vapours in the formation of the volatiles during biomass pyrolysis remains unknown, which hinders a thorough understanding of the formation mechanisms of the volatiles during biomass pyrolysis. To this regard, this study has developed a novel method to estimate the contributions of the ejected aerosols and the evaporated vapours to the formation of the volatiles during cellulose pyrolysis at different heating rates. A wire mesh reactor (WMR) has been used to minimise the secondary reactions of primary volatiles in the vapour phase, thus facilitating the collection of primary volatiles from cellulose pyrolysis. The results of this study will greatly enhance the understanding of the important role of thermal ejection during cellulose fast pyrolysis.

4.2 The yields of the ejected aerosols and the evaporated vapours collected from cellulose pyrolysis at different heating rates

The yields of the ejected aerosols and the evaporated vapours collected from cellulose pyrolysis at different heating rates are presented in Figure 4.1 The yields of the ejected aerosols and the evaporated vapours collected from cellulose pyrolysis at 600 ℃ with a particle size at 106-150μm and a holding time of 10s at different heating rates of 1–1000 °C/s, together with the total tar yields. The calculation of the yields of ejection and evaporation is presented in the following equations:

$$\mathbf{Y}\,(\boldsymbol{ejection}) = \frac{\mathbf{W(ejected\ aerosols)}}{\mathbf{W(sample)}} \tag{4-1}$$

$$\mathbf{Y}\,(\,\boldsymbol{evaporation}) = \frac{\mathbf{W(evaporated\ vapours)}}{\mathbf{W(sample)}} \tag{4-2}$$

where Y refers to the yield of collected ejected or evaporated products, while W refers to the weight of samples. Increasing the heating rate from 1 to 100 °C/s leads to an increase in the yield of the ejected aerosols but a slight decrease in the yield of the evaporated vapours. However, further increasing the heating rate from 100 to 1000 °C/s leads to reduction in the yields of both the ejected aerosols and the evaporated vapours. Thus, the maximal yield of the evaporated vapours (~39%) was achieved at 1 °C/s, while the maximal collected yield of the ejected aerosols (~28%) was achieved at 100 ℃/s. The results suggest that a higher heating rate seems to promote the formation of the ejected aerosols but suppress the formation of the evaporated vapours. This phenomenon is reasonable since the formation of the liquid intermediate phase is enhanced at higher heating rates,[16] resulting in more aerosols ejected from the molten liquid.

The total yields of the ejected aerosols and the evaporated vapours collected from cellulose pyrolysis were also calculated and compared with the yields of the total tar yields under all heating rate conditions. The total collected yield of the ejected aerosols and the evaporated vapours is much lower than the total tar yield. For example, the total collected yield of the ejected aerosols and the evaporated vapours is only ~40% at 1 °C/s, much lower than the total tar yield of ~76% at the same heating rate. The total collected yield of the ejected aerosols and the evaporated vapours increases when the heating rate increases from 1 to 100 °C/s but decreases when the heating rate further increases to 1000 °C/s. Thus, the total yield of the ejected aerosols and the evaporated vapours achieves the maximum value of ~63% at 100 °C/s. In contrast, the total tar yield slightly increases with increasing the heating rate from 76 to 86% from 1 to 1000 °C/s. Such data demonstrates that the current method is unable to collect the ejected aerosols and the evaporated vapours. Thus, the above yields cannot represent the actual yields of the ejected aerosols and the evaporated vapours from cellulose pyrolysis.

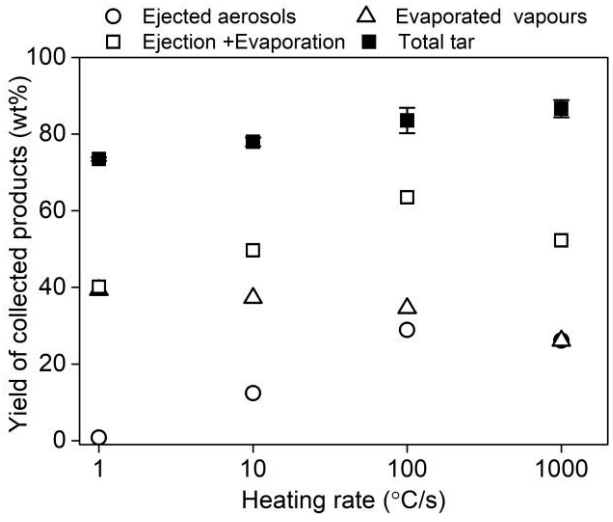

Figure 4.1 The yields of the ejected aerosols and the evaporated vapours collected from cellulose pyrolysis at 600 °C with a particle size at 106-150μm and a holding time of 10s at different heating rates of 1–1000 °C/s

4.3 Characterisation of the ejected aerosols and the evaporated vapours collected from cellulose pyrolysis at different heating rates

4.3.1 Particle size distribution of the ejected aerosols droplets

The ejected aerosol droplets captured by the glass slide were first analysed using a light microscope, and the microscope photos at 10 – 1000 K/s are shown in Figure 4.2. It should be mentioned that the microscope photo of the ejected aerosols at 1 K/s is not presented as the light microscope could not identify any droplets under this condition. The microscopy photos clearly show that the ejected aerosols can be successfully collected as droplets in the glass slide, and the size and number of droplets seem to increase with the heating rate. This indicates that thermal ejection is enhanced at a higher heating rate. The microscope photos were also processed using ImageJ[108, 278] for estimating the particle size distribution of the aerosol droplets, with results also presented in Figure 4.2. Further analysis of the particle size distribution of the aerosol droplets shows that majority of the droplets have a particle size <5 μm at10 °C/s. The percentage of larger droplets increases with an increased heating rate, indicating that the particle size of the ejected aerosols shifts from small to large particle size as the heating rate increases. This could be due to the formation of larger gas bubbles at higher heating rates. Once the surface tension reaches the critical point, the burst of gas bubbles is capable of carrying a considerable amount of liquid aerosol droplets, which is subsequently captured by the glass slide.

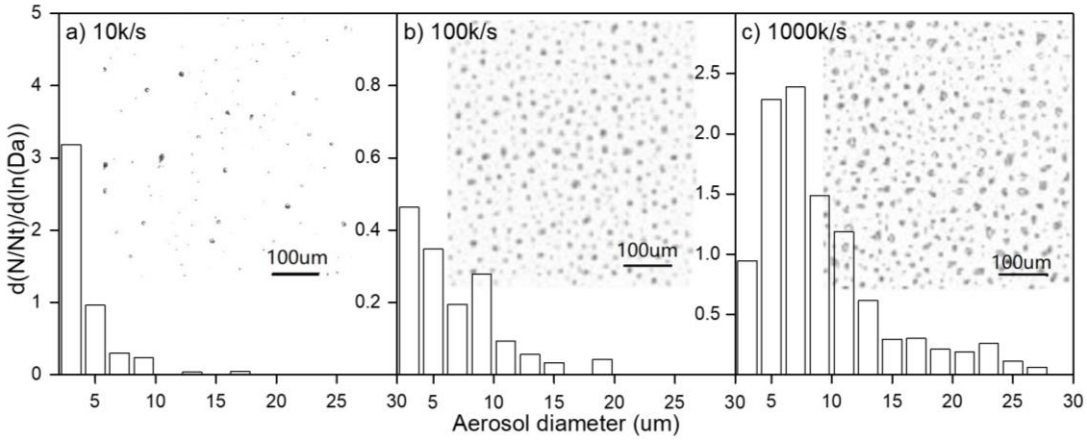

Figure 4.2 Particle size distribution of the ejected aerosols droplets during cellulose pyrolysis at 600 °C with a particle size at 106-150μm and a holding time of 10s at different heating rates

4.3.2 Yields of key compounds in the ejected aerosols and the evaporated vapours

In our previous studies, [16, 25, 284]it has been reported that anhydro-sugars (i.e., AC1-AC5) account for a considerable amount of the primary tar product from cellulose pyrolysis. In order to understand the compositional difference between the ejected aerosols and the evaporated vapours, the water-soluble liquid samples from the ejected aerosols and evaporated vapours were analysed by HPAEC-PAD. Various compounds such as anhydro-sugars and 5-HMF were identified with available standards. The evaporated vapours mainly contains AC1, AC2, and 5-HMF, while anhydro-sugars with the degree of polymerisation (DP) up to 5 can be detected in the ejected aerosols. With increasing the heating rate, the amount of anhydro-sugars with larger DPs increases. It is a common understanding that AC1 easily evaporates because of its low

boiling point (i.e., 385 °C[287]). It can be found that AC2 (with a boiling point of ~581 °C[288-290]) is also present in the evaporated vapours, which is due to the high pyrolysis temperature of 600 °C used in this study. It is worth pointing out that 5-HMF is only detected in the evaporated vapours, due to its low boiling point (114-116 °C).

The yields of key compounds in the ejected aerosols and the evaporated vapours were further calculated and compared to their yields in the total tar, as shown in Figure 4.3. For the key compounds in total tar (see Figure 4.3a), their yields are strongly dependent on the heating rate, however with different trends. For instance, the yield of AC1 increases from ~14% to ~23% when the heating rate increases from 1 to 1000 °C/s. On the contrary, the yield of 5-HMF decreases with increasing the heating rate, i.e., from ~1.2% at 1 °C/s to ~0.8% at 1000 °C/s. For other anhydro-sugars, the yields of AC2-AC5 increase with the heating rate and reach the maximal values at 10 °C/s, but start to decrease as the heating rate further increases to 1000 °C/s. For example, the yields of AC2-AC5 increases from 1.2%, 0.2%, 0.07 and 0.03% at 1 °C/s to the maximal values of 3.5%, 0.9%, 0.12% and 0.07% at 10 °C/s, then reduces to 2.2%, 0.5%, 0.06% and 0.04% at 1000 °C/s, respectively. The results indicate that the heating rate greatly affects the tar composition during cellulose pyrolysis.

As for the ejected aerosols during cellulose pyrolysis, anhydro-sugars with DPs up to 5 can be identified, but their yields decrease with DP under all conditions. Among the quantified anhydro-sugars, the yield of AC1 increases continuously with the heating rate, from ~ 0.01% at 1 °C/s to ~2.34% at 10 °C/s, then to ~6.26% at 1000 °C/s. However, other anhydro-sugars shows different trends as the heating rate increases. The yields of AC2-AC5 increase first with the heating rate from 1 to 100 °C/s, but a further increase in the heating rate leads to a slight decrease in their yields. In contrast, only two anhydro-sugars (AC1 and AC2) are present in the evaporated aerosol together

with 5-HMF, obviously due to their low boiling points which allow those compounds to evaporate easily from the liquid intermediate phase. Both the yields of AC1 and 5-HMF reduce with increasing the heating rate, from 9.8% and 1.10% at 1 °C/s to 7.4% and 0.76% at 1000 °C/s, while the yield of AC2 increases from ~0.66% at 1 °C/s to ~1.47% at 1000 °C/s.

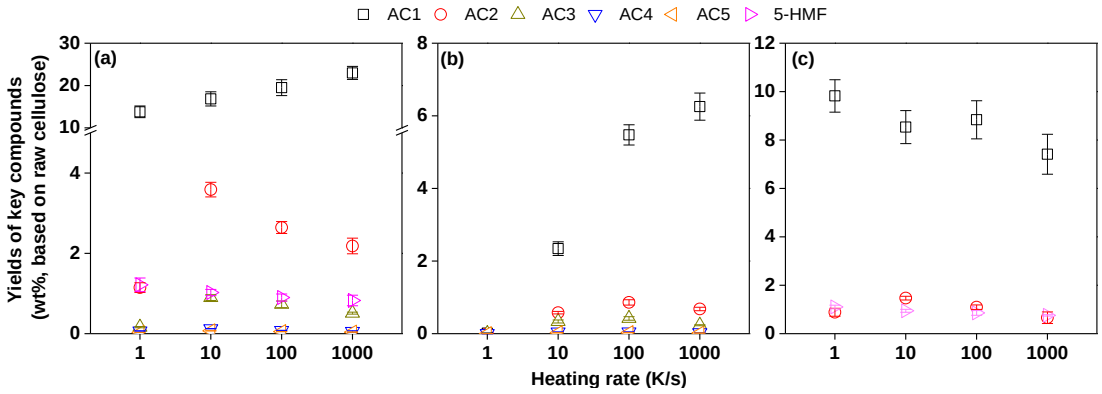

Figure 4.3 The yields of key compounds in the total tar, the ejected aerosols and the evaporated vapours during cellulose pyrolysis at 600 °C with a particle size at 106-150μm and a holding time of 10s at 1–1000 K/s. (a) Total tar; (b) Ejected aerosols; (c) Evaporated vapours.

4.3.3 Collection efficiencies of key compounds in the ejected aerosols and evaporated vapours

As shown in Figure 4.1, the total collected yield of the ejected aerosols and the evaporated vapours collected from cellulose pyrolysis experiments is much lower than the total tar yield, indicating that part of the ejected aerosols and the evaporated vapours are lost during the collection process. Since the total tar from cellulose pyrolysis can be collected, it allows us to estimate the collection efficiency of each

compound in the ejected aerosols and the evaporated vapours by normalising the amount of each compound in the ejected aerosols (or evaporated vapours) to the amount of the same compound in the total tar. The collection efficiencies of key components in the ejected aerosols and the evaporate vapour were further calculated, and the results are shown in Figure 4.4. And the calculations of collection efficiency (CE) are shown in the following equations:

$$\mathbf{y}(\boldsymbol{ACi}) = \frac{\mathbf{w(ACi)}}{\mathbf{w(cellulose\ sample\ for\ ejection\ or\ evaporation)}} (\boldsymbol{i} = \mathbf{3,4,5}) \quad (4\text{-}3)$$

$$\boldsymbol{y_t}(\boldsymbol{ACi}) = \frac{\mathbf{w(ACi)}}{\mathbf{w(cellulose\ sample\ for\ total\ tar)}} (\boldsymbol{i} = \mathbf{3,4,5}) \quad (4\text{-}4)$$

$$\mathbf{CE}\ (\boldsymbol{ejection}) = \frac{\mathbf{y(ACi)}}{\boldsymbol{y_t}\mathbf{(ACi)}} (\boldsymbol{i} = \mathbf{3,4,5}) \quad (4\text{-}5)$$

$$\mathbf{CE}\ (\boldsymbol{evaporation}) = \frac{\mathbf{y(5-HMF)}}{\boldsymbol{y_t}\mathbf{(5-HMF)}} \quad (4\text{-}6)$$

where y and y_t present collection efficiency, the yield of collected ejected or evaporated products, and the yield in total tar, respectively.

As discussed above, both AC1 and AC2 exist in the ejected aerosols and the evaporated vapours, while AC3-AC5 are only present in the ejected aerosols and 5-HMF only exists in the evaporated vapours. Theoretically, the collection efficiencies of AC3-AC5 in the ejected aerosols and the collection efficiency of 5-HMF in the evaporated vapours should be 100% if there are no losses during the collection of the ejected aerosols and the evaporated vapours. However, the collection efficiencies of AC3-AC5 are much lower than 100%, further confirming that a large amount of AC3-AC5 is lost during the aerosol collection process.

It is also interesting to see that AC3-AC5 almost have the same collection efficiency, which indicates that the collection efficiencies of compounds that only exist in the ejected aerosols may be independent on the species of the compound.

It can be seen that the collection efficiencies of AC3-AC5 first increase from ~2.8% at 1 °C/s to the maximal value of ~58.5% at 100°C/s, followed by a decrease to ~45.5% as the heating rate further increases to 1000 °C/s. The low collection efficiencies of AC3-AC5 are probably due to the configuration of the wire mesh reactor for collecting the ejected aerosols. The application of a glass slide tends to influence the direction of the gas stream, resulting in a considerable amount of generated volatiles travelling downwards or sidewards. At a low heating rate, the smaller size of the aerosol may lead to more aerosol droplets carried away by the gas stream, thus greatly reducing the collection efficiency of the ejected aerosols. In contrast, the collection efficiency of 5-HMF is over 90% under all heating rate conditions, indicating that majority of the evaporated vapours can be collected in this study. Also, the heating rate has a negligible effect on the collection efficiency of the evaporated vapours.

However, such observations cannot be applied to AC1 and AC2, which are present in both the ejected aerosols and the evaporated vapours. As shown in Figure 4.4, the collection efficiencies of AC1 and AC2 in the ejected aerosols at 1 K/s are very low (only ~0.1 and 0.4%), but increase to 27 and 31% at 1000 °C/s, respectively. On the contrary, the collection efficiencies of AC1 and AC2 in the evaporated vapours reduce with increasing the heating rate, from 71 and 77% at 1 °C/s to 32 and 30% at 1000 °C/s, respectively. This indicates that AC1 and AC2 are mainly released into volatiles via evaporation, especially at low heating rates. However, at high heating rates, a large amount of AC1 and AC2 are released into volatiles via thermal ejection. Compared to those of AC2, the collection efficiency of AC1 in the evaporated vapours is slightly

higher, while its collection efficiency in the ejected aerosols is marginally lower, mainly due to the lower boiling point of AC1.

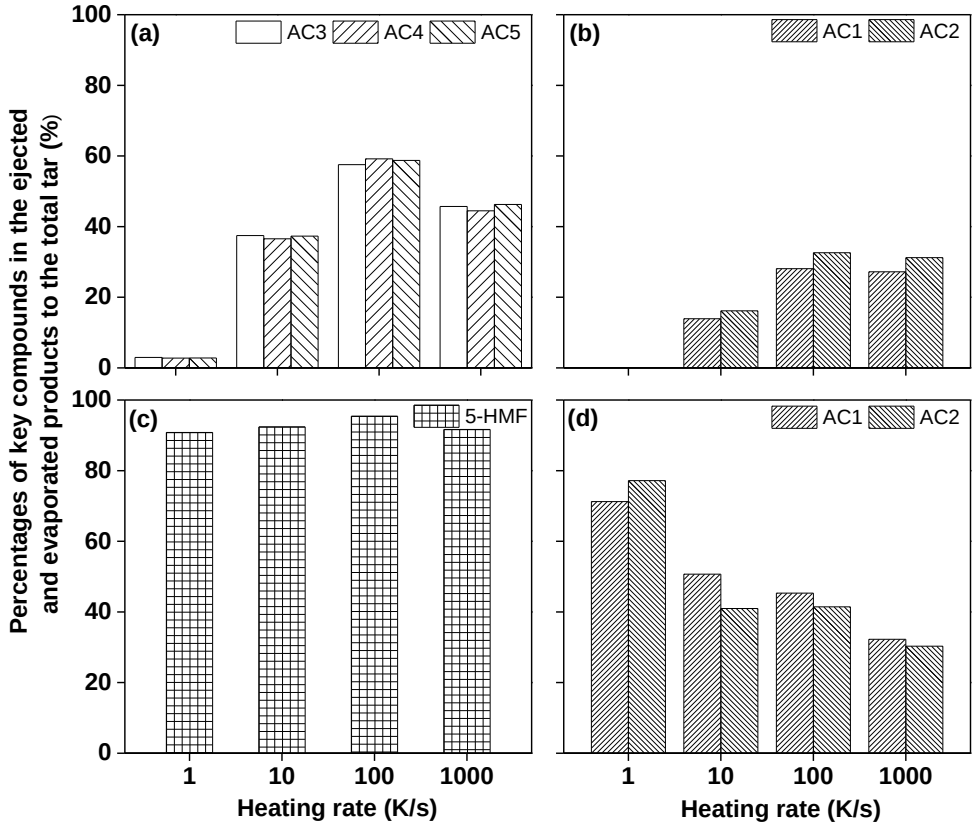

Figure 4.4 The collection efficiencies of the key compounds in the ejected aerosols and the evaporated vapours during cellulose pyrolysis at 600 °C with a particle size at 106-150μm and a holding time of 10s at 1–1000 K/s. (a) AC3-AC5 in the ejected aerosols; (b) AC1-AC2 in the ejected aerosols; (c) 5-HMF in the evaporated vapours; (d) AC1-AC2 in the evaporated vapours.

4.4 Estimation of the true yields of the ejected aerosols and the evaporated vapours from cellulose pyrolysis at different heating rates

The above data have clearly demonstrated that thermal ejection plays an essential role in the formation of volatiles during cellulose pyrolysis, especially at high heating rates. However, the yields of the ejected aerosols and the evaporated vapours collected from cellulose pyrolysis experiments cannot represent their true yields, due to their significant losses (especially for the ejected aerosols) during the collection processes. To estimate the true yields of the ejected aerosols and the evaporated vapours, it is important to know the overall collection efficiencies of the ejected aerosols and the evaporated vapours, which are difficult to obtain from the current experiments. Further analysis of the collection efficiency data leads to an important observation that some key compounds that only exist in the ejected aerosols (i.e., AC3-AC5) or the evaporated vapours (i.e., 5-HMF) have almost the same collection efficiencies (see Figure 4.4). Therefore, it is reasonable to use the collection efficiencies of key compounds that only exist in the ejected aerosols and the evaporated vapours to represent the overall collection efficiencies of the ejected aerosols and the evaporated vapours, respectively.

Further calculations were conducted to estimate the true yields of the ejected aerosols and the evaporated vapours based on their yields from experiments divided by their overall collection efficiencies.

$$\mathrm{P_{ej}} = \frac{\mathrm{Y}_{ej}}{\mathrm{CE_{ej}}} \tag{4-7}$$

$$\mathrm{P_{ev}} = \frac{\mathrm{Y}_{ev}}{\mathrm{CE_{ev}}} \tag{4-8}$$

where P_{ej} and P_{ev} represent the estimated yields of the ejected aerosols and the evaporated vapours, respectively. It should be noted that the overall collection efficiencies of the ejected aerosols (or the evaporated vapours) were determined based on the average collection efficiencies of the key compounds that only exist in the ejected aerosols (or the evaporated vapours).

The estimated yields of the ejected aerosols and the evaporated vapours are shown in Figure 4.5, together with the yields of the ejected aerosols and the evaporated vapours collected from experiments as well as the yield of the total tar. The estimated yield of the ejected aerosols continuously increases with the heating rate, from 29% at 1 °C/s to 57% at 1000 °C/s. Although the estimated yield of the evaporated vapours continuously decreases with the heating rate, from 43% at 1 °C/s to 28% at 1000 °C/s, the estimated total tar yield still increases with the heating rate (from 72% at 1 °C/s to 86% at 1000 °C/s). It is interesting to see that the total tar yields based on the estimated yields of the ejected aerosols and the evaporated vapours match well with the total tar yields measured from experiments under all heating rate conditions. Based on the research findings, it can be stated that the proposed method can be successfully used to predict the true yields of the ejected aerosols and the evaporated vapours during cellulose pyrolysis at various heating rates.

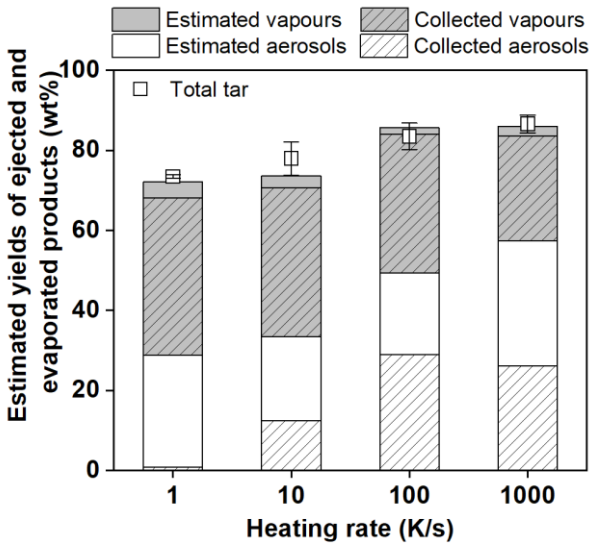

Figure 4.5 The estimated yields of the ejected aerosols and the evaporated vapours during cellulose pyrolysis at 600 °C with a particle size at 106-150μm and a holding time of 10s at 1–1000 K/s. Note: the yields of the ejected aerosols and the evaporated vapours collected from experiments (hatched) are also presented for comparisons.

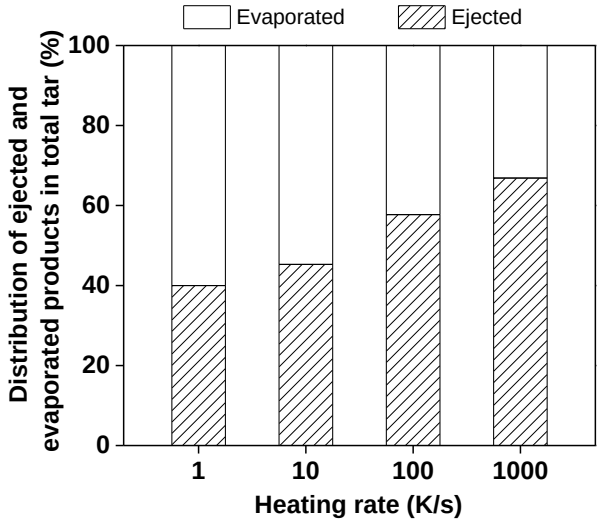

Figure 4.6 Distribution of ejected and evaporated products in the total tar during cellulose pyrolysis at 600 °C with a particle size at 106-150μm and a holding time of 10s at 1–1000 K/s.

The successful estimation of the true yields of the ejected aerosols and the evaporated vapours allows us to obtain an in-depth understanding of the formation mechanism of primary volatiles during cellulose pyrolysis. The contributions of thermal ejection and evaporation to tar formation during cellulose pyrolysis at various heating rates were further calculated based on the estimated yields of the ejected aerosols and the evaporated vapours, and the results are shown in Figure 4.6. Thermal ejection contributes significantly to tar formation during cellulose pyrolysis. The contribution of thermal ejection increases with the heating rate, from ~40% at 1 °C/s to ~67% at 1000 °C/s. The results also demonstrate the importance of thermal ejection during cellulose pyrolysis at different heating rates.

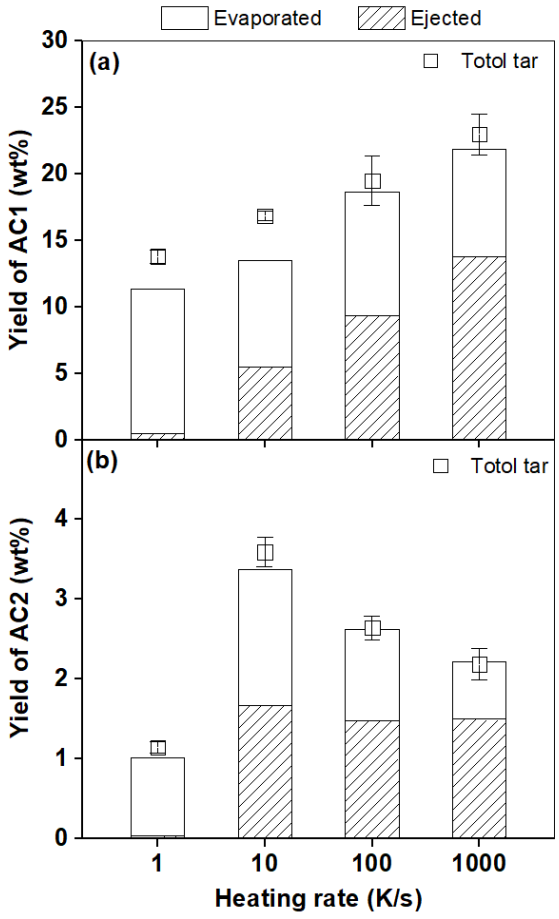

Figure 4.7 The estimated yields of the ejected and evaporated AC1 (panel a) and AC2 (panel b) during cellulose pyrolysis at 600 °C with a particle size at 106-150μm and a holding time of 10s at different heating rates.

To further verify the accuracy of the estimated contributions of thermal ejection and evaporation, the (true) yields of the ejected and evaporated AC1 and AC2 were further estimated based on the collection efficiencies of thermal ejection and evaporation, and compared with the yields of AC1 and AC2 in the total tar in Figure 8. It can be found that the yield of the ejected AC1 increases as the heating rate increases, while the yield of the evaporated AC1 decreases slightly as the heating rate increases. As for AC2, both the yields of the ejected and evaporated AC2 reach maximal values at 10 K/s, then decrease as the heating rate further increases. Overall, the estimated total yields of AC1 and AC2 based on the collection efficiencies of thermal ejection and evaporation match well with the yields of AC1 and AC2 in the total tar under all heating rate conditions. This further proves that the proposed method can be also applied to estimate the true yield of each compound in the ejected aerosols and the evaporated vapours.

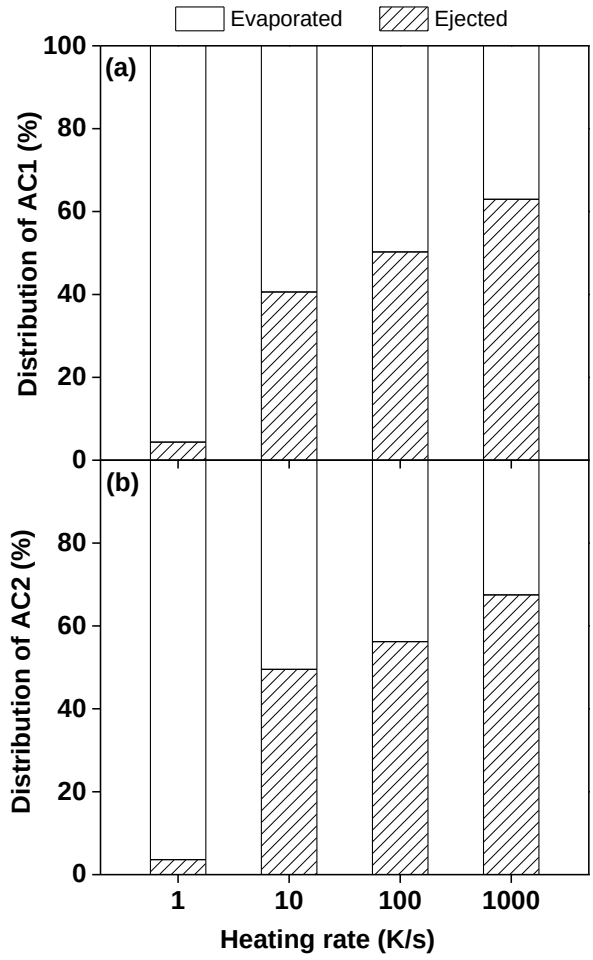

Figure 4.8 Distribution of the ejected and evaporated AC1 (panel a) and AC2 (panel b) in the total tar during cellulose pyrolysis at 600 °C with a particle size at 106-150μm and a holding time of 10s at 1–1000 K/s.

The contributions of thermal ejection and evaporation to the formation of AC1 and AC2 during cellulose pyrolysis at 1–1000 K/s were also estimated and the results are shown in Figure 9. It can be seen that ~95% of AC1 and ~96% of AC2 in the total tar are released due to evaporation during cellulose pyrolysis at 1 K/s. As the heating rate increases, the contribution of evaporation decreases while the contribution of thermal ejection increases. During cellulose pyrolysis at 1000 K/s, ~63% of AC1 and ~68% of AC2 are released due to thermal ejection. This demonstrates that a higher heating rate

can lead to increased releases of some volatile species (i.e., AC1) as aerosols instead of vapours, due to enhanced thermal ejection.

4.5 Further discussion on the formation mechanism of primary volatiles during cellulose fast pyrolysis

The understanding of aerosol formation from biomass pyrolysis via thermal ejection is still in the infancy stage. As the first in the field, this study proposes a novel method to estimate the true yields of the ejected aerosols and the evaporated vapours from cellulose fast pyrolysis. This allows us to understand the important role of thermal ejection in the formation of primary volatiles from cellulose fast pyrolysis. Particularly, several important findings on the formation of the ejected aerosols during cellulose pyrolysis are discussed below.

First, this study has identified some volatile compounds (i.e., 5-HMF) that are only present in the evaporated vapours (i.e., released via evaporation), and some non-volatile compounds (i.e., AC3-AC5) that are only present in the ejected aerosols (i.e., released via thermal ejection). Those key compounds can be considered as the "tracers" to estimate the average collection efficiencies of the ejected aerosol and the evaporated vapours, which are critical to the estimation of the true yields of the ejected aerosols and the evaporated vapours during cellulose pyrolysis. However, it should be noted that the collection efficiency of the ejected aerosols can be greatly affected by the pyrolysis conditions, especially the heating rate. At a lower heating rate, the smaller size of the aerosol droplet may lead to more aerosols carried away by the gas stream, thus greatly reducing the collection efficiency of the ejected aerosols. In contrast, the effect of the heating rate on the collection efficiency of the evaporated vapours is

negligible. To estimate the true yields of the ejected aerosols and the evaporated vapours under different experimental conditions (i.e., temperature, heating rate, feedstock, reactor system), the collection efficiencies of both the ejected aerosols and the evaporated vapours should be determined before the true yields can be estimated.

Second, the current results clearly demonstrate the important role of thermal ejection in the formation of primary volatiles during cellulose pyrolysis, under the current pyrolysis conditions. Previous modelling studies[126, 291286] reported the highest aerosol yield of 25% for a 1 mm particle at a high heating rate (similar to that in a fluidised bed reactor). In this study, the estimated true yield of the ejected aerosols continuously increases with the heating rate, from 29% at 1 K/s to 57% at 1000 K/s, accompanied by the continuous decrease in the yield of the evaporated vapours from 43% at 1 K/s to 28% at 1000 K/s. Such a difference in the yield of the ejected aerosols indicates that the formation of the ejected aerosols can be greatly affected by the particle properties and the pyrolysis conditions. Overall, the total tar yield of cellulose pyrolysis still increases with the heating rate, from 72% at 1 K/s to 86% at 1000 K/s. This leads to the contribution of thermal ejection increasing from 40% at 1 K/s to 67% at 1000 K/s. The results confirm that the volatile formation mechanism is largely affected by the heating rate, with more volatiles released via the thermal ejection mechanism at higher heating rates. This can explain why a higher bio-oil yield can be obtained at a higher heating rate during cellulose/biomass pyrolysis. More importantly, the results further indicate that biomass pyrolysis knowledge (i.e., kinetics, mechanism, etc) obtained at slow pyrolysis conditions (i.e., in a thermogravimetric analyser) cannot be directly applied to fast pyrolysis conditions (i.e., in a fluidised bed reactor), due to different volatile formation mechanisms at different heating rates. Also, thermal ejection

mechanism must be considered in the modelling of biomass pyrolysis process, particularly for fast pyrolysis conditions.

Third, the composition of primary volatiles from cellulose pyrolysis can also be affected by the enhanced formation of the ejected aerosols at higher heating rates. Although a higher heating rate leads to the formation of more AC1, but not for other anhydro-sugars (i.e., AC2-AC5). In fact, the yields of AC2-AC5 reach the maximal values at 10 K/s, and a higher heating rate results in reductions in their yields. In contrast, the yield of 5-HMF decreases with increasing the heating rate. The results indicate that a higher heating rate enhances the yield of the ejected AC1, thus suppressing the decomposition of AC1 in the liquid intermediate phase to form lower-molecular-weight species such as 5-HMF. However, the formation mechanisms of AC2-AC5 are still unclear. Since the secondary reactions of primary volatiles are minimised in the WMR, it is more likely that the reactions of AC1 in the liquid intermediate phase largely determine the formation of the anhydro-sugars with higher DPs. Further research is required to understand the chemistry in the liquid intermediate phase.

4.6 Conclusions

This study reports a novel method to determine the true yields of the ejected aerosols and the evaporated vapours from cellulose fast pyrolysis using a wire mesh reactor. Separate experiments have been developed to collect the ejected aerosols and the evaporated vapours from the primary volatiles produced during cellulose fast pyrolysis at 600 °C and various heating rates of 1 – 1000 K/s. Using some key compounds in the ejected aerosols and the evaporated vapours as the “tracers”, the average collection efficiencies of the ejected aerosol and the evaporated vapours have been estimated to

determine the true yields of the ejected aerosols and the evaporated vapours. Based on this novel method, this study has successfully estimated the true yield of the ejected aerosols from cellulose pyrolysis, which continuously increases with the heating rate from 29% at 1 K/s to 57% at 1000 K/s. In contrast, the yield of the evaporated vapours continuously decreases with increasing the heating rate, from 43% at 1 K/s to 28% at 1000 K/s. Since total tar yield of cellulose pyrolysis can also be determined (i.e., 72% at 1 K/s to 86% at 1000 K/s), this allows us to estimate the contributions of thermal ejection and evaporation to the formation of primary volatiles during cellulose pyrolysis. It can be found that the contribution of thermal ejection increases from 40% at 1 K/s to 67% at 1000 K/s, with the contribution of evaporation decreasing from 60% at 1 K/s to 33% at 1000 K/s. Obviously, thermal ejection plays a key role in the formation of primary volatiles from cellulose fast pyrolysis, especially at higher heating rates. The enhanced thermal ejection at increased heating rates greatly influences the yields and compositions of the generated volatiles (and the condensed bio-oil) during cellulose fast pyrolysis. The current results further suggest that thermal ejection mechanism must be considered in the modelling of biomass pyrolysis process, particularly for fast pyrolysis conditions (i.e., in a fluidised bed reactor).

CHAPTER 5 Formation of Reaction Intermediates and Primary Volatiles during Acid-catalysed Fast Pyrolysis of Cellulose

5.1 Introduction

Fast pyrolysis is a promising technology for producing renewable biofuels and biochemicals from biomass[6]. Particularly, acid-catalysed biomass pyrolysis is considered as an important method to produce value-added chemicals (i.e., levoglucosan, levoglucosenone)[26, 292]. Previous studies[38-40] have reported that acid loading not only passivates the catalytic effect of inherent inorganic species in biomass, but also promotes the dehydration reactions for producing desired chemicals.

However, there is considerable scope for research into understanding fundamental reaction mechanisms during biomass fast pyrolysis under acidic conditions. As one of the major components in biomass, cellulose is generally used as a model compound to study the acid-catalysed pyrolysis mechanism. It is well documented that fast pyrolysis of cellulose proceeds through the formation of a liquid (or molten) intermediate phase[122, 123, 284], where significant reactions take place to form primary volatiles[9]. Therefore, the reactions in the liquid intermediate phase play important roles in determining the composition of primary volatiles during cellulose pyrolysis. However, due to the short-lived nature of reaction intermediates, it is difficult to collect and characterise those intermediates in the liquid intermediate phase. In addition, one major shortcoming of conventional reactor systems is the incapability of minimising the secondary reactions of primary volatiles in the vapour phase so that the collection

of primary volatiles is impossible[9]. Therefore, previous studies[24, 38-40] mainly focused on product distribution during acid-catalysed cellulose pyrolysis, with little having been done on the liquid-phase chemistry[28]. To clearly understand the liquid-phase chemistry, it is critical to understand the composition of the reaction intermediates in the liquid phase and the primary volatiles in the vapour phase. This requires a reactor system with unique features for rapid quenching of reaction intermediates in the liquid phase, with the minimisation of secondary reactions of primary volatiles in the vapour phase. For example, our previous work[16] has employed a wire-mesh reactor (WMR) to facilitate the collection of both reaction intermediates and primary volatiles from cellulose pyrolysis. Therefore, the main objective of this study is to understand the liquid-phase chemistry during acid-catalysed cellulose pyrolysis by quantifying the key compounds in the reaction intermediates and primary volatiles produced in a WMR. An in-depth understanding of the liquid phase chemistry is important to optimise the reaction conditions for producing value-added chemicals from cellulose or biomass pyrolysis.

5.2 Cellulose conversion during the pyrolysis of the raw and acid-impregnated cellulose

Figure 5.1 presents the cellulose conversions based on weight, carbon and sugar during pyrolysis of the raw and acid-impregnated cellulose as a function of pyrolysis temperature. The results show that the acid-catalysed cellulose pyrolysis starts at ~160 °C, much lower than that (~250 °C) for the raw cellulose. The lower start temperature for the acid-impregnated cellulose pyrolysis is attributed to the partial destruction of crystalline structure and hydrogen bonding network within the raw

cellulose (that is known to take place during acid treatment[293]). The conversion of the raw cellulose on a weight basis increases from ~6% at 320 °C to ~87% at 450 °C. The cellulose conversions on three bases for the raw cellulose follow an order of sugar basis > weight basis > carbon basis, but only with small differences. This indicates that the raw cellulose pyrolysis mainly proceeds with depolymerisation reactions, which is consistent with our previous work[294].

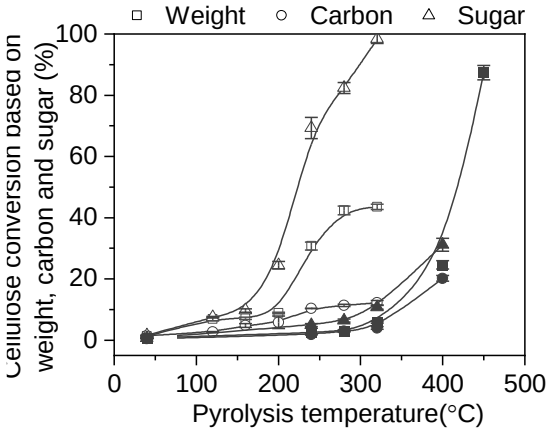

Figure 5.1 Cellulose conversions based on weight, carbon and sugar during the pyrolysis of the raw (solid symbol) and acid-impregnated (open symbol) cellulose at different temperatures

In contrast, the cellulose conversions for the acid-impregnated cellulose are substantially higher than those for the raw cellulose at temperatures < 320 °C. For example, the conversion of the acid-impregnated cellulose on a weight basis increases rapidly from ~9% at 200 °C to ~42% at 280 °C, but levels off as the pyrolysis temperature further increases to 320 °C, compared to that of only ~6% for the raw cellulose at 320 °C. Although the cellulose conversions on three bases still follow an

order of sugar basis > weight basis > carbon basis, the conversions on a sugar basis are much higher than the conversions on a weight basis, which are considerably higher than the conversions on a carbon basis. This clearly demonstrates that acid-catalysed cellulose pyrolysis mainly proceeds with dehydration reactions. In particular, almost all sugar structures are decomposed at 320 °C, although the conversion on a carbon basis is only ~12%. Such enhanced dehydration reactions tend to retain more carbon in the solid residue[39, 40], enhancing char formation during acid-catalysed cellulose pyrolysis.

5.3 Yields of the water-soluble products in the solid residue and tar during the pyrolysis of the raw and acid-impregnated cellulose

Our previous studies [16, 284] have demonstrated that the water-soluble fraction in the solid residue (or char) contains important reaction intermediates from cellulose pyrolysis, while the water-soluble fraction in the tar contains key compounds in the primary volatiles. Therefore, the yields of the water-soluble products in both solid residue and tar from the pyrolysis of the raw and acid-impregnated cellulose at different temperatures were determined and presented in Figure 5.2. For the raw cellulose, the water-soluble intermediates in the solid residue start to form at ~280 °C with the yield increasing to ~5% at 320 °C, while the water-soluble tar starts to form at ~320 °C. For the acid-impregnated cellulose, a small amount of the water-soluble compounds (~2%) is already present in the sample even after acid impregnation. The yield of the water-soluble intermediates in the solid residue increases with temperature to ~7% at 200 °C, followed by a reduction as temperature further increases. At 320 °C, the yield of the water-soluble intermediates reduces to almost zero. Interestingly, the

water-soluble tar starts to form at 200 °C, at which the yield of the water-soluble intermediates starts to decrease with increasing pyrolysis temperature. The yield of the water-soluble tar also increases with temperature, from ~3% at 240 °C to ~5% at 320 °C. These results demonstrate that the water-soluble tar is produced from the water-soluble intermediates in the solid residue.

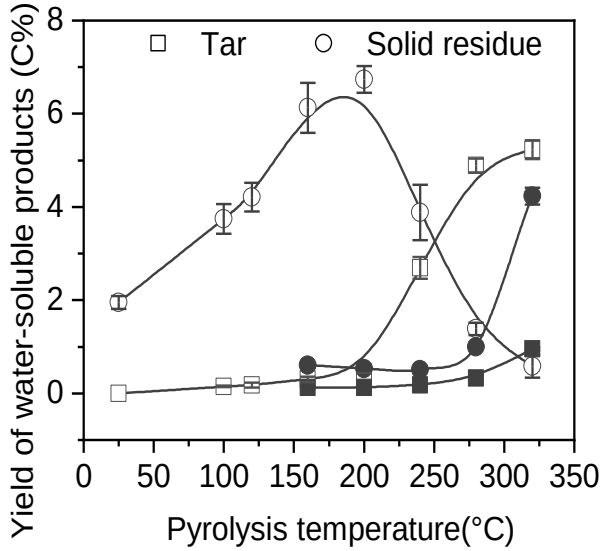

Figure 5.2 Yields of the water-soluble products in the solid residue and tar produced from the pyrolysis of the raw (solid symbol) and acid-impregnated cellulose (open symbol) at different temperatures

5.4 Characterisation of the water-soluble products in the solid residue and tar produced from the pyrolysis of the raw and acid-impregnated cellulose

The major compounds (i.e., C1-2, AC1-3, AGF, LGO, 5-HMF) in the water-soluble intermediates and tar were identified and quantified, and the respective yields and selectivities are presented in Figure 5.3 and Figure 5.4. For the raw cellulose, the major compound in the water-soluble intermediates is levoglucosan, which starts to form at ~280 °C. The levoglucosan yield in the water-soluble intermediates increases with

temperature from ~0.1% at 280 °C to ~1.2% at 320 °C, with its selectivity in the water-soluble intermediates increasing from ~13 to ~30%, respectively. This confirms that levglucosan is indeed a major primary product from cellulose pyrolysis. As for the water-soluble tar (see Figure 5.4), levoglucosan is also the major compound which can be identified in the tar at 280 °C. The levoglucosan yield in the tar increases with temperature from 0.03% at 280 °C to 0.8% at 320 °C, contributing to ~20% and ~86% of the water-soluble tar, respectively.

For the acid-impregnated cellulose, glucose oligomers are present in the water-soluble intermediates at temperatures < 100 °C. The glucose yield increases with temperature due to the hydrolysis reactions, with the maximal yield of ~0.2% achieved at 160 ˚C, but its selectivity is low (<4%) and continuously decreases with temperature. The yield of C2 is even lower than that of C1. For the dehydrated sugars, AGF and levoglucosan are produced at 120 °C. The AGF yield first increases from ~0.3% at 120 °C to a maximal value of ~0.6% at 200 °C, then reduces to ~0.1% as the pyrolysis temperature further increases to 320 °C. The AGF selectivity in the water-soluble intermediates increases from ~8% at 120 °C to ~11% at 280 °C. The formation pathways of AGF have been proposed previously [129, 295, 296]. One pathway is that glucose undergoes intramolecular dehydration to produce AGF and levoglucosan [129]. Other pathways include the dehydration of glucose via isomerisation to fructose [296] or acyclic glucose [295]. The results in this study indicate that AGF is more likely produced from glucose, since only glucose is present in the water-soluble intermediates before AGF is formed. Compared to AGF, levoglucosan has much lower yields, which also increases with temperature from ~0.1% at 120 °C to a maximal value of ~0.2% at 200 °C, followed by a reduction to close to zero as temperature further increases to 320 °C. This confirms that the presence of acid inhibits the formation of levoglucosan during

cellulose pyrolysis [23, 38]. Another major dehydrated product LGO starts to form at ~160 °C, and its yield first increases from ~0.2% at 200 °C to a maximal value of ~0.8% at 240 °C, then reduces to ~0.1% as the pyrolysis temperature further increases to 320 °C. The LGO selectivity in the water-soluble intermediates increases from ~4% at 200 °C to ~20% at 280 °C, followed by a reduction to ~14% at 320 °C. It was reported that LGO could be produced from DHGP [297]. However, DHGP was only detected in water-soluble tar from the pyrolysis of the acid-impregnated cellulose under current experimental conditions, with both very low yield (< 0.1% on a carbon basis) and selectivity (<0.2% on carbon basis). This confirms that LGO is a major product from acid-catalysed cellulose pyrolysis [23, 27], mostly produced from the dehydration of levoglucosan or AGF [292, 298].

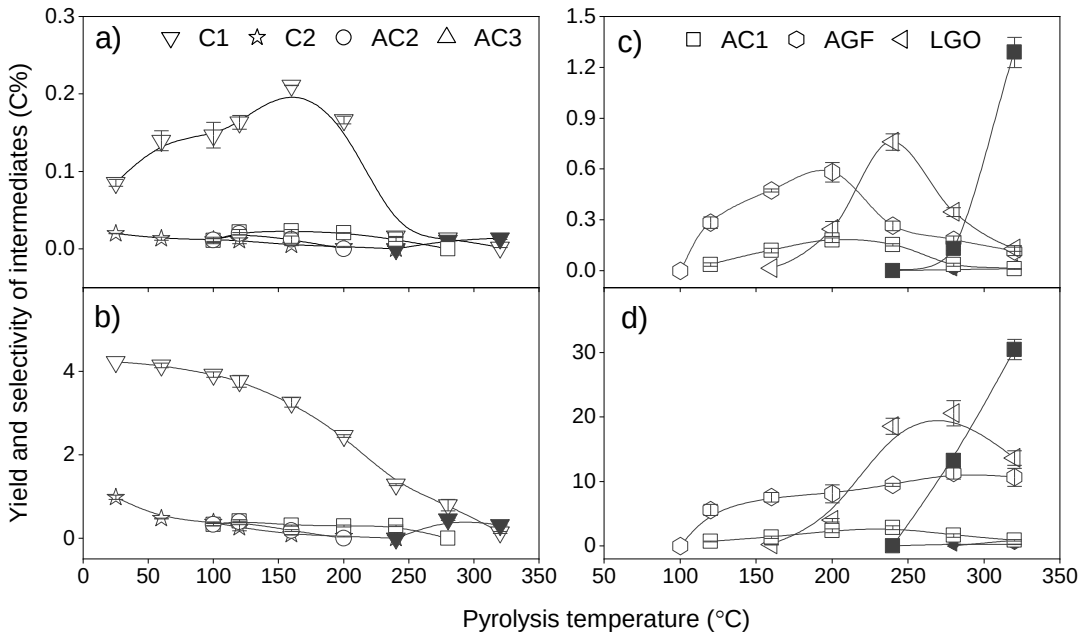

Figure 5.3 Yields (Panel a and c) and selectivities (Panel b and d) of the major compounds in the water-soluble intermediates from the pyrolysis of the raw (solid symbol) and acid-impregnated cellulose (open symbol) at different temperatures

As for the water-soluble tar from the acid-impregnated cellulose (see Figure 5.4), the yields of the major compounds in the water-soluble tar follow an order of AGF > LGO > 5-HMF > AC1 > C1. These products are produced in the tar at ~200 °C, with the respective yields increasing with temperature to maximal values (i.e., 1.4% for AGF, 1.3% for LGO, 0.65% for 5-HMF, 0.15% for AC1 and 0.004% for C1) at 280 °C, followed by decreases as the pyrolysis temperature further increases. As a result, AGF, LGO and 5-HMF contribute to ~42, ~31, ~14% of the water-soluble tar at 280 °C, respectively. In comparison, the levoglucosan selectivity in the water-soluble tar is low (<8%), while the glucose selectivity is even lower (<1%).

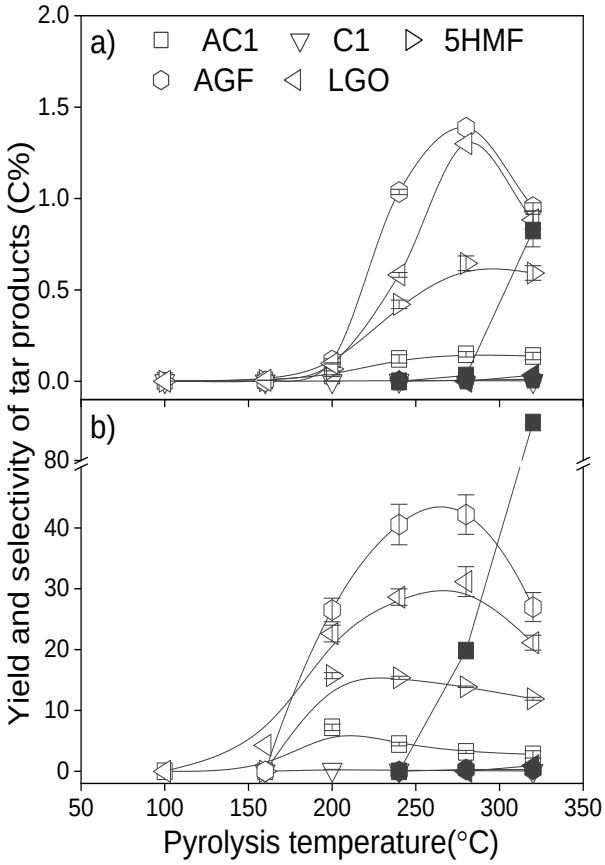

Figure 5.4 Yields (Panel a) and selectivities (Panel b) of the major compounds in the water-soluble tar from the pyrolysis of the raw (solid symbol) and acid-impregnated cellulose (open symbol) at different temperatures

Further efforts were taken to calculate the distributions of key compounds (i.e., AC1, AGF and LGO) in both reaction intermediates and primary volatiles during acid-catalysed cellulose pyrolysis, with the results presented in Figure 5.5. These key compounds gradually release from the liquid intermediate phase to the vapour phase as the temperature increases, but the distributions of these compounds are largely depending on the respective physical properties such as melting and boiling points. At 160 °C, the majority of these compounds are present in the reaction intermediates, i.e., ~95, ~100 and ~74% for AC1, AGF and LGO, respectively. Almost all AGF is in the reaction intermediates at 160 °C, indicating that it is difficult to evaporate into the vapour phase due to its high boiling point (i.e. ~416 °C [299]). It is interesting to see that AGF starts to release into the vapour phase at 200 °C, much lower than its boiling point. It is known that AGF has a low melting point of ~110 °C. Therefore, AGF is unlikely to evaporate into the vapour phase. Instead, AGF is mainly released into the vapour phase as aerosols via thermal ejection mechanism, or carried away by the carrier gas. AC1 follows a similar mechanism to release into the vapour phase due to its high boiling point. As for LGO, ~74% is present in the reaction intermediates at 160 °C. LGO is unable to evaporate at this temperature, which is much lower than its boiling point of ~254 °C. As the temperature increases to 280 °C, LGO rapidly evaporates into the vapour phase, with ~87% in the vapour phase. As the temperature increases to 320 °C, the majority of those products are present in the vapour phase, i.e., ~94, ~89 and ~87 for AC1, AGF and LGO. Although 5-HMF is not identified in the water-soluble intermediates, it can be easily produced from glucose under acidic conditions [300, 301]. In addition, the boiling point of 5-HMF is only ~116 °C, which makes it easy to evaporate into the vapour phase once it is formed.

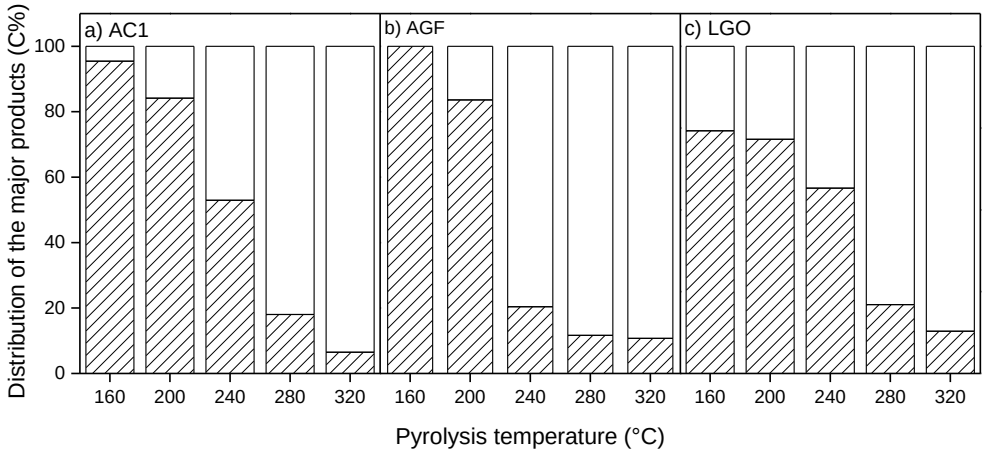

Figure 5.5 Distribution of the major compounds in the reaction intermediates (hatched) and primary volatiles (empty) as a function of temperature

The above results clearly show that the reaction intermediates in the solid residue are significantly different during acid-catalysed cellulose pyrolysis. The raw cellulose pyrolysis produces levoglucosan as the major reaction intermediate through depolymerisation reactions. However, during acid-catalysed cellulose pyrolysis, glucose is firstly produced at ~60 °C via hydrolysis, followed by its dehydration to produce AGF at ~120 °C. The depolymerisation of cellulose to produce levoglucosan is largely suppressed in the presence of acid, and levoglucosan and AGF are also easily converted to LGO at ~160 °C. The changes of reaction intermediates in the solid residue also lead to changes in the composition of the primary volatiles. While levoglucosan is the major product in the primary volatiles from cellulose pyrolysis, the dehydrated products such as AGF, LGO and 5-HMF are major products in the primary volatiles from acid-catalysed cellulose pyrolysis.

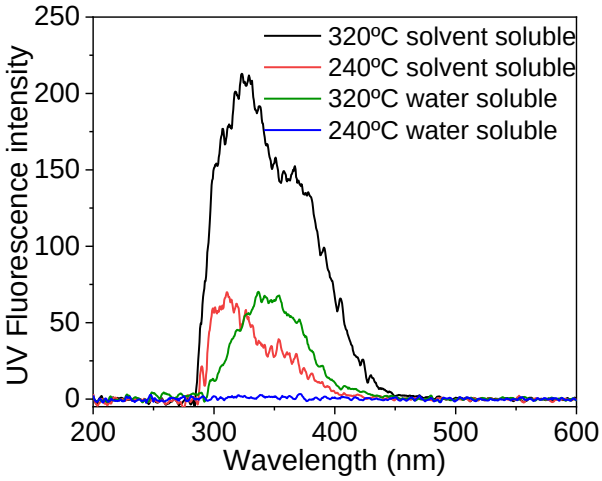

Figure 5.6 Constant energy (-2800 cm^{-1}) synchronous spectra of the solvent-soluble tars produced from the pyrolysis of acid-impregnated cellulose at 240 and 320 °C

While the compounds in the tar from the raw cellulose pyrolysis are mostly soluble in water, half of the compounds in the tar from the pyrolysis of acid-impregnated cellulose are insoluble in water. For example, the yield of the water-soluble tar (on a carbon basis) is only ~6% at 320 °C, although the conversion on a carbon basis is ~12%. Therefore, some water-insoluble compounds are present in the tar from the acid-catalysed cellulose pyrolysis. To verify this point, the tar products soluble in water and a solvent mixture of chloroform and methanol (80:20 in volume) were subject to UV fluorescence analysis to identify the aromatic compounds in the tar, as presented in Figure 5.6. It can be seen that little aromatic compounds can be detected in the water-soluble tar at 240 °C, but some aromatic compounds are present in the solvent-soluble tar. At 320 °C, even some aromatic compounds with 2-5 fused rings can be detected in the water-soluble tar. Because the secondary reactions of the primary volatiles are minimised in the WMR, the aromatic compounds with fused rings must be released from the reaction intermediates in the solid residue. The results clearly

demonstrate the formation of aromatic structures via condensation reactions during acid-catalysed cellulose pyrolysis at 240 °C or above.

5.5 Discussion on the acid-catalysed cellulose pyrolysis mechanism

The results in this study provide new insights into the chemistry in the liquid intermediate phase during acid-catalysed cellulose pyrolysis, via the quantification of key compounds in the reaction intermediates and primary volatiles. Figure 5.7 summarises the fundamental reaction mechanisms of acid-catalysed cellulose pyrolysis under the reaction conditions. Acid impregnation can break the hydrogen bonding networks in crystalline cellulose, leading to the formation of sugar oligomers in the acid-impregnated cellulose. Due to the presence of acid and water in the acid-impregnated cellulose, hydrolysis reactions can easily take place to produce glucose at temperatures <100 °C. At 120 °C, levoglucosan is also produced via depolymerisation reactions from sugar oligomers, and AGF is formed via glucose dehydration. At 160 °C, various dehydrated compounds such as LGO and 5-HMF can be produced from glucose, levoglucosan or AGF via acid-catalysed dehydration reactions. For example, LGO can be produced from both levoglucosan and AGF, while 5-HMF can be produced from glucose. Therefore, dehydration reactions are the dominant reactions during acid-catalysed cellulose pyrolysis, with AGF, LGO and 5-HMF as major primary pyrolysis products. At temperatures of 240 °C or above, aromatic compounds are also produced as important primary pyrolysis products during acid-catalysed cellulose pyrolysis. Once produced, these primary products can be released into the vapour phase via either evaporation (e.g. 5-HMF) or thermal ejection (e.g. AGF, LGO).

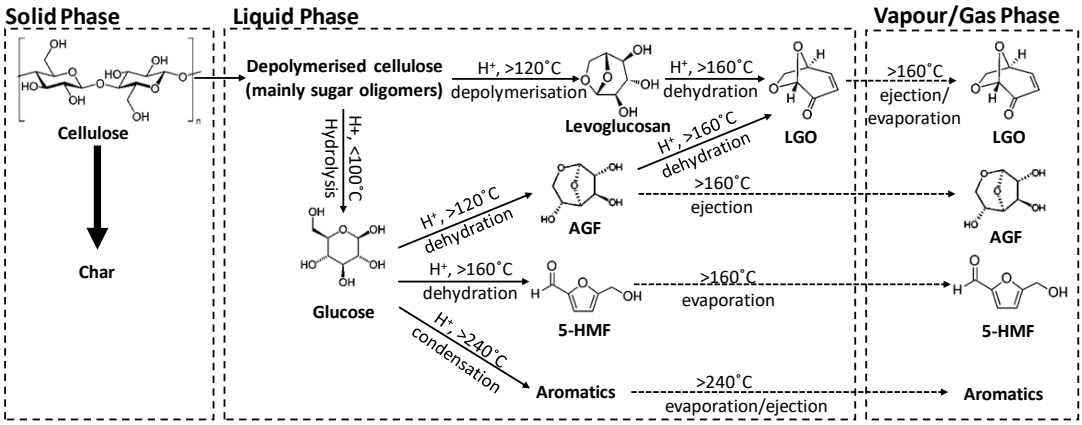

Figure 5.7 Proposed acid-catalysed cellulose pyrolysis mechanism

5.6 Conclusions

This study reports the formation of reaction intermediates and primary volatiles produced from the pyrolysis of the raw and acid-impregnated cellulose at 40–320 °C in a WMR. While cellulose pyrolysis mainly proceeds with depolymerisation reactions to produce levoglucosan, acid-catalysed pyrolysis is dominated by dehydration reactions. The pyrolysis of the acid-impregnated cellulose has a lower start temperature compared to that for the raw cellulose pyrolysis, due to weakened hydrogen bonding networks during acid impregnation process. At temperatures <100 °C, hydrolysis reactions can take place to form glucose due to the presence of acid and water. Once glucose is formed, it can be easily dehydrated to form AGF at ~120 °C, which is a major primary pyrolysis product from acid-catalysed cellulose pyrolysis. A small amount of levoglucosan is also formed at ~120 °C. At temperatures >160 °C, significant dehydration reactions of glucose, levgolucosan and AGF take place to form 5-HMF and LGO. Once those compounds are produced, they can be released into the vapour phase via either evaporation or thermal ejection. When

the temperature increases to 240 °C, aromatic compounds are formed and released into the vapour phase as part of the primary volatiles.

CHAPTER 6 `The Release and Transformation of Organic and Inorganic Sodium during Fast Pyrolysis of the Sodium Impregnated Lignin

6.1 Introduction

Alkali lignin is considered as an alternative to producing valuable biofuels and chemicals[302] under thermochemical utilisation methods, especially pyrolysis. Alkali and alkaline earth metals (AAEM), existing within the three-dimension lignin structure, cause severe ash related issues, such as slagging and corrosion during the thermal utilisation process.[303, 304] Those AAEM species play a vital role during lignin thermal decomposition, increasing char yield and decreasing of organic volatile yield.[29, 37] Sodium (Na), as one of the most abundant metal species in alkali lignin,[305] exists in lignin matrix inorganically as well as organically attaching to carboxylic and phenolic groups[30]. Investigations also reported that the organically bonded intraparticles and inorganic extraparticles have distinct catalytic effects on lignin pyrolysis[3,31]. In addition, the transformation of different forms of alkalis is partly responsible for the releasing characteristics of volatile products. At low temperatures, the release of alkalis is attributed to the devolatilisation of organic bonded compounds with low melting points,[215, 306] while the inorganic AAEM species are thermally or chemically released to vapour phase at higher temperatures[307, 308]. Therefore, the understanding of the release and transformation behaviour of AAEM, particularly Na, is vital to provide fundamental research to achieve both economically and environment-friendly application of biomass pyrolysis.

With all the effort on the catalytic effect of AAEM species during biomass pyrolysis, the release and transformation of sodium in primary tar and char residues require further clarification. Therefore, the main objective of this chapter is to investigate the catalytic effect, the release and transformation of different types of sodium during lignin pyrolysis under a wide range of experimental temperatures with a high heating rate. Three different types of lignin, including acid-washed lignin, organic sodium and inorganic sodium loaded lignin, were pyrolysed in a wire mesh reactor to achieve minimised secondary reactions. The effect of sodium additives with different chemical forms on the product yield and characteristics was investigated. Furthermore, the distribution of organic and inorganic sodium in tar and char residues and their physico-chemical transformations during pyrolysis were reported and elucidated.

As detailed in section 3.3.1, The pre-treated samples with sodium sulphate and sodium acetate were referred to as In-Na-lignin and Or-Na-lignin. Those samples were subjected to a predesigned ashing process[309] for the examination of sodium content. The total loaded sodium in both lignin samples was 0.15 mmol (Na) /g (lignin). The proximate, ultimate and ash compositional analysis of three lignin samples are listed in Table 6-1.

.

Table 6-1 proximate, ultimate and ash compositional analysis of three lignin samples

	Alkali lignin[305]	A-lignin	Or-lignin	In-lignin
Proximate analysis (wt% dry basis)				
Moisture	3.43	2.20	3.01	3.57
Ash	3.83	0.10	1.64	1.46
Volatile	67.46	63.9	64.91	64.40
	28.71	33.8	30.44	30.57
Ultimate analysis (% dry and ash free)				
C	65.80	64.79	62.43	62.65
H	6.24	5.61	5.51	5.28
N	1.02	0.23	0.78	0.57
S	2.12	1.18	2.83	3.73
O	24.82	28.19	28.45	27.77
Ash compositional analysis (mg/kg dry basis)				
K	1255.46±1.99	Not detected	6.77±0.39	2.88±0.16
Mg	192.15±9.00	58.29±1.54	91.96±8.42	66.42±6.49
Na	11567.10±148.17	Not detected	3503.66±29.65	3489.35±37.14
Ca	106.77±15.63	120.01±2.41	107.43±3.69	100.13±0.63

6.2 Product distribution during the pyrolysis of different types of lignin

Table 6-2 presents the char, tar and gas yields of three lignin samples pyrolysis as a function of temperature. As can be seen, the char yield of acid-washed lignin is continually lower than that of sodium loaded lignin under all temperatures, which demonstrates that AAEM loading promotes the char yield during lignin pyrolysis[29]. However, the different types of sodium loaded lignin show different tendencies. For example, the char yield of In-Na-lignin is 86% at 300 °C, higher than that of Or-Na-lignin of 83% at 300 °C. While oppositely, at temperatures above 450 °C, the char yield of Or-Na-lignin is slightly higher. This phenomenon demonstrates that the organic sodium bonded structure tends to evaporate to form volatiles[310] or can be easily ejected as liquids at lower temperatures. As for condensed tar yield, the yield of In-Na-lignin tar is continually higher than that of acid-washed lignin and Or-Na-lignin

after 300 °C, suggesting that the inorganic sodium have a stronger catalytic effect on tar production. Despite that Or-Na-lignin tar yield is higher than that of acid-washed lignin at temperatures below 500 °C, the yield of acid-washed lignin tar takes over at temperatures above 500 °C. The data indicate that inorganic sodium enhances the production of tar under all elevated temperature ranges, while organic sodium promotes tar yields below 500 °C and inhibits its tar yield at higher temperatures. The presented gas yield was calculated by difference. It is clearly shown that the gas yield follows an increasing tendency with increasing temperatures, with the gas yield of acid-washed lignin higher than Or-Na-lignin, and followed by In-Na-lignin. For example, the gas yields of acid-washed lignin, Or-Na-lignin and In-Na-lignin are ~11%, 4% and 6% at 300 °C, and increase to ~32%, 28% and 29% at 800 °C, respectively. Those results strongly imply that the addition of sodium inhibits the generation of light gaseous products at the current temperature range. Meanwhile, Or-Na-lignin generates more volatiles with lower molecular weight that cannot be quenched by the liquid nitrogen cooled tar trap, than In-Na-lignin.

In conclusion, Na-impregnation increases char yield and decrease light non-condensable gas products under the current temperature range. Different types of sodium show divergent catalytic effects at different temperature ranges. While inorganic sodium promotes the production of condensable tar products, organic sodium tends to generate more low- molecule-weight compounds, especially at the low-temperature range.

Table 6-2 Product yields during the pyrolysis of the lignin samples at different temperatures

Temperature (°C)		300	400	500	600	700	800
Char yield (%)	Acid-lignin	80.35±2.49	57.71±1.25	39.92±0.64	32.21±3.40	26.89±2.24	24.05±2.05
	In-lignin	85.98±3.16	61.22±5.00	40.11±2.14	34.16±3.17	28.42±0.57	27.46±0.16
	Or-lignin	83.07±0.65	57.99±3.56	43.02±0.24	33.56±1.43	30.82±2.48	29.17±0.70
Tar yield (%)	Acid-lignin	8.35±0.69	18.58±0.99	34.76±1.31	42.11±0.36	42.89±0.50	44.33±0.98
	In-lignin	10.20±0.32	23.94±1.21	41.32±1.66	42.41±1.26	44.13±2.25	47.58±2.89
	Or-lignin	11.19±2.99	22.57±2.01	34.98±2.99	38.60±1.21	39.54±3.17	42.31±2.26
Gas yield (by difference) (%)	Acid-lignin	11.30	23.71	25.32	26.68	30.22	31.61
	In-lignin	3.81	14.84	18.56	23.43	27.44	27.96
	Or-lignin	5.73	19.44	22.00	24.84	29.63	28.53

6.3 Characterization of tar and char products during the pyrolysis of organic and inorganic sodium loaded lignin

6.3.1 FT-IR analysis of lignin samples and the char residues

The FT-IR spectra of lignin samples and their char residues are presented in Figure 6.1, while the peak assignments are listed in Table 6-3 according to previous literature[311-313]. As shown in Figure 6.1, three types of lignin samples display the same main structures. Although the pyrolysis of three samples at 300 °C for 10 seconds yields less than 20% light volatiles, it rarely has notable effects on the functional groups. This indicates that, at the early pyrolysis stage, the generation of light volatiles

is likely due to the ejection effect of molten lignin intermediates as well as the evaporation of light molecule weight compounds. When the temperature reaches 600 °C, the function groups decrease dramatically. The reduction of C-O stretching of aromatic acetoxy at 1766 cm^{-1} and aromatic skeletal vibration at 1513, 1462, 1423 cm^{-1} indicates that the release of tar product could be attributed to the release of aromatic structures. When samples are pyrolysed at 800 °C, functional groups barely remain in the char residues for all three lignin samples. Compared with the other two samples, sodium loaded lignin char samples tended to retain more carbon in char, yet show a negatable difference with regards to functional groups. This phenomenon indicates that sodium impregnation promoted carbonation reactions. It can also be seen in Figure 6.1c, the impregnation of different occurrences of sodium influences the function group of C-O aromatic acetoxy stretching at 1766 cm^{-1}, as well as the aromatic C-H deformations at 1766 cm^{-1}. The decrease of main aromatic structures during the pyrolysis of sodium impregnated lignin samples suggests that the generation of aromatic volatiles is enhanced.

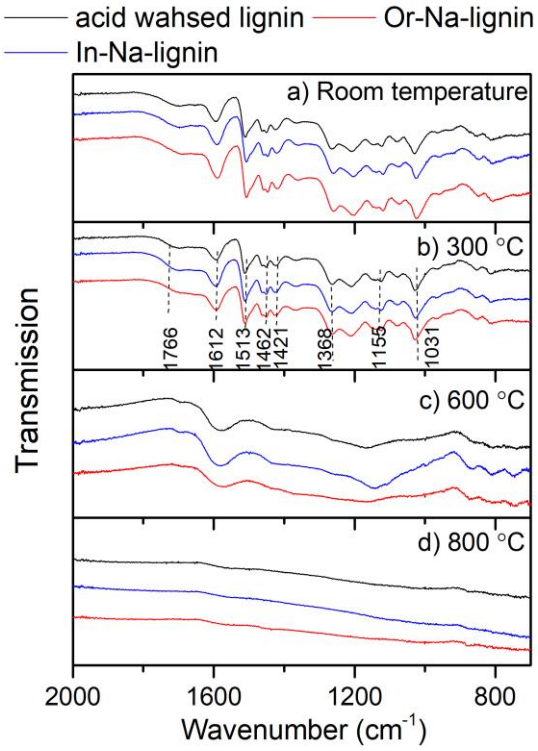

Figure 6.1 FT-IR spectra of lignin char samples from different pyrolysis temperatures in the region of 700–2000 cm^{-1}

Table 6-3 Peak assignments for FT-IR spectra

Wavenumbers (cm^{-1})	Assignments
1766	C-O stretching of aromatic acetoxy
1612	C=O stretching and C=C aromatic vibration
1509-1513	Aromatic skeletal vibration
1461-1462	C-H bending vibration, CH_3, CH_2 asymmetric bending vibration aromatic skeletal vibration.
1421-1423	Aromatic skeletal vibration and C-H in-plane bending
1368	OH in-plane bending, CH bending, Syringyl ring breathing with C-O stretching
1155	Aromatic C-H deformations of guaiacyl ring
1126	Aromatic C-H deformations of syringyl ring, C-H aromatic -plane bending vibration, C-O stretching vibration
1031	C-H aromatic in-plane bending vibration, C=O stretching

6.3.2 UV fluorescence analysis of tar samples

To verify the effect of different forms of sodium on the aromatic structures in tar samples, the UV fluorescence spectra at various pyrolysis temperatures were normalised to per gram of lignin sample as well as per gram of tar samples are presented in Figure 6.2. Overall, it is observed that acid-washed lignin tar products contain aromatic with more low-fused-rings structures, while In-Na-lignin yields aromatics with more fused rings, even at the early pyrolysis stage. It further proves that the loading of sodium will intensify the ejection effect during lignin pyrolysis, as the existence of aromatic structures with high fused rings tends to have high boing points thus cannot be attributed to evaporation. As shown in Figure 6.2a and Figure 6.2d, the aromatics that existing in acid-washed lignin volatile samples are higher than the other two samples at 300 °C. As the temperature increases, the fraction of aromatic structures with more fused rings (> 400nm) increases. The intensity of the aromatic structures for these three types of lignin samples shows neglectable differences when normalised to per gram of lignin samples. However, when normalised to tar products, the spectrum shows slightly different trends. At 300 °C, the sodium loaded lignin samples, Or-Na-lignin in particular, have considerably lower intensity compared to the acid-washed lignin. The results demonstrate that sodium impregnated lignin yields more incondensable gaseous products at low temperatures. And organic sodium tended to produce more aromatic structures with low molecular weight, compared with In-Or-lignin. When the temperature reaches 600 °C and 800 °C, the intensity of aromatic structures is slightly higher in Or-Na-lignin. In conclusion, sodium impregnation slightly enhances the release of aromatic structures during lignin pyrolysis, while organic sodium tends to yield more low-molecule-weight incondensable compounds at low temperatures.

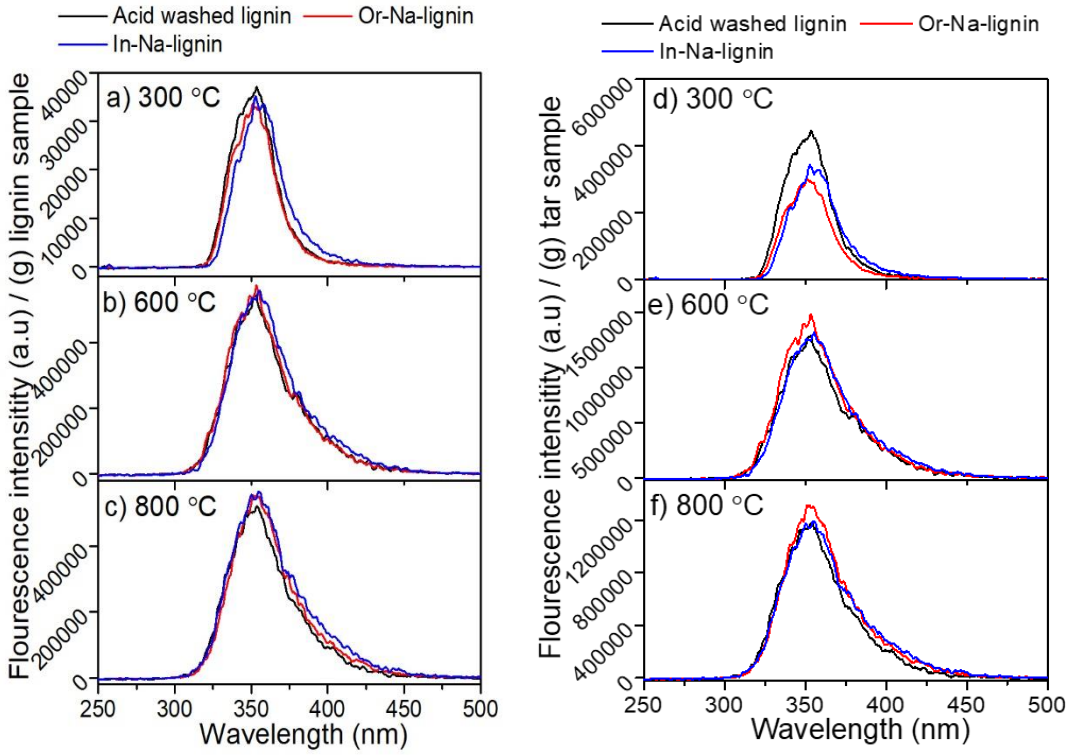

Figure 6.2 Constant energy (-2800 cm^{-1}) synchronous spectra of the solvent-soluble tar produced from the pyrolysis of lignin samples at different temperatures

6.4 Sodium distribution and transformation in the tar and char residues during the pyrolysis of organic and inorganic sodium loaded lignin

6.4.1 Sodium retention

The sodium retention of both sodium loaded samples are presented in Figure 6.3. As can be seen, ~90% or more sodium was collected in both samples, with more than 75% in the char residues. As for Or-Na-lignin, sodium retention in char is highest, reaching ~88% at 300 °C. With increasing temperature, the sodium retention in char slightly decreases and then remains stable at ~76%. On the contrary, the amount of sodium in tar is rising consistently from ~7% at 300 °C to ~14% at 800 °C. For the In-Na-lignin

pyrolysis products, the sodium retention at all temperatures remains relatively stable. ~ 80% to ~ 85% of total sodium are retained in char residues, and ~9~11% sodium is transferred to volatile products. The high sodium retention in char residues shows consistency with the findings in high-Na coal pyrolysis[314].

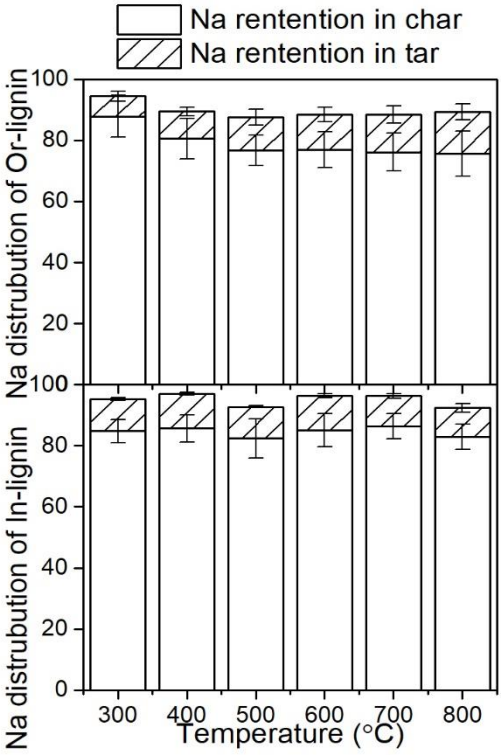

Figure 6.3 Sodium retention during the pyrolysis of sodium loaded lignin samples at different temperatures

6.4.2 Organic and inorganic sodium distribution in the tar and char residues

To have a better understanding of the evolution and transformation of sodium during lignin pyrolysis, the organic and inorganic occurrence of sodium were separately collected and analysed with detailed methods described below. The solid residue was subjected to an ashing procedure to obtain ash. The collected ash and tar samples were digested in the concentrated HNO_3/H_2O_2 acid solution. After acid digestion, the

remaining was dissolved using diluted methanesulfonic acid for total sodium content in both tar and char products. In another set of experiments, the tar trap was washed with ultra-pure water to collect the inorganic sodium in the tar (hereby referred to as In-Na-Tar), while the solid residue sample was subjected to water leaching process to extract inorganic sodium in char (hereby referred to as In-Na-Char). Subsequently, liquid samples were filtered via a 0.45 um syringe filter. The acquired liquid solution was further analysed in an ion chromatography. Therefore, the organic sodium remaining in tar and char samples can be calculated by difference respectively, and were denoted as Or-Na-Tar and Or-Na-Char.

The sodium contents with different forms within tar and char residue were quantified and presented in Figs.4 and 5. For the inorganic sodium loaded lignin, some inorganic sodium is transferred to the water-insoluble form at a temperature as low as 300 °C. In particular, with regards to the sodium distribution in char residues, the content of organic sodium grows steadily from ~17% at 300 °C to ~37% at 800 °C. On the contrary, the content of preloaded inorganic sodium decreases continuously, but to a smaller extent, from ~67% at 300 °C to ~42% at 800 °C. It could be concluded that even under the pyrolysis temperature of 300 °C, the transformation of sodium forms already commences, which results from the ion exchangeable liquid intermediate phase during lignin pyrolysis, where free hydrogen ions can be replaced by the inorganic sodium. And with increasing temperature, the transformation becomes more severe. In terms of tar products, sodium in different forms are identified, and their amount remains steady at all temperatures. Inorganic sodium in tar products is less likely to be generated through evaporation, as the boiling point of sodium and sodium salts are greater than 800 °C. It is reported that lignin pyrolysis undergoes an intermediates phase, during which process ejection and evaporation occur.[13] The

ejected aerosols are clearly captured by a high-speed camera. The same author reported the primary ejected aerosols containing calcium during cellulose pyrolysis, which also undergoes a molten liquid phase.[12] It is also evident that the "tar ball" from the collect aerosols from biomass burning contains variable inorganic species, and is the most abundant particles in smoke.[315] Therefore, it can be assumed that the different types of sodium transferred within the molten phase can be partially ejected to the liquid phase, which is subsequently captured in a liquid nitrogen-cooled tar trap.

As described in Figure 6.5, the sodium distribution of Or-Na-lignin shows a different tendency. As speculated, the content of organic sodium decreases rapidly with increased temperature, from ~79% at 300 °C to ~28% at 800 °C. The decreased amount of organic sodium in the char residues of Or-Na-lignin is more than three times the involved inorganic sodium in In-Na-lignin. However, the increased amount of inorganic sodium is only 38% in the char products, which is considerably lower than the decreased organic sodium. As for the sodium form in tar products, the yield of inorganic sodium slightly increases with increasing temperature, but to a smaller extent and lower value, compared with the organic sodium in tar samples. Therefore, some of the reduced organic sodium could be released to the volatile phase by evaporation. Also, at temperatures above 600 °C, the amount of inorganic sodium in char exceeds the amount of initial organic sodium. It is spectacled that the chemical bond of carboxylic and phenolic sodium is broken due to the massive loss of aromatics. Therefore, at high temperature, some organic sodium tend to be left in the char matrix and become free sodium ions. Meanwhile, some sodium can attach to the low molecule weight compound thus is released to the vapour phase. It is also reported that the addition of AAEM of lignin pyrolysis results in the reduction of reaction energies.[33] As a result, the exchange of free radicals and sodium in lignin structure are

significantly enhanced. Also the data suggest that the occurrence of sodium forms in lignin char is strongly dependent on pyrolysis temperature under fast heating conditions. However, the amount of different types of sodium in tar products grows slightly with increasing temperature.

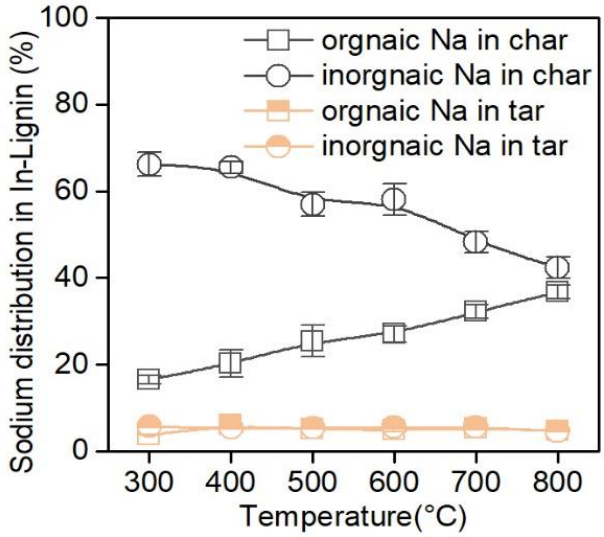

Figure 6.4 Sodium distribution during the pyrolysis of In-Na-lignin

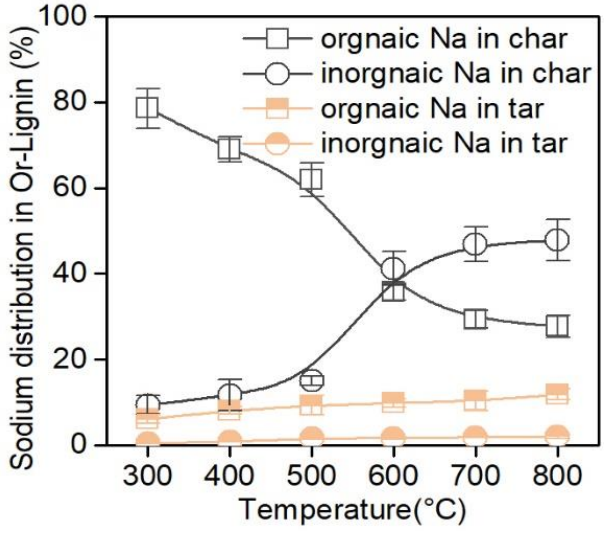

Figure 6.5 Sodium distribution during the pyrolysis of Or-Na-lignin

Based on above data, it can be concluded that the ejection effects occur during the heating periods when the transformation of sodium already happens. Also, the transformation between different types of sodium mainly happens inside liquid intermediates, as the secondary reaction in the volatile phase is minimised. With increasing temperatures, the transformation between organic and inorganic sodium during pyrolysis is intensified. As a result, the sodium existence in tar products can be distributed into two parts. Firstly, the active ejection effect during biomass pyrolysis is able to deliver sodium into tar, which consists of both types of sodium. Secondly, as the evolution continues, the organic bonded sodium in lignin structure also starts to decompose and evaporate into the liquid phase, while inorganic sodium is retained in the solid phase. However, it can also be assumed that the ejection of liquid components is intense in the initial pyrolysis process and starts to calm down during char burn-out stage. Therefore, it could partly explain that even the tar yield doubles as temperature increases, the total amount of released sodium does not seriously change. Also, the amount of ejected sodium is not severely reinforced by increasing temperature.

6.4.3 Sodium transformation in the tar and char residues

To further investigate the overall physio-chemical transformation of sodium, the comparison of the amount of organic and inorganic sodium during Na loaded lignin pyrolysis is presented in Figure 6.6. As for Or-Na-lignin, it is shown that with the increasing temperature, the amount of organic sodium within the products declines gradually until 600 °C, then remains stable when temperature increase to 800 °C. It is notable that the amount of inorganic sodium exceeds that of original loaded organic and reaches ~56% at 800 °C. Similarly, for the inorganic sodium loaded lignin, the change in terms of inorganic sodium follows the same decreasing manner, while the

organic sodium shows the opposite tendency. However, the amount of inorganic remains higher than that of organic sodium, decreasing from 78% at 300 °C to 53% at 800 °C. It appears that the sodium forms existing in the intermediates tend to exist and stabilise in inorganic form. Those results are consistent with the previous results that organic sodium tends to generate higher yields of volatiles and light organic gaseous products during lignin pyrolysis, compared with inorganic sodium. Also, the transformation of sodium not only occurs during devolatilisation but also following stabilising stage within molten lignin, which is consistent with the findings of potassium releasing.[316]

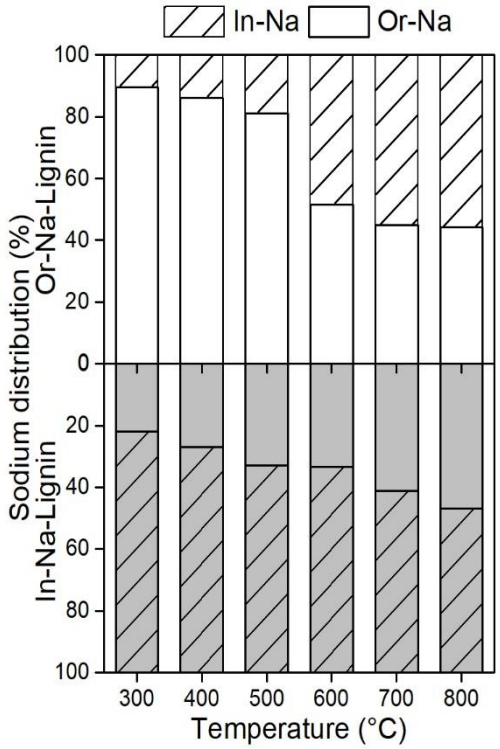

Figure 6.6 Inorganic and organic sodium distribution during the pyrolysis of lignin samples

The detailed Or-Na-Tar, Or-Na-Char, In-Na-Tar and In-Na-Char distribution is also listed to comprehend the transformation of sodium in different forms. As can be seen

from Figure 6.7, for both samples, the original form of sodium is gradually transferred to the other form in solid residues, but to different extents. Unlike the evolution of sodium forms in the solid, sodium in tar products is more stable with much slighter changes. However, in both samples, the percentage of inorganic sodium in tar is always lower than that in char residues. As clarified previously, inorganic sodium is unlikely to be released to vapor phase through evaporation, but more likely via thermal ejection. However, the proportion of the two sodium in tar is not the same as that in char. The results indicate that some organic sodium is also released to the vapour phase, with some low molecule weight compounds. Also, from the slight change of sodium forms in tar, it can be concluded that the ejection of sodium is not intensified with increasing temperature. This phenomenon is probably because that the ejection happens in the early stage of heating, but further increasing temperature leads to limited influence.

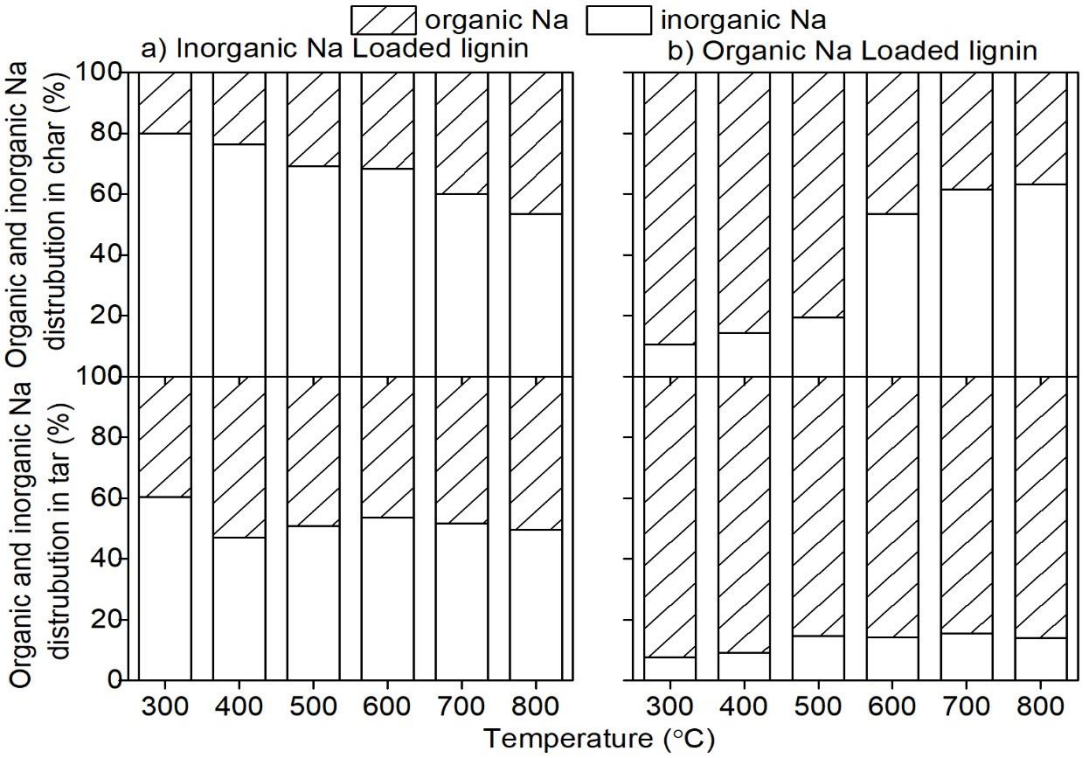

Figure 6.7 Organic and inorganic sodium distribution in char and tar during the pyrolysis of lignin samples

6.5 Discussion on the release and transformation of different sodium during lignin pyrolysis

The release and transformation of inorganic and organic sodium are discussed in this study with their detailed distribution in primary tar and char residues. The proposed transformation is elucidated in Figure 6.8. Sodium occurrence in lignin samples can be divided into two parts: inorganic sodium within the pores of lignin structures and organic sodium attached to carboxylic and phenolic groups. During the pyrolysis process, lignin undergoes a molten intermediate phase where the transformation and evolution of different sodium occurs. And the transformation is intensified with increasing temperature. Upon heating, the free radicals can replace the organic attached sodium or in the opposite direction. At low temperatures, the ejection effect already occurs under the high heating rate condition, generating aerosols that consist of organic and inorganic sodium. Besides, some organically bonded sodium components with low boiling points can be released to the tar phase via evaporation. Those ejected aerosols and evaporated organic components make up the primary tar products. As the ejection and evaporation undergo, the evolution of sodium forms within the molten phase continues. In addition, because of the limited ejection and evaporation effect, most sodium is still retained in char residues.

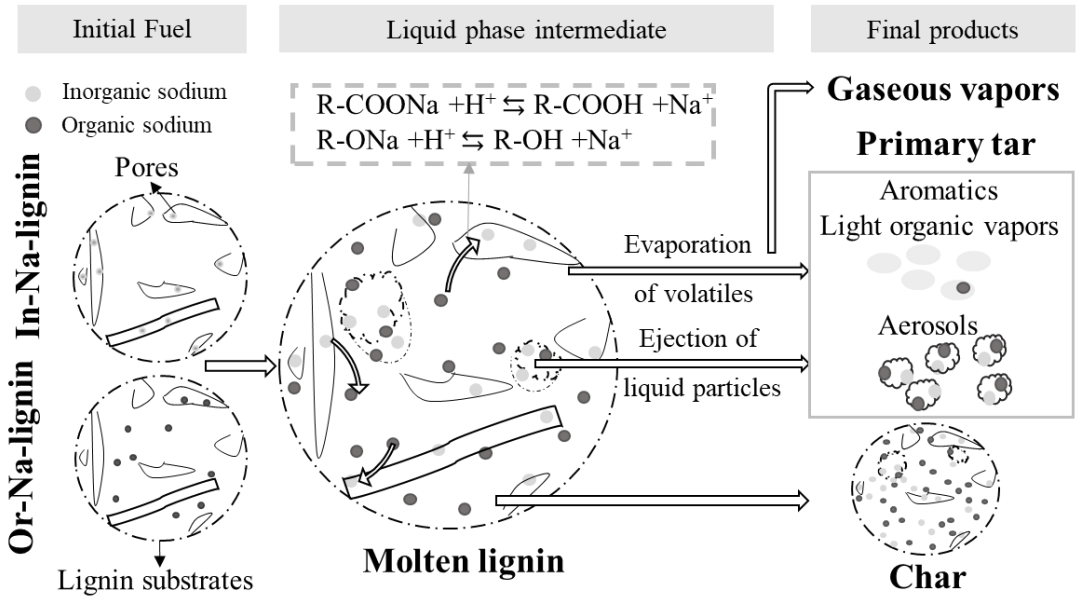

Figure 6.8 Proposed release and transformation of various sodium during lignin pyrolysis

6.6 Conclusions

This study investigates the catalytic effect and transformation of inorganic and organic sodium during lignin fast pyrolysis at 300- 800 °C in a wire mesh reactor. Both forms of sodium additive lead to an increased char yield, while organic sodium tends to generate more light gaseous products than inorganic sodium. In addition, the sodium impregnation promotes the breakage of aromatic functional groups, yielding more aromatic structures with more fused rings. The transformation between various types of sodium occurs in an early stage and is intensified with increasing temperature. The molten phase of lignin provides the environment for the replacement of free hydrogen and inorganic ions and organic bonded ions. Also, the transformation of sodium in different occurrences takes place in the molten lignin phase, while no such evolution in the tar phase occurs as secondary reactions are minimised in this study. Also, it

appears that inorganic sodium is more stable than organic sodium, as the transformation from inorganic sodium to organic form is far less than the opposite evolution. More than 70% sodium is retained in char residues in both cases, while more than 15% sodium is released to tar. The existence of sodium in tar products results from two possible reasons. While some organic sodium can be released to the liquid phase by evaporation through the decomposition of lignin structure, the inorganic sodium and other organic sodium are ought to be attributed to the ejection effect of the molten intermediate phase of lignin.

CHAPTER 7 Effect of Carbon Dioxide Torrefaction on the Fast Pyrolysis of Lignin

7.1 Introduction

Lignocellulosic biomass is of increasingly widespread interest to be utilised as the potential alternative for fossil fuel due to the aggravating environmental issues. And pyrolysis is a promising method to convert the lignocellulosic biomass into liquid bio-fuel or valued chemicals. Lignin is one of the main components (15- 35%wt) in lignocellulosic biomass with a 3D structure of branched aromatic rings.[60] In addition, lignin and pyrolytic lignin often significantly influence the black liquor or the conventional pulp industry. However, the undesired properties of lignin with large molecule weight components containing a high amount of moisture and oxygen, hinder their further utilisation. Therefore, some pre-treatment methods are employed to improve the properties of lignin. Among the pre-treatment methods, torrefaction which normally occurs at a temperature between 200 ºC and 300 ºC under inert atmospheres is one of the most potential methods. It is reported that torrefaction of biomass reduces the moisture and oxygen content, enhances the carbon concentration, boosts energy density, increases the grindability of the pellet,[35] and thus favours the following treatment of biomass such as pyrolysis and combustion[41]. The effect of torrefaction on the subsequent pyrolysis of biomass, confirms more pyrolytic lignin and phenols are enriched in the bio-oil.[34, 36, 317-319] It is reported that the torrefaction of lignin involves deoxygenation[320] and demethoxylation[321] reactions and alters the pyrolytic product distribution[322], with increased phenol yield and decreased aromatic hydrocarbon yield[323]. Despite plenty of researches focusing on torrefaction on biomass, the

torrefaction effect on individual lignin components, especially the subsequent thermal utilisation, needs a more thorough understanding.

Even though torrefaction has been proved to be effective to improve the properties of biomass, the requirement of inert atmospheres, on the other hand, is a drawback in the economic aspect. However, if the flue gas consisting of oxygen, carbon dioxide and nitrogen, from a burner, could be utilised in the torrefaction process, the extra input of torrefied biomass under inert atmospheres could be diminished to achieve both economic and environmental efficiency. CO_2, as a massive output product during the thermal utilisation of fossil or lignocellulosic fuels, has been applied to the biomass torrefaction process.[231, 232, 235] It is reported that the introduction of CO_2 into inert atmospheres leads to more mass loss, higher energy yield and improved grindability.[238] Those promising results suggest that CO_2 can be served as a prospective medium for the torrefaction of biomass to yield bio-fuel with higher quality yet lower costs.

Therefore, the objective of this chapter is to obtain a better understanding in terms of the effect of temperature as well as CO_2 addition on the torrefaction of organosolv lignin and the subsequent pyrolysis. The physical properties and chemical compositions of the torrefied samples were analysed and compared. Also, UV fluorescence spectra were obtained for the aromatics in torrefied and subsequent pyrolysed lignin samples. These results will provide fundamental understandings for producing high-quality bio-fuel and desired value-added platform chemicals on the torrefaction and subsequent pyrolysis behaviour of lignin.

7.2 Characterisation of organosolv lignin torrefied under various temperatures and atmospheres

7.2.1 Conversion of the torrefied organosolv lignin

The mass yield of torrefied lignin under three different atmospheres and temperatures are presented in Figure 7.1. As can be seen, the increase of temperature leads to the decrease of solid yields in all three atmospheres, yet to various extend. In addition, the difference intensifies as the temperature evolves. While the addition of 5% of CO_2 shows a neglectable difference compared to the inert environment, the introduction of 15% of CO_2 results in a more noticeable decrease in all temperatures. For example, the mass yields decrease to 81.5%, 81.3% and 77.9% from 95.4%, 95.9% and 95.3% for pure nitrogen, co-feed with 5% CO_2 and 15% CO_2 respectively. The results comply with previous studies that the addition of CO_2 results in more mass loss during biomass, which could be attributed to the reactions of CO_2 with the fixed carbon within biomass[231] and enhanced thermal degradation[235].

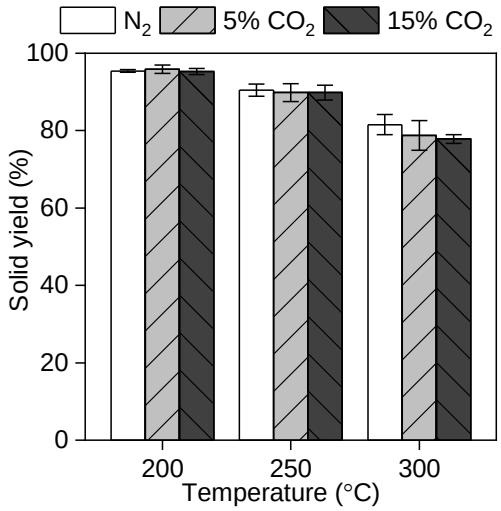

Figure 7.1 Solid yield of torrefied organosolv lignin under different atmospheres and temperatures

7.2.2 Elementary composition of the torrefied organosolv lignin

Further characterisation and comparison of the solid torrefied products under various temperatures and atmospheres are presented in Table 7-1. The ash content has a minor increase while the moisture content is largely reduced under all conditions. The fixed carbon content in the torrefied lignin samples is enhanced by the increase of torrefaction temperature. Also, generally, the addition of CO_2 yields torrefied lignin with higher carbon content. In addition, a higher torrefaction temperature results in a higher loss of hydrogen and oxygen. At the condition of 15% of CO_2 and 300 ºC, the oxygen content is the lowest. This result suggests that the introduction of CO_2 can facilitate oxygen removal efficiency. The HHV results show that torrefaction leads to an increase of HHV compared with raw lignin. And the addition of CO_2 has a minor influence on the HHV value. With the 5% introduction of CO_2 in the torrefaction atmosphere at 200 and 250 ºC, the HHV is higher than that in inert atmospheres. And at the atmosphere of 15% CO_2, the HHV is slightly lower at all torrefaction temperatures compared with lignin torrefied under N_2. The lower HHV value at other conditions with CO_2 addition could be attributed to the enhanced carbon loss. As for the energy yield, the effect of temperature and atmosphere follows the same trend as that of HHV.

Table 7-1 Ultimate, proximate analysis, estimated HHV and EY of torrefied lignin

Sample	Ultimate analysis				Proximate analysis (wt %)				HHV	EY	
	C	H	N	O*	Ash	Moisture	Volatile	Fixed carbon	(MJ/Kg)	(%)	
Raw-40	65.13	6.19	0.18	28.32	0.05	2.49	64.25	33.22	25.77	100.00	
N_2-200	65.86	5.97	0.16	28.01	0.14	0.98	65.42	33.45	25.79	95.48	
N_2-250	67.67	5.59	0.19	26.57	0.15	1.00	65.40	33.45	26.11	91.67	
N_2-300	68.94	5.49	0.25	25.32	0.09	1.28	65.61	33.02	26.62	84.22	
5% CO_2-200	67.17	6.10	0.28	26.45	0.06	0.90	65.38	33.65	26.04	96.90	
5% CO_2-250	68.10	5.46	0.19	26.25	0.07	1.03	65.52	33.65	26.45	92.21	
5% CO_2-300	69.05	5.43	0.18	25.35	0.05	1.42	64.92	33.61	26.57	81.88	
15% CO_2-200	66.51	5.73	0.18	27.59	0.11	0.92	65.94	33.03	25.64	94.78	
15% CO_2-250	66.75	5.57	0.18	27.51	0.06	1.06	65.25	33.64	25.77	89.85	
15% CO_2-300	69.75	4.99	0.18	25.09	0.08	1.36	65.41	33.15	26.23	77.47	

The van Krevelen plot is also illustrated in Figure 7.2. As can be seen, the atomic ratios of H/C and O/C in three atmospheres decrease with increasing temperature. With the addition of 5% CO_2, the O/C ratio is slightly reduced compared with inert atmospheres. And the addition of 15% CO_2 significantly lower both H/C and O/C ratios, especially at 300 ºC. In addition, the slopes for three atmospheres are 3.1, 3.6 and 4.0 respectively for N_2, 5% CO_2 and 15% CO_2. This result indicates that, with the introduction of CO_2, the slope inclines to the direction of losing more hydrogen than oxygen. In all samples, the slope is larger than that caused by dehydration reaction, with the slope being 2. This phenomenon indicates that the presence of demethoxylation reactions results in the release of methoxyl and methyl groups, and CO_2 facilitate those processes.

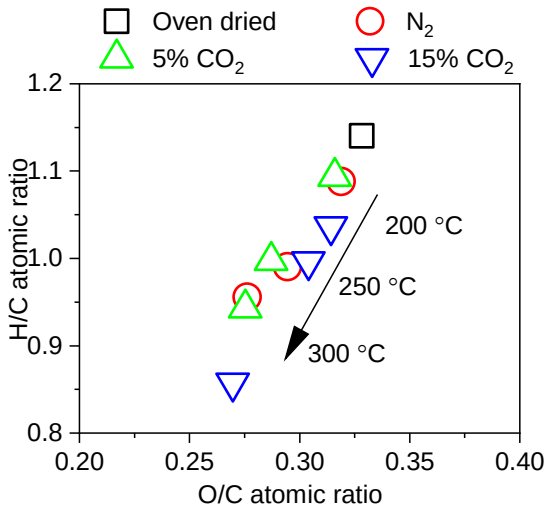

Figure 7.2 Van Krevelen plot of torrefied lignin under various temperatures and atmospheres

7.2.3 Morphological changes of the torrefied organosolv lignin

After torrefaction under various atmospheres and temperatures, the morphological changes of the samples were compared. As the temperature increases, the colour of the

sample evolves from brown to dark brown or black. Macroscopically, the torrefied lignin samples under inert atmospheres barely show large vesicles, compared to the hollow porous structure in lignin samples treated in CO_2. Also, the introduction of CO_2 yields a more crunchy structure, as a result of the enhanced reaction between CO_2 and generated volatiles.[324] In terms of the microscopical structure changes, the SEM photographs of the lignin samples before and after torrefaction under various temperatures and atmospheres are diagrammed in Figure 7.5. As shown in the photo, the raw lignin samples (oven-dried) present a semi-spherical porous structure. At all atmospheres, and even under a temperature as low as 200 ºC, the plasticisation of lignin began with the softening, melting and fusion into the lignin matrix. As a consequence, the cross-linked vesicles are gradually formed with the release of volatiles from the torrefied samples. In addition, presumably due to capillary and hydrophobic forces[325], the molten lignin samples will flow to form more densified structures with smaller inner pores. With the evolving temperature, the pore size within the residue structure tends to decrease, leaving a smooth, flat and almost nonporous surface with densified and homogeneous cubic structure. For comparison, the addition of CO_2, tends to yield a clear cross-section with fewer pores. In addition, higher CO_2 concentration leads to smoother and finer surfaces. Those physical changes indicate that high torrefaction temperature and CO_2 leads to intensified volatile release, thus leaving a frame with finer and densified inner structure but with large vesicles overall.

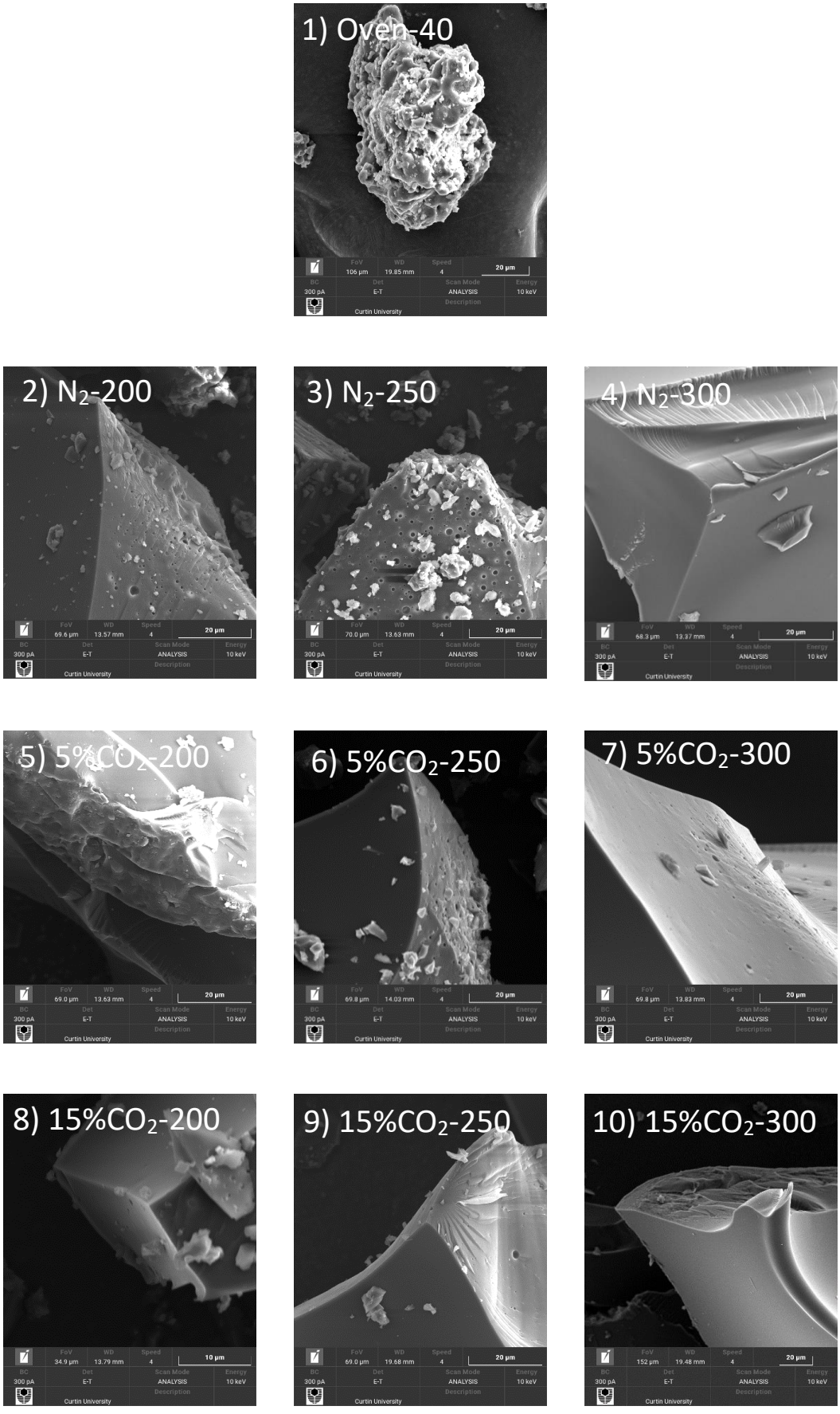

Figure 7.3 SEM photos of organosolv lignin samples before and after torrefaction

7.2.4 FTIR spectrum of the torrefied organosolv lignin

The FTIR spectrum of raw organoslov lignin and the torrefied lignin samples is presented in Figure 7.4, and the corresponding peak assignments are given in table 2. All lignin samples show the band at 3460 cm^{-1} for OH Stretching vibration, and its slight decrease with increasing temperature indicates the occurrence of dehydration reaction during torrefaction. The bands at 2925 and 1462 cm^{-1} are ascribed to CH_2 and CH_3 stretching vibrations, and the band at 2856 cm^{-1} is assigned to the C-H stretching of methyl or methoxyl groups. The sharp decrease of these bands with increased temperatures is likely due to the spitting of propyl side chains and methoxyls in lignin samples.[322] The bands at 1600, 1504 and 1422 cm^{-1} are corresponding to the aromatic skeletal vibration, C=C stretching vibration in aromatic rings and aromatic skeletal vibration together with C-H in-plane bending vibration, respectively. The reduction of the peak intensities suggests the release of aromatic rings in lignin[321]. In addition, the decline of signals at bands 1155, 1108 and 817 cm^{-1}, which are assigned to aromatic C-H deformations, aromatic C-H in-plane deformation and aromatic C-H out of plane bending, also suggests that the degradation of guaiacyl and syringyl structures. Those results are consistent with the results of the UV fluorescence spectrum that the introduction of CO_2 leads to more release of aromatics. The C-H bending and stretching in methyl and phenolic alcohol was observed at 1370 cm^{-1}. The bands at 1317, 1264, 1226, 988 and 896 cm^{-1}, which decrease with evaluated temperatures, are mainly assigned to C-O stretching. The decrease of those signals could be indicators[36] of the breakage of β-O-4 bonds and demethoxylation[322] and polycondensation reactions of lignin samples during torrefaction.

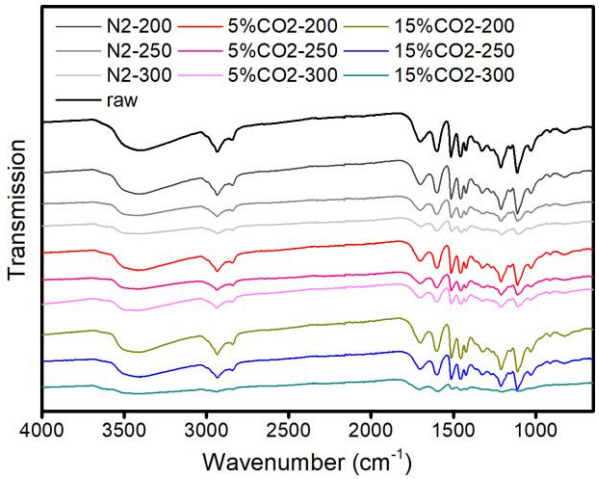

Figure 7.4 FT-IR spectra of lignin char samples from different pyrolysis temperatures in the region of 700–2000 cm^{-1}

Table 7-2 FTIR peak assignment of torrefied lignin samples[326-330]

Wavenumbers (cm^{-1})	Band assignments
3460	OH Stretching vibration
2925	Asymmetric –CH2–, symmetric –CH3 and –CH2– stretching vibrations
2856	C-H stretching of methyl/ methoxyl groups
1600	Aromatic skeletal vibration
1504	C=C stretching vibration in aromatic rings
1462	C-H bending vibration, CH3, CH2 asymmetric bending vibration aromatic skeletal vibration
1422	Aromatic skeletal vibration and C-H in-plane bending vibration
1370	C-H bending, C-H stretching in methyl and phenol OH
1317	C-O stretching of C5 substituted aromatic units
1264	C-O stretching
1226	C-C, C-O, C=O stretching
1155	Aromatic C-H deformations of guaiacyl ring
1108	Aromatic C-H in plane deformation
988	C-O stretching or –CH=CH- out of plane bending
896	C-O-C stretching
817	Aromatic C-H out of plane bending

7.2.5 UV-fluorescence spectrum of the solvent-soluble torrefied organosolv lignin and its generated volatiles

Figure 7.5 and Figure 7.6 show the UV spectra of the aromatic structures in the generated gaseous products and solvent-soluble residues. With increasing temperatures, the solvent-soluble gaseous aromatic shifts towards the direction with more fused rings. Besides, the addition of CO_2, especially with a higher concentration of 15%, results in yielding more aromatic structures with more fused rings. As for the lignin residues after torrefaction, all aromatic structures in three sample matrics experience a drop with increasing temperature. The intensity of aromatics follows a trend of 15% CO_2 < 5% CO_2 < N_2 at all three temperatures. This result suggests that the addition of CO_2 tends to release a large amount of aromatics from the solids to the volatile phase, and the process is intensified with a higher concentration of CO_2.

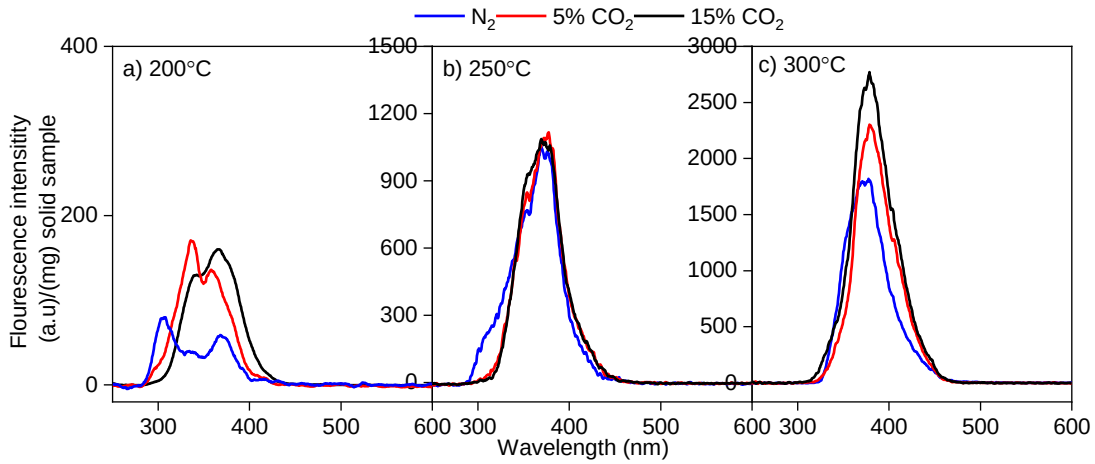

Figure 7.5 Constant energy (-2800 cm^{-1}) synchronous spectra of the solvent-soluble volatiles from the torrefaction of lignin at different temperatures and atmospheres

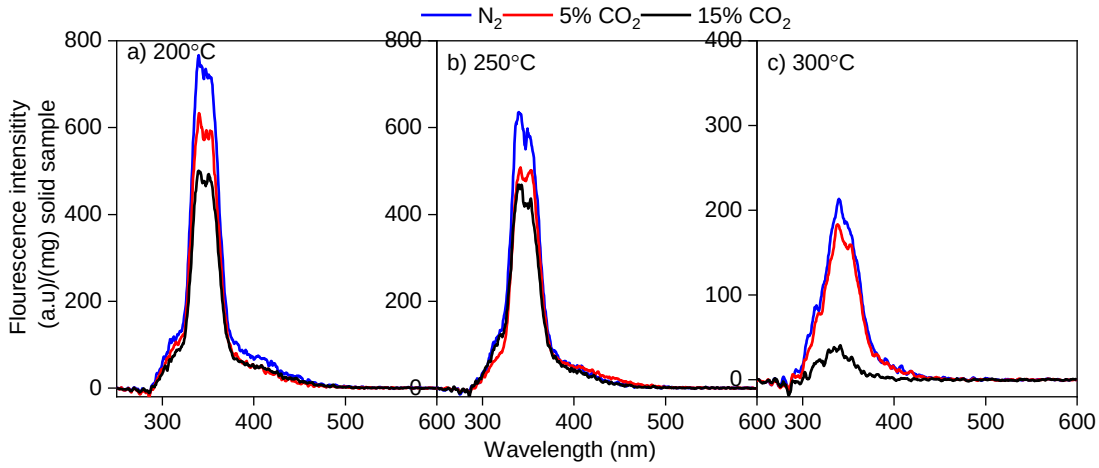

Figure 7.6 Constant energy (-2800 cm^{-1}) synchronous spectra of the solvent-soluble residues from the torrefaction of lignin at different temperatures and atmospheres

7.3 Effect of torrefaction on pyrolysis

7.3.1 Conversion of the torrefied organosolv lignin after pyrolysis

The product yields from pyrolysis of torrefied organosolv lignin at 500 ºC are listed in Figure 7.7. Higher torrefaction temperature results in the increasing char yield. For example, the char yield of torrefied lignin under three atmospheres is ~30% at 200 ºC, evaluated to ~34% at 250 ºC. Further increase of temperature leads to a sharp rise regarding char yield of ~41% to 61% under various atmospheres. As for the volatile yield, the increase of torrefaction temperature causes the reduction of tar yield, especially at high torrefaction temperature. For instance, only ~18% of tar is produced from the pyrolysis of torrefied lignin under 300 ºC and 15% CO_2 addition. In terms of the effect of CO_2 addition, at torrefaction temperatures of 200 and 250 ºC, the higher concentration of CO_2 exists in the torrefied atmosphere, and the more volatile is released from the pyrolysis of torrefied lignin. However, at 300 ºC, the addition of a high level of 15% CO_2 boosts the char yield dramatically and suppress the generation

of primary volatile. It suggests that CO_2 inclines toward the reaction with hydrogenated and oxygenated groups, generating carbon-abundant char.[331] As clarified in previous sections, the structure of torrefied lignin under 300 ºC with 15% CO_2 addition is very stable with only minor functional groups available and a small amount of aromatics existing. In addition, as shown in the SEM pictures, the more densified morphology of lignin samples after torrefied with CO_2 addition, provide less opportunity for the generation and escape of gaseous products. This phenomenon could lead to less testified ejection effect which is widely occurred during lignin pyrolysis. As a result, fewer condensable volatiles is generated and collected compared with other torrefied lignin samples. Similarly, while the torrefaction temperature is less intense, porous structures remain in lignin matrix and are less visible with the addition of CO_2. Therefore, fewer gas products are produced.

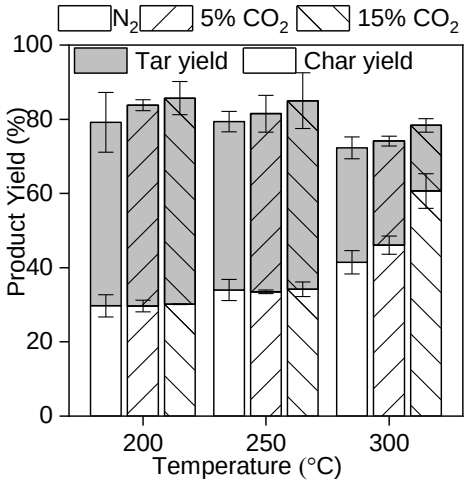

Figure 7.7 Pyrolysis product yields of torrefied organosolv lignin samples at 500 ºC

7.3.2 UV-fluorescence spectrum of the pyrolysis of torrefied organosolv lignin

In order to have an understanding of the evolution of aromatics from the pyrolysis of torrefied lignin under various conditions, the UV spectra are presented in Figure 7.8 and Figure 7.9. For the solvent-soluble gaseous products, the increase of torrefied temperature leads to a minor increase of aromatics released during pyrolysis in the N_2 torrefied lignin samples. While the increase of temperature from 200 to 250 ºC shows neglectable effects in the conditions of CO_2 addition, the further increase of temperature results in the sharp decrease of aromatic volatiles produced from the pyrolysis of 15% CO_2 torrefied lignin. This result is consistent with previous research[332] that tar generated in CO_2 atmosphere is less aromatic than N_2 atmosphere during pyrolysis. As for the dissolved char residues, it shows a completely different tendency. The amount of aromatics within the char residues in three atmospheres under 200 ºC is almost identical, while only aromatics in samples treated with 15% CO_2 is more than the aromatic char in other temperatures. In addition, in terms of the pyrolysed char of 15% CO_2 torrefied lignin, the aromatics remained only shows minor change with the evaluated temperature but is significantly higher than that treated in the other atmospheres at temperature 250 to 300 ºC.

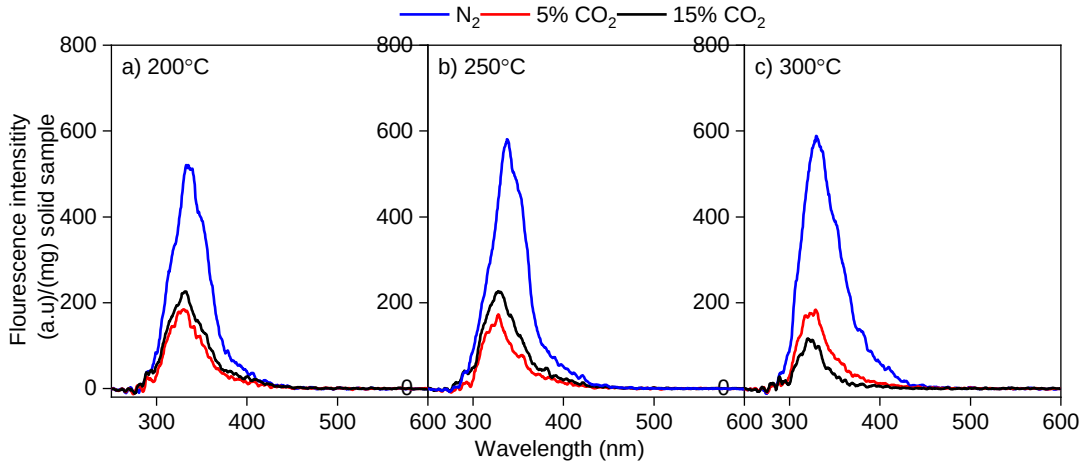

Figure 7.8 Constant energy (-2800 cm^{-1}) synchronous spectra of the solvent-soluble volatiles from the pyrolysis of torrefied lignin at different temperatures and atmospheres

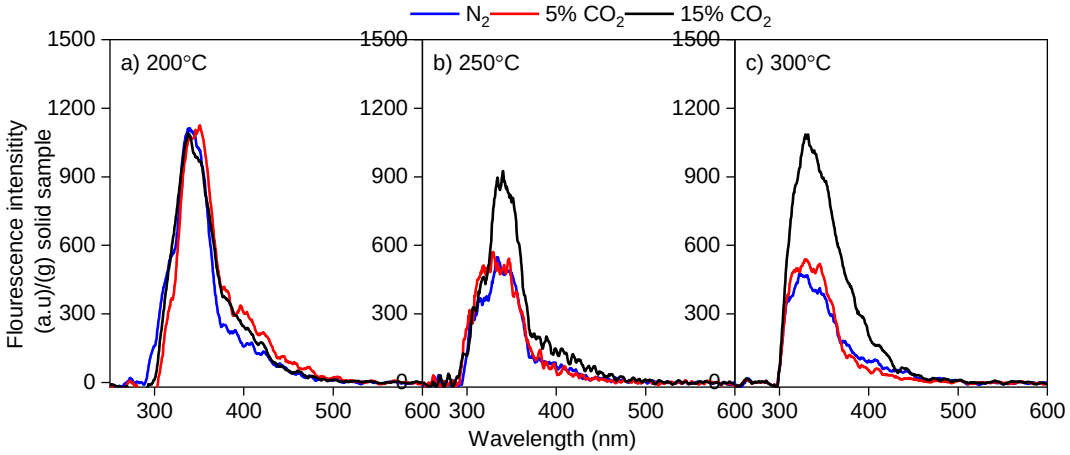

Figure 7.9 Constant energy (-2800 cm^{-1}) synchronous spectra of the soluble solid residues from the pyrolysis of torrefied lignin at different temperatures and atmospheres

7.4 Conclusions

This study reports the effect of CO_2 assisted torrefaction on lignin and the subsequent pyrolysis process. During torrefaction, a series of reactions takes place, such as breakage of β-O-4 bonds, demethoxylation to release methoxyl and methyl groups and polycondensation reactions. Those reactions result in char residues with better grindability and higher heating value. The addition of CO_2 facilitates the thermal degradation of lignin, resulting in more weight loss. Higher CO_2 concentration leads to smoother and finer surfaces, releasing more aromatic structures with more fused rings to the gaseous products. For the subsequent pyrolysis, higher torrefaction temperature leads to significantly higher char yield. And the addition of 15% CO_2 tends to reserve more aromatics in the char residues at 300 ºC.

CHAPTER 8 Conclusions and Recommendations

8.1 Introduction

This chapter presents the key discoveries of this PhD study with recommendations for future work. Overall, this research has investigated the chemistry of pyrolytic behaviour of biomass model components and biomass-derived products, with a focus on the primary products with minimised secondary reactions. A new quantification method for determining the contribution of thermal ejection and evaporation during cellulose pyrolysis has been proposed in this research. In addition, this study also characterises the physical properties and chemical reaction pathways during the pyrolysis of biomass-derived products.

8.2 Conclusions

Several conclusions can be drawn based on the above information in Chapter 4−7.

8.2.1 Contributions of thermal ejection and evaporation to primary tar formation during cellulose pyrolysis in a wire mesh reactor at various heating rates

- Up to 29% of ejected aerosol and ~ 39% of evaporated vapour were collected with different compositions.
- While AC3-5 present in the ejected products, 5-HMF only occurs in the evaporated vapours.

- The collection efficiency of ejection and evaporation reach up to 58% and 95% respectively in this research.
- The proportion of ejection is enhanced by the intensified heating rates, accounting for 29% to 57% of cellulose intermediates while the proportion of evaporation is inhibited from 43% to 28%.
- The ejection process is remarkably intensified by the increasing heating rate, producing aerosols with larger particle diameters.

8.2.2 Formation of reaction intermediates and primary volatiles during acid-catalysed fast pyrolysis of cellulose in a wire-mesh reactor

- At temperatures <100 ºC, hydrolysis reactions can take place to form glucose due to the presence of acid and water.
- Once glucose is formed, it can be easily dehydrated to form AGF at ~120 ºC.
- At temperatures >160 ºC, dehydration reactions of glucose, levoglucosan and AGF take place to form 5-HMF and LGO.
- When the temperature increases to 240 ºC, aromatic compounds are formed.
- Once those compounds are produced, they can be released into the vapour phase via either evaporation or thermal ejection.

8.2.3 The release and transformation of organic and inorganic sodium during the fast pyrolysis of sodium impregnated lignin

- During the pyrolysis process, lignin experiences a molten intermediate phase where the transformation and evolution of different sodium occurs.
- The transformation is intensified with increasing temperature.

- At low temperatures, the ejection effect already occurs under the high heating rate condition, generating aerosols that not only consists of organic but also inorganic sodium.
- Some organic bonded sodium components with low boiling points can be released to the tar phase via evaporation.
- As the ejection and evaporation undergoes, the evolution of sodium forms within the molten phase continues, but most sodium is still retained in char residues.

8.2.4 Effect of carbon dioxide assisted torrefaction on the fast pyrolysis of lignin in a wire-mesh reactor

- During torrefaction, a series of reactions takes place, such as breakage of β-O-4 bonds, demethoxylation to release methoxyl and methyl groups and polycondensation reactions. Those reactions result in residues with better grindability and higher heating value.
- The addition of CO_2 facilitates the thermal degradation of lignin, resulting in more weight loss. Higher CO_2 concentration leads to smoother and finer surfaces, releasing more aromatic structures with more fused rings to the gaseous products.
- For the subsequent pyrolysis, higher torrefaction temperature leads to significantly higher char yield. And the addition of 15% CO_2 tends to reserve more aromatics in the char residues at 300 ºC.

8.3 Recommendations

Based on the above findings in this study, future research should be addressed to supplement the following research gaps:

- Contribution and characterisation of ejection and evaporation of other biomass components, and biomass-derived products during pyrolysis process should be further investigated. And the parameters affecting the ejection mechanism and the product distribution, such as particle size, temperature and inorganics, should be clarified. Basing on the individual pyrolytic behaviours and contribution of ejection, a systematic model should be developed to predict the ejected aerosols and evaporated vapours according to the compositions of the feedstock.
- The pyrolysis acid and AAEM catalysed biomass can be conducted using a fixed bed reactor where secondary reactions cannot be minimised. Analysing the generated product, together with the current research findings, the mechanism of secondary reaction is able to be revealed.
- The effect of different atmospheres during lignin torrefaction, especially the product distribution should be systematic addressed.

REFERENCES

1. Smeets EM, Faaij AP, Lewandowski IM, Turkenburg WC. A bottom-up assessment and review of global bio-energy potentials to 2050. Progress in Energy and combustion science. 2007;33(1):56-106.

2. Czernik S, Bridgwater A. Overview of applications of biomass fast pyrolysis oil. Energy & fuels. 2004;18(2):590-598.

3. Mohan D, Pittman CU, Steele PH. Pyrolysis of wood/biomass for bio-oil: a critical review. Energy & fuels. 2006;20(3):848-889.

4. Oasmaa A, Czernik S. Fuel oil quality of biomass pyrolysis oils state of the art for the end users. Energy & Fuels. 1999;13(4):914-921.

5. Huber GW, Iborra S, Corma A. Synthesis of transportation fuels from biomass: chemistry, catalysts, and engineering. Chemical reviews. 2006;106(9):4044-4098.

6. Bridgwater A, Meier D, Radlein D. An overview of fast pyrolysis of biomass. Organic geochemistry. 1999;30(12):1479-1493.

7. McKendry P. Energy production from biomass (part 1): overview of biomass. Bioresource technology. 2002;83(1):37-46.

8. Yang H, Yan R, Chen H, Zheng C, Lee DH, Liang DT. In-depth investigation of biomass pyrolysis based on three major components: hemicellulose, cellulose and lignin. Energy & Fuels. 2006;20(1):388-393.

9. Mettler MS, Vlachos DG, Dauenhauer PJ. Top ten fundamental challenges of biomass pyrolysis for biofuels. Energy & Environmental Science. 2012;5(7):7797-7809.

10. Bridgwater AV, Czernik S, Diebold J, Meier D, Oasmaa A, Peacocke C, et al. Fast pyrolysis of biomass: a handbook. CPL press Newbury; 1999.

11. Lédé J, Li HZ, Villermaux J, Martin H. Fusion-like behaviour of wood pyrolysis. Journal of analytical and applied pyrolysis. 1987;10(4):291-308.

12. Teixeira AR, Gantt R, Joseph KE, Maduskar S, Paulsen AD, Krumm C, et al. Spontaneous aerosol ejection: origin of inorganic particles in biomass pyrolysis. ChemSusChem. 2016;9(11):1322-1328.

13. Teixeira AR, Mooney KG, Kruger JS, Williams CL, Suszynski WJ, Schmidt LD, et al. Aerosol generation by reactive boiling ejection of molten cellulose. Energy & Environmental Science. 2011;4(10):4306-4321.

14. Pollard AS, Rover MR, Brown RC. Characterization of bio-oil recovered as stage fractions with unique chemical and physical properties. Journal of Analytical and Applied Pyrolysis. 2012;93:129-138.

15. Tzanetakis T, Ashgriz N, James D, Thomson M. Liquid fuel properties of a hardwood-derived bio-oil fraction. Energy & Fuels. 2008;22(4):2725-2733.

16. Gong X, Yu Y, Gao X, Qiao Y, Xu M, Wu H. Formation of anhydro-sugars in the primary volatiles and solid residues from cellulose fast pyrolysis in a wire-mesh reactor. Energy & Fuels. 2014;28(8):5204-5211.

17. Anthony DB, Howard JB, Hottel HC, Meissner HP. Rapid devolatilisation and hydrogasification of bituminous coal. Fuel. 1976;55(2):121-128.

18. Suuberg EM, Peters WA, Howard JB. Product composition and kinetics of lignite pyrolysis. Industrial & Engineering Chemistry Process Design and Development. 1978;17(1):37-46.

19. Guell AJ, Kandiyoti R. Development of a gas-sweep facility for the direct capture of pyrolysis tars in a variable heating rate high-pressure wire-mesh reactor. Energy & fuels. 1993;7(6):943-952.

20. Li C-Z, Bartle KD, Kandiyoti R. Characterization of tars from variable heating rate pyrolysis of maceral concentrates. Fuel. 1993;72(1):3-11.

21. Chaala A, Ba T, Garcia-Perez M, Roy C. Colloidal properties of bio-oils obtained by vacuum pyrolysis of softwood bark: aging and thermal stability. Energy & fuels. 2004;18(5):1535-1542.

22. Lu Q, Li W-Z, Zhu X-F. Overview of fuel properties of biomass fast pyrolysis oils. Energy conversion and management. 2009;50(5):1376-1383.

23. Dobele G, Dizhbite T, Rossinskaja G, Telysheva G, Meier D, Radtke S, et al. Pre-treatment of biomass with phosphoric acid prior to fast pyrolysis: a promising method for obtaining 1, 6-anhydrosaccharides in high yields. Journal of Analytical and Applied Pyrolysis. 2003;68:197-211.

24. Hu B, Lu Q, Wu Y-t, Zhang Z-x, Cui M-s, Liu D-j, et al. Catalytic mechanism of sulfuric acid in cellulose pyrolysis: A combined experimental and computational investigation. Journal of analytical and applied pyrolysis. 2018;134:183-194.

25. Long Y, Yu Y, Chua YW, Wu H. Acid-catalysed cellulose pyrolysis at low temperatures. Fuel. 2017;193:460-466.

26. Oudenhoven S, Westerhof RJM, Aldenkamp N, Brilman DWF, Kersten SR. Demineralization of wood using wood-derived acid: Towards a selective pyrolysis process for fuel and chemicals production. Journal of analytical and applied pyrolysis. 2013;103:112-118.

27. Sui X-w, Wang Z, Liao B, Zhang Y, Guo Q-x. Preparation of levoglucosenone through sulfuric acid promoted pyrolysis of bagasse at low temperature. Bioresource technology. 2012;103(1):466-469.

28. Wang Z, Zhou S, Pecha B, Westerhof RJ, Garcia-Perez M. Effect of pyrolysis temperature and sulfuric acid during the fast pyrolysis of cellulose and douglas fir in an atmospheric pressure wire mesh reactor. Energy & fuels. 2014;28(8):5167-5177.

29. Dalluge DL, Kim KH, Brown RC. The influence of alkali and alkaline earth metals on char and volatile aromatics from fast pyrolysis of lignin. Journal of analytical and applied pyrolysis. 2017;127:385-393.

30. Guo D-l, Wu S-b, Liu B, Yin X-l, Yang Q. Catalytic effects of NaOH and Na2CO3 additives on alkali lignin pyrolysis and gasification. Applied Energy. 2012;95:22-30.

31. Guo D-l, Yuan H-y, Yin X-l, Wu C-z, Wu S-b, Zhou Z-q. Effects of chemical form of sodium on the product characteristics of alkali lignin pyrolysis. Bioresource technology. 2014;152:147-153.

32. Wang S, Li Z, Bai X, Yi W, Fu P. Influence of inherent hierarchical porous char with alkali and alkaline earth metallic species on lignin pyrolysis. Bioresource technology. 2018;268:323-331.

33. Wang W-L, Ren X-Y, Li L-F, Chang J-M, Cai L-P, Geng J. Catalytic effect of metal chlorides on analytical pyrolysis of alkali lignin. Fuel Processing Technology. 2015;134:345-351.

34. Meng J, Park J, Tilotta D, Park S. The effect of torrefaction on the chemistry of fast-pyrolysis bio-oil. Bioresource technology. 2012;111:439-446.

35. Van der Stelt M, Gerhauser H, Kiel J, Ptasinski K. Biomass upgrading by torrefaction for the production of biofuels: A review. Biomass and bioenergy. 2011;35(9):3748-3762.

36. Zheng A, Jiang L, Zhao Z, Huang Z, Zhao K, Wei G, et al. Impact of torrefaction on the chemical structure and catalytic fast pyrolysis behavior of hemicellulose, lignin, and cellulose. Energy & Fuels. 2015;29(12):8027-8034.

37. Jakab E, Faix O, Till F, Székely T. The effect of cations on the thermal decomposition of lignins. Journal of analytical and applied pyrolysis. 1993;25:185-194.

38. Dobele G, Rossinskaja G, Telysheva G, Meier D, Faix O. Cellulose dehydration and depolymerization reactions during pyrolysis in the presence of phosphoric acid. Journal of Analytical and Applied Pyrolysis. 1999;49(1-2):307-317.

39. Dobele G, Meier D, Faix O, Radtke S, Rossinskaja G, Telysheva G. Volatile products of catalytic flash pyrolysis of celluloses. Journal of Analytical and Applied Pyrolysis. 2001;58:453-463.

40. Julien S, Chornet E, Overend R. Influence of acid pre-treatment (H2SO4, HCl, HNO3) on reaction selectivity in the vacuum pyrolysis of cellulose. Journal of Analytical and Applied Pyrolysis. 1993;27(1):25-43.

41. Chen D, Cen K, Jing X, Gao J, Li C, Ma Z. An approach for upgrading biomass and pyrolysis product quality using a combination of aqueous phase bio-oil washing and torrefaction pre-treatment. Bioresource technology. 2017;233:150-158.

42. Wang Q, Song H, Pan S, Dong N, Wang X, Sun S. Initial pyrolysis mechanism and product formation of cellulose: An Experimental and Density functional theory (DFT) study. Scientific reports. 2020;10(1):1-18.

43. Lehto J, Oasmaa A, Solantausta Y, Kytö M, Chiaramonti D. Review of fuel oil quality and combustion of fast pyrolysis bio-oils from lignocellulosic biomass. Applied Energy. 2014;116:178-190.

44. Oasmaa A, Elliott DC, Korhonen J. Acidity of biomass fast pyrolysis bio-oils. Energy & Fuels. 2010;24(12):6548-6554.

45. Czernik S, Johnson DK, Black S. Stability of wood fast pyrolysis oil. Biomass and Bioenergy. 1994;7(1-6):187-192.

46. Stefanidis SD, Kalogiannis KG, Iliopoulou EF, Michailof CM, Pilavachi PA, Lappas AA. A study of lignocellulosic biomass pyrolysis via the pyrolysis of cellulose, hemicellulose and lignin. Journal of analytical and applied pyrolysis. 2014;105:143-150.

47. Xu F, Yu J, Tesso T, Dowell F, Wang D. Qualitative and quantitative analysis of lignocellulosic biomass using infrared techniques: a mini-review. Applied energy. 2013;104:801-809.

48. Bajpai P. Structure of lignocellulosic biomass. In: Pre-treatment of lignocellulosic biomass for biofuel production: Springer; 2016. p. 7-12.

49. McGinnis G, Shafizadeh F. Cellulose and hemicellulose. Pulp and paper chemistry and chemical technology. 1980;1:3.

50. Yu H, Zhang Z, Li Z, Chen D. Characteristics of tar formation during cellulose, hemicellulose and lignin gasification. Fuel. 2014;118:250-256.

51. Liu L, Sun J, Cai C, Wang S, Pei H, Zhang J. Corn stover pre-treatment by inorganic salts and its effects on hemicellulose and cellulose degradation. Bioresource technology. 2009;100(23):5865-5871.

52. Bridgwater A, Peacocke G. Fast pyrolysis processes for biomass. Renewable and sustainable energy reviews. 2000;4(1):1-73.

53. Bridgwater A, Cottam M. Opportunities for biomass pyrolysis liquids production and upgrading. Energy & Fuels. 1992;6(2):113-120.

54. Di Blasi C. Modeling chemical and physical processes of wood and biomass pyrolysis. Progress in energy and combustion science. 2008;34(1):47-90.

55. Wyman CE. Ethanol from lignocellulosic biomass: technology, economics, and opportunities. Bioresource Technology. 1994;50(1):3-15.

56. Mood SH, Golfeshan AH, Tabatabaei M, Jouzani GS, Najafi GH, Gholami M, et al. Lignocellulosic biomass to bioethanol, a comprehensive review with a focus on pre-treatment. Renewable and Sustainable Energy Reviews. 2013;27:77-93.

57. Bridgewater AV. Biomass fast pyrolysis. Thermal science. 2004;8(2):21-50.

58. Bridgwater A. Principles and practice of biomass fast pyrolysis processes for liquids. Journal of analytical and applied pyrolysis. 1999;51(1-2):3-22.

59. Wright MM, Daugaard DE, Satrio JA, Brown RC. Techno-economic analysis of biomass fast pyrolysis to transportation fuels. Fuel. 2010;89:S2-S10.

60. Wang S, Dai G, Yang H, Luo Z. Lignocellulosic biomass pyrolysis mechanism: a state-of-the-art review. Progress in Energy and Combustion Science. 2017;62:33-86.

61. Lédé J, Diebold J, Peacocke G, Piskorz J. The nature and properties of intermediate and unvaporized biomass pyrolysis materials. In: Developments in thermochemical biomass conversion: Springer; 1997. p. 27-42.

62. Tiarks JA, Dedic CE, Meyer TR, Brown RC, Michael JB. Visualization of physicochemical phenomena during biomass pyrolysis in an optically accessible reactor. Journal of Analytical and Applied Pyrolysis. 2019;143:104667.

63. Kan T, Strezov V, Evans TJ. Lignocellulosic biomass pyrolysis: A review of product properties and effects of pyrolysis parameters. Renewable and Sustainable Energy Reviews. 2016;57:1126-1140.

64. Bridgwater AV. Renewable fuels and chemicals by thermal processing of biomass. Chemical engineering journal. 2003;91(2-3):87-102.

65. Goyal H, Seal D, Saxena R. Bio-fuels from thermochemical conversion of renewable resources: a review. Renewable and sustainable energy reviews. 2008;12(2):504-517.

66. Yu J, Paterson N, Blamey J, Millan M. Cellulose, xylan and lignin interactions during pyrolysis of lignocellulosic biomass. Fuel. 2017;191:140-149. doi:10.1016/j.fuel.2016.11.057

67. Butler E, Devlin G, Meier D, McDonnell K. Characterisation of spruce, salix, miscanthus and wheat straw for pyrolysis applications. Bioresource technology. 2013;131:202-209.

68. Collard F-X, Blin J, Bensakhria A, Valette J. Influence of impregnated metal on the pyrolysis conversion of biomass constituents. Journal of Analytical and Applied Pyrolysis. 2012;95:213-226.

69. Mamleev V, Bourbigot S, Le Bras M, Yvon J. The facts and hypotheses relating to the phenomenological model of cellulose pyrolysis: Interdependence of the steps. Journal of Analytical and Applied Pyrolysis. 2009;84(1):1-17.

70. Van de Velden M, Baeyens J, Brems A, Janssens B, Dewil R. Fundamentals, kinetics and endothermicity of the biomass pyrolysis reaction. Renewable energy. 2010;35(1):232-242.

71. Lu Q, Yang X-c, Dong C-q, Zhang Z-f, Zhang X-m, Zhu X-f. Influence of pyrolysis temperature and time on the cellulose fast pyrolysis products: Analytical Py-GC/MS study. Journal of Analytical and Applied Pyrolysis. 2011;92(2):430-438.

72. Hosoya T, Kawamoto H, Saka S. Role of methoxyl group in char formation from lignin-related compounds. Journal of Analytical and Applied Pyrolysis. 2009;84(1):79-83.

73. Elyounssi K, Collard F-X, Mateke J-aN, Blin J. Improvement of charcoal yield by two-step pyrolysis on eucalyptus wood: A thermogravimetric study. Fuel. 2012;96:161-167.

74. Wooten JB, Seeman JI, Hajaligol MR. Observation and characterization of cellulose pyrolysis intermediates by 13C CPMAS NMR. A new mechanistic model. Energy & fuels. 2004;18(1):1-15.

75. Collard F-X, Blin J. A review on pyrolysis of biomass constituents: Mechanisms and composition of the products obtained from the conversion of cellulose, hemicelluloses and lignin. Renewable and Sustainable Energy Reviews. 2014;38:594-608.

76. Neves D, Thunman H, Matos A, Tarelho L, Gómez-Barea A. Characterization and prediction of biomass pyrolysis products. Progress in Energy and Combustion Science. 2011;37(5):611-630.

77. Akhtar J, Amin NS. A review on operating parameters for optimum liquid oil yield in biomass pyrolysis. Renewable and Sustainable Energy Reviews. 2012;16(7):5101-5109.

78. Anca-Couce A. Reaction mechanisms and multi-scale modelling of lignocellulosic biomass pyrolysis. Progress in Energy and Combustion Science. 2016;53:41-79.

79. Demirbaş A. Mechanisms of liquefaction and pyrolysis reactions of biomass. Energy conversion and management. 2000;41(6):633-646.

80. Carpenter D, Westover TL, Czernik S, Jablonski W. Biomass feedstocks for renewable fuel production: a review of the impacts of feedstock and pre-treatment on the yield and product distribution of fast pyrolysis bio-oils and vapors. Green Chemistry. 2014;16(2):384-406.

81. McGrath TE, Chan WG, Hajaligol MR. Low temperature mechanism for the formation of polycyclic aromatic hydrocarbons from the pyrolysis of cellulose. Journal of Analytical and Applied Pyrolysis. 2003;66(1-2):51-70.

82. Pastorova I, Botto RE, Arisz PW, Boon JJ. Cellulose char structure: a combined analytical Py-GC-MS, FTIR, and NMR study. Carbohydrate research. 1994;262(1):27-47.

83. Scheirs J, Camino G, Tumiatti W. Overview of water evolution during the thermal degradation of cellulose. European Polymer Journal. 2001;37(5):933-942.

84. Cetin E, Moghtaderi B, Gupta R, Wall T. Influence of pyrolysis conditions on the structure and gasification reactivity of biomass chars. Fuel. 2004;83(16):2139-2150.

85. Guerrero M, Ruiz M, Alzueta M, Bilbao R, Millera A. Pyrolysis of eucalyptus at different heating rates: studies of char characterization and oxidative reactivity. Journal of Analytical and Applied Pyrolysis. 2005;74(1-2):307-314.

86. Olsson JG, Jäglid U, Pettersson JB, Hald P. Alkali metal emission during pyrolysis of biomass. Energy & Fuels. 1997;11(4):779-784.

87. Werkelin J, Skrifvars B-J, Zevenhoven M, Holmbom B, Hupa M. Chemical forms of ash-forming elements in woody biomass fuels. Fuel. 2010;89(2):481-493.

88. Obernberger I. Strategy for the application of novel characterization methods for biomass fuels: case study of straw. Energy & fuels. 2014;28(2):1041-1052.

89. Jahirul MI, Rasul MG, Chowdhury AA, Ashwath N. Biofuels production through biomass pyrolysis—a technological review. Energies. 2012;5(12):4952-5001.

90. Piskorz J, Scott D, Radlein D Pyrolysis oils from biomass: Producing analyzing and upgrading. Symposium Series; 1988 American Chemical Society Washington, DC; p.

91. Scholze B, Hanser C, Meier D. Characterization of the water-insoluble fraction from fast pyrolysis liquids (pyrolytic lignin): Part II. GPC, carbonyl goups, and 13C-NMR. Journal of Analytical and Applied Pyrolysis. 2001;58:387-400.

92. Bai X, Kim KH, Brown RC, Dalluge E, Hutchinson C, Lee YJ, et al. Formation of phenolic oligomers during fast pyrolysis of lignin. Fuel. 2014;128:170-179.

93. Piskorz J, Majerski P, Radlein D. In Biomass. A Growth Opportunity in Green Energy and Value-Added Products, RP Overend and E. Chronet (Eds.) Elsevier Science, Amsterdam; 1999.

94. Dauenhauer PJ, Colby JL, Balonek CM, Suszynski WJ, Schmidt LD. Reactive boiling of cellulose for integrated catalysis through an intermediate liquid. Green Chemistry. 2009;11(10):1555-1561.

95. Wang Z, McDonald AG, Westerhof RJ, Kersten SR, Cuba-Torres CM, Ha S, et al. Effect of cellulose crystallinity on the formation of a liquid intermediate and on product distribution during pyrolysis. Journal of analytical and applied pyrolysis. 2013;100:56-66.

96. Zhou S, Pecha B, van Kuppevelt M, McDonald AG, Garcia-Perez M. Slow and fast pyrolysis of Douglas-fir lignin: Importance of liquid-intermediate formation on the distribution of products. Biomass and Bioenergy. 2014;66:398-409.

97. Montoya J, Pecha B, Janna FC, Garcia-Perez M. Micro-explosion of liquid intermediates during the fast pyrolysis of sucrose and organosolv lignin. Journal of Analytical and Applied Pyrolysis. 2016;122:106-121.

98. Montoya J, Pecha B, Janna FC, Garcia-Perez M. Single particle model for biomass pyrolysis with bubble formation dynamics inside the liquid intermediate and its contribution to aerosol formation by thermal ejection. Journal of Analytical and Applied Pyrolysis. 2017;124:204-218.

99. Fratini E, Bonini M, Oasmaa A, Solantausta Y, Teixeira J, Baglioni P. SANS analysis of the microstructural evolution during the aging of pyrolysis oils from biomass. Langmuir. 2006;22(1):306-312.

100. Lédé J, Broust F, Ndiaye F-T, Ferrer M. Properties of bio-oils produced by biomass fast pyrolysis in a cyclone reactor. Fuel. 2007;86(12-13):1800-1810.

101. Wiinikka H, Carlsson P, Johansson A-C, Gullberg M, Ylipää C, Lundgren M, et al. Fast pyrolysis of stem wood in a pilot-scale cyclone reactor. Energy & Fuels. 2015;29(5):3158-3167.

102. Piskorz J, Majerski P, Radlein D. Pyrolysis of biomass-aerosol generation: properties, applications, and significance for process engineers. 1999

103. Chen T, Deng C, Liu R. Effect of selective condensation on the characterization of bio-oil from pine sawdust fast pyrolysis using a fluidized-bed reactor. Energy & Fuels. 2010;24(12):6616-6623.

104. Jendoubi N, Broust F, Commandre J-M, Mauviel G, Sardin M, Lede J. Inorganics distribution in bio oils and char produced by biomass fast pyrolysis: The key role of aerosols. Journal of Analytical and Applied Pyrolysis. 2011;92(1):59-67.

105. Wiinikka H, Johansson A-C, Sandström L, Öhrman OG. Fate of inorganic elements during fast pyrolysis of biomass in a cyclone reactor. Fuel. 2017;203:537-547.

106. Johansson A-C, Wiinikka H, Sandström L, Marklund M, Öhrman OG, Narvesjö J. Characterization of pyrolysis products produced from different Nordic biomass types in a cyclone pilot plant. Fuel processing technology. 2016;146:9-19.

107. Johansson A-C, Iisa K, Sandström L, Ben H, Pilath H, Deutch S, et al. Fractional condensation of pyrolysis vapors produced from Nordic feedstocks in cyclone pyrolysis. Journal of Analytical and Applied Pyrolysis. 2017;123:244-254.

108. Montoya J, Pecha B, Janna FC, Garcia-Perez M. Methodology for estimation of thermal ejection droplet size distribution and intensity during the pyrolysis of sugarcane bagasse and model compounds. Journal of Analytical and Applied Pyrolysis. 2017;125:69-82.

109. Iisa K, Johansson A-C, Pettersson E, French RJ, Orton KA, Wiinikka H. Chemical and physical characterization of aerosols from fast pyrolysis of biomass. Journal of Analytical and Applied Pyrolysis. 2019;142:104606.

110. Jenkins B, Baxter L, Miles Jr T, Miles T. Combustion properties of biomass. Fuel processing technology. 1998;54(1-3):17-46.

111. Obernberger I, Biedermann F, Widmann W, Riedl R. Concentrations of inorganic elements in biomass fuels and recovery in the different ash fractions. Biomass and bioenergy. 1997;12(3):211-224.

112. Hansen LA, Nielsen HP, Frandsen FJ, Dam-Johansen K, Hørlyck S, Karlsson A. Influence of deposit formation on corrosion at a straw-fired boiler. Fuel processing technology. 2000;64(1-3):189-209.

113. Krässig HA. Cellulose: structure, accessibility and reactivity. Gordon and Breach Science Publ.; 1993.

114. Zhao X, Zhang L, Liu D. Biomass recalcitrance. Part I: the chemical compositions and physical structures affecting the enzymatic hydrolysis of lignocellulose. Biofuels, Bioproducts and Biorefining. 2012;6(4):465-482.

115. Poletto M, Ornaghi HL, Zattera AJ. Native cellulose: structure, characterization and thermal properties. Materials. 2014;7(9):6105-6119.

116. Karimi K, Shafiei M, Kumar R. Progress in physical and chemical pre-treatment of lignocellulosic biomass. In: Biofuel technologies: Springer; 2013. p. 53-96.

117. Festucci-Buselli RA, Otoni WC, Joshi CP. Structure, organization, and functions of cellulose synthase complexes in higher plants. Brazilian Journal of Plant Physiology. 2007;19(1):1-13.

118. Mettler MS, Paulsen AD, Vlachos DG, Dauenhauer PJ. The chain length effect in pyrolysis: bridging the gap between glucose and cellulose. Green Chemistry. 2012;14(5):1284-1288.

119. Mazeau K, Heux L. Molecular dynamics simulations of bulk native crystalline and amorphous structures of cellulose. The Journal of Physical Chemistry B. 2003;107(10):2394-2403.

120. Richards G. Chemistry of pyrolysis of polysaccharides and lignocellulosics. In: Advances in Thermochemical Biomass Conversion: Springer; 1993. p. 727-745.

121. Boutin O, Ferrer M, Lédé J. Radiant flash pyrolysis of cellulose—Evidence for the formation of short life time intermediate liquid species. Journal of analytical and applied pyrolysis. 1998;47(1):13-31.

122. Lédé J. Cellulose pyrolysis kinetics: An historical review on the existence and role of intermediate active cellulose. Journal of Analytical and Applied Pyrolysis. 2012;94:17-32.

123. Lédé J, Blanchard F, Boutin O. Radiant flash pyrolysis of cellulose pellets: products and mechanisms involved in transient and steady state conditions. Fuel. 2002;81(10):1269-1279.

124. Shen D, Gu S. The mechanism for thermal decomposition of cellulose and its main products. Bioresource technology. 2009;100(24):6496-6504.

125. Shafizadeh F, Fu Y. Pyrolysis of cellulose. Carbohydrate Research. 1973;29(1):113-122.

126. Lin Y-C, Cho J, Tompsett GA, Westmoreland PR, Huber GW. Kinetics and mechanism of cellulose pyrolysis. The Journal of Physical Chemistry C. 2009;113(46):20097-20107.

127. Kilzer FJ, Broido A. Speculations on the nature of cellulose pyrolysis. Pyrodynamics. 2: 151-163. 1965;2:151-163.

128. Ponder GR, Richards GN, Stevenson TT. Influence of linkage position and orientation in pyrolysis of polysaccharides: A study of several glucans. Journal of Analytical and Applied Pyrolysis. 1992;22(3):217-229.

129. Patwardhan PR, Satrio JA, Brown RC, Shanks BH. Product distribution from fast pyrolysis of glucose-based carbohydrates. Journal of Analytical and Applied Pyrolysis. 2009;86(2):323-330.

130. Shafizadeh F. Introduction to pyrolysis of biomass. Journal of analytical and applied pyrolysis. 1982;3(4):283-305.

131. Piskorz J, Radlein DSA, Scott DS, Czernik S. Pre-treatment of wood and cellulose for production of sugars by fast pyrolysis. Journal of Analytical and Applied Pyrolysis. 1989;16(2):127-142.

132. Banyasz J, Li S, Lyons-Hart J, Shafer K. Gas evolution and the mechanism of cellulose pyrolysis. Fuel. 2001;80(12):1757-1763.

133. Banyasz JL, Li S, Lyons-Hart JL, Shafer KH. Cellulose pyrolysis: the kinetics of hydroxyacetaldehyde evolution. Journal of Analytical and Applied Pyrolysis. 2001;57(2):223-248.

134. Bradbury AG, Sakai Y, Shafizadeh F. A kinetic model for pyrolysis of cellulose. Journal of applied polymer science. 1979;23(11):3271-3280.

135. Xin S, Yang H, Chen Y, Yang M, Chen L, Wang X, et al. Chemical structure evolution of char during the pyrolysis of cellulose. Journal of analytical and applied pyrolysis. 2015;116:263-271.

136. Worasuwannarak N, Sonobe T, Tanthapanichakoon W. Pyrolysis behaviors of rice straw, rice husk, and corncob by TG-MS technique. Journal of Analytical and Applied Pyrolysis. 2007;78(2):265-271.

137. Yang H, Yan R, Chen H, Lee DH, Zheng C. Characteristics of hemicellulose, cellulose and lignin pyrolysis. Fuel. 2007;86(12-13):1781-1788.

138. Wang S, Guo X, Liang T, Zhou Y, Luo Z. Mechanism research on cellulose pyrolysis by Py-GC/MS and subsequent density functional theory studies. Bioresource technology. 2012;104:722-728.

139. Patwardhan PR, Dalluge DL, Shanks BH, Brown RC. Distinguishing primary and secondary reactions of cellulose pyrolysis. Bioresource technology. 2011;102(8):5265-5269.

140. Bridgwater AV. Upgrading biomass fast pyrolysis liquids. Environmental Progress & Sustainable Energy. 2012;31(2):261-268.

141. Milosavljevic I, Oja V, Suuberg EM. Thermal effects in cellulose pyrolysis: relationship to char formation processes. Industrial & Engineering Chemistry Research. 1996;35(3):653-662.

142. Antal MJJ, Varhegyi G. Cellulose pyrolysis kinetics: the current state of knowledge. Industrial & Engineering Chemistry Research. 1995;34(3):703-717.

143. Srinivasan V, Adhikari S, Chattanathan SA, Park S. Catalytic pyrolysis of torrefied biomass for hydrocarbons production. Energy & Fuels. 2012;26(12):7347-7353.

144. Boerjan W, Ralph J, Baucher M. Lignin biosynthesis. Annual review of plant biology. 2003;54(1):519-546.

145. Burhenne L, Messmer J, Aicher T, Laborie M-P. The effect of the biomass components lignin, cellulose and hemicellulose on TGA and fixed bed pyrolysis. Journal of Analytical and Applied Pyrolysis. 2013;101:177-184.

146. Whetten RW, MacKay JJ, Sederoff RR. Recent advances in understanding lignin biosynthesis. Annual review of plant biology. 1998;49(1):585-609.

147. Pérez J, Munoz-Dorado J, De la Rubia T, Martinez J. Biodegradation and biological treatments of cellulose, hemicellulose and lignin: an overview. International microbiology. 2002;5(2):53-63.

148. Salmén L. Micromechanical understanding of the cell-wall structure. Comptes rendus biologies. 2004;327(9-10):873-880.

149. Ramiah M. Thermogravimetric and differential thermal analysis of cellulose, hemicellulose, and lignin. Journal of applied polymer science. 1970;14(5):1323-1337.

150. Williams PT, Besler S. The influence of temperature and heating rate on the slow pyrolysis of biomass. Renewable energy. 1996;7(3):233-250.

151. Liu C, Hu J, Zhang H, Xiao R. Thermal conversion of lignin to phenols: Relevance between chemical structure and pyrolysis behaviors. Fuel. 2016;182:864-870.

152. Jung KA, Woo SH, Lim S-R, Park JM. Pyrolytic production of phenolic compounds from the lignin residues of bioethanol processes. Chemical engineering journal. 2015;259:107-116.

153. Liu Q, Wang S, Zheng Y, Luo Z, Cen K. Mechanism study of wood lignin pyrolysis by using TG–FTIR analysis. Journal of Analytical and Applied Pyrolysis. 2008;82(1):170-177.

154. Brebu M, Tamminen T, Spiridon I. Thermal degradation of various lignins by TG-MS/FTIR and Py-GC-MS. Journal of analytical and applied pyrolysis. 2013;104:531-539.

155. Lv G, Wu S. Analytical pyrolysis studies of corn stalk and its three main components by TG-MS and Py-GC/MS. Journal of Analytical and Applied Pyrolysis. 2012;97:11-18.

156. Kawamoto H, Horigoshi S, Saka S. Effects of side-chain hydroxyl groups on pyrolytic β-ether cleavage of phenolic lignin model dimer. Journal of wood science. 2007;53(3):268-271.

157. Kawamoto H, Saka S. Role of side‐chain hydroxyl groups in pyrolytic reaction of phenolic β‐ether type of lignin dimer. Journal of wood chemistry and technology. 2007;27(2):113-120.

158. Nowakowski DJ, Bridgwater AV, Elliott DC, Meier D, de Wild P. Lignin fast pyrolysis: Results from an international collaboration. Journal of Analytical and Applied Pyrolysis. 2010;88(1):53-72.

159. Orfão JJ, Antunes FJ, Figueiredo JL. Pyrolysis kinetics of lignocellulosic materials—three independent reactions model. Fuel. 1999;78(3):349-358.

160. Gellerstedt G, Sjöholm E, Brodin I. The wood-based biorefinery: A source of carbon fiber? The Open Agriculture Journal. 2010;4(1)

161. Huang J, He C, Wu L, Tong H. Thermal degradation reaction mechanism of xylose: A DFT study. Chemical physics letters. 2016;658:114-124.

162. Wang S, Ru B, Lin H, Luo Z. Degradation mechanism of monosaccharides and xylan under pyrolytic conditions with theoretic modeling on the energy profiles. Bioresource technology. 2013;143:378-383.

163. Huang J, He C, Wu L, Tong H. Theoretical studies on thermal decomposition mechanism of arabinofuranose. Journal of the Energy Institute. 2017;90(3):372-381.

164. Räisänen U, Pitkänen I, Halttunen H, Hurtta M. Formation of the main degradation compounds from arabinose, xylose, mannose and arabinitol during pyrolysis. Journal of thermal analysis and calorimetry. 2003;72(2):481-488.

165. Baruah J, Nath BK, Sharma R, Kumar S, Deka RC, Baruah DC, et al. Recent trends in the pre-treatment of lignocellulosic biomass for value-added products. Frontiers in Energy Research. 2018;6:141.

166. McMillan JD. Pre-treatment of lignocellulosic biomass. In: ACS Publications; 1994.

167. Brodeur G, Yau E, Badal K, Collier J, Ramachandran K, Ramakrishnan S. Chemical and physicochemical pre-treatment of lignocellulosic biomass: a review. Enzyme research. 2011;2011

168. Mosier N, Wyman C, Dale B, Elander R, Lee Y, Holtzapple M, et al. Features of promising technologies for pre-treatment of lignocellulosic biomass. Bioresource technology. 2005;96(6):673-686.

169. El-barbary MH, Steele PH, Ingram L. Characterization of fast pyrolysis bio-oils produced from pretreated pine wood. Applied biochemistry and biotechnology. 2009;154(1):3-13.

170. Shafiei M, Kumar R, Karimi K. Pre-treatment of lignocellulosic biomass. In: Lignocellulose-based bioproducts: Springer; 2015. p. 85-154.

171. Taherzadeh MJ, Karimi K. Pre-treatment of lignocellulosic wastes to improve ethanol and biogas production: a review. International journal of molecular sciences. 2008;9(9):1621-1651.

172. Wyman CE, Dale BE, Elander RT, Holtzapple M, Ladisch MR, Lee Y. Coordinated development of leading biomass pre-treatment technologies. Bioresource technology. 2005;96(18):1959-1966.

173. Fengel D, Wegener G. Wood: chemistry, ultrastructure, reactions. Walter de Gruyter; 2011.

174. Xiang Q, Kim JS, Lee Y. A comprehensive kinetic model for dilute-acid hydrolysis of cellulose. In: Biotechnology for Fuels and Chemicals: Springer; 2003. p. 337-352.

175. Jacobsen SE, Wyman CE Cellulose and hemicellulose hydrolysis models for application to current and novel pre-treatment processes. Twenty-first symposium on biotechnology for fuels and chemicals; 2000 Springer. 81-96 p.

176. Muranaka Y, Suzuki T, Sawanishi H, Hasegawa I, Mae K. Effective production of levulinic acid from biomass through pre-treatment using phosphoric acid, hydrochloric acid, or ionic liquid. Industrial & Engineering Chemistry Research. 2014;53(29):11611-11621.

177. Söderström J, Pilcher L, Galbe M, Zacchi G. Combined use of H 2 SO 4 and SO 2 impregnation for steam pre-treatment of spruce in ethanol production. Applied biochemistry and biotechnology. 2003;105(1):127-140.

178. Kim SB, Lee Y. Diffusion of sulfuric acid within lignocellulosic biomass particles and its impact on dilute-acid pre-treatment. Bioresource technology. 2002;83(2):165-171.

179. Torget R, Himmel ME, Grohmann K. Dilute sulfuric acid pre-treatment of hardwood bark. Bioresource Technology. 1991;35(3):239-246.

180. Harris J, Baker A, Zerbe J. Two-stage, dilute sulfuric acid hydrolysis of hardwood for ethanol production. Energy biomass wastes. 1984;8:1151-1170.

181. Nguyen QA, Tucker MP, Keller FA, Eddy FP Two-stage dilute-acid pre-treatment of softwoods. Twenty-first Symposium on biotechnology for fuels and chemicals; 2000 Springer. 561-576 p.

182. Hong T, WANG S-r. Experimental study of the effect of acid-washing pre-treatment on biomass pyrolysis. Journal of Fuel Chemistry and Technology. 2009;37(6):668-672.

183. Harris E, Beglinger E, Hajny G, Sherrard E. Hydrolysis of wood-treatment with sulfuric acid in a stationary digester. Industrial & Engineering Chemistry. 1945;37(1):12-23.

184. Zeitsch KJ. The chemistry and technology of furfural and its many by-products. Elsevier; 2000.

185. Xin X, Pang S, de Miguel Mercader F, Torr KM. The effect of biomass pre-treatment on catalytic pyrolysis products of pine wood by Py-GC/MS and principal component analysis. Journal of Analytical and Applied Pyrolysis. 2019;138:145-153.

186. Higgins F, Ho G. Hydrolysis of cellulose using HCl: a comparison between liquid phase and gaseous phase processes. Agricultural Wastes. 1982;4(2):97-116.

187. Goldstein IS, Pereira H, Pittman JL, Strouse B, Scaringelli F Hydrolysis of cellulose with superconcentrated hydrochloric acid. Biotechnol. Bioeng. Symp.;(United States); 1983 North Carolina State Univ., Raleigh; p.

188. Israilides C, Grant G, Han Y. Sugar level, fermentability, and acceptability of straw treated with different acids. Applied and Environmental Microbiology. 1978;36(1):43-46.

189. Villota EM, Lei H, Qian M, Yang Z, Villota SMA, Zhang Y, et al. Optimizing microwave-assisted pyrolysis of phosphoric acid-activated biomass: impact of concentration on heating rate and carbonization time. ACS Sustainable Chemistry & Engineering. 2018;6(1):1318-1326.

190. Mourant D, Wang Z, He M, Wang XS, Garcia-Perez M, Ling K, et al. Mallee wood fast pyrolysis: effects of alkali and alkaline earth metallic species on the yield and composition of bio-oil. Fuel. 2011;90(9):2915-2922.

191. Mahadevan R, Adhikari S, Shakya R, Wang K, Dayton D, Lehrich M, et al. Effect of alkali and alkaline earth metals on in-situ catalytic fast pyrolysis of lignocellulosic biomass: a microreactor study. Energy & Fuels. 2016;30(4):3045-3056.

192. Cen K, Zhang J, Ma Z, Chen D, Zhou J, Ma H. Investigation of the relevance between biomass pyrolysis polygeneration and washing pre-treatment under different severities: Water, dilute acid solution and aqueous phase bio-oil. Bioresource technology. 2019;278:26-33.

193. Zhou S, Xue Y, Cai J, Cui C, Ni Z, Zhou Z. An understanding for improved biomass pyrolysis: Toward a systematic comparison of different acid pre-treatments. Chemical Engineering Journal. 2021;411:128513.

194. Vassilev SV, Baxter D, Andersen LK, Vassileva CG. An overview of the chemical composition of biomass. Fuel. 2010;89(5):913-933.

195. Vassilev SV, Baxter D, Andersen LK, Vassileva CG, Morgan TJ. An overview of the organic and inorganic phase composition of biomass. Fuel. 2012;94:1-33.

196. Williams PT, Horne PA. The role of metal salts in the pyrolysis of biomass. Renewable Energy. 1994;4(1):1-13.

197. Nik-Azar M, Hajaligol M, Sohrabi M, Dabir B. Mineral matter effects in rapid pyrolysis of beech wood. Fuel Processing Technology. 1997;51(1-2):7-17.

198. Yu J, Guo Q, Gong Y, Ding L, Wang J, Yu G. A review of the effects of alkali and alkaline earth metal species on biomass gasification. Fuel Processing Technology. 2021;214:106723.

199. Zhao D, Dai Y, Chen K, Sun Y, Yang F, Chen K. Effect of potassium inorganic and organic salts on the pyrolysis kinetics of cigarette paper. Journal of Analytical and Applied Pyrolysis. 2013;102:114-123.

200. Scott DS, Paterson L, Piskorz J, Radlein D. Pre-treatment of poplar wood for fast pyrolysis: rate of cation removal. Journal of Analytical and Applied Pyrolysis. 2001;57(2):169-176.

201. Pan W-P, Richards GN. Influence of metal ions on volatile products of pyrolysis of wood. Journal of Analytical and Applied Pyrolysis. 1989;16(2):117-126.

202. Bridgwater AV. Advances in thermochemical biomass conversion. Springer Science & Business Media; 2013.

203. Eom I-Y, Kim J-Y, Kim T-S, Lee S-M, Choi D, Choi I-G, et al. Effect of essential inorganic metals on primary thermal degradation of lignocellulosic biomass. Bioresource technology. 2012;104:687-694.

204. Haddad K, Jeguirim M, Jellali S, Guizani C, Delmotte L, Bennici S, et al. Combined NMR structural characterization and thermogravimetric analyses for the assessment of the AAEM effect during lignocellulosic biomass pyrolysis. Energy. 2017;134:10-23.

205. Dayton D, Jenkins B, Turn S, Bakker R, Williams R, Belle-Oudry D, et al. Release of inorganic constituents from leached biomass during thermal conversion. Energy & Fuels. 1999;13(4):860-870.

206. Wyman CE. Aqueous pre-treatment of plant biomass for biological and chemical conversion to fuels and chemicals. John Wiley & Sons; 2013.

207. Lv D, Xu M, Liu X, Zhan Z, Li Z, Yao H. Effect of cellulose, lignin, alkali and alkaline earth metallic species on biomass pyrolysis and gasification. Fuel Processing Technology. 2010;91(8):903-909.

208. Okuno T, Sonoyama N, Hayashi J-i, Li C-Z, Sathe C, Chiba T. Primary release of alkali and alkaline earth metallic species during the pyrolysis of pulverized biomass. Energy & Fuels. 2005;19(5):2164-2171.

209. Long J, Song H, Jun X, Sheng S, Lun-Shi S, Kai X, et al. Release characteristics of alkali and alkaline earth metallic species during biomass pyrolysis and steam gasification process. Bioresource technology. 2012;116:278-284.

210. Keown DM, Favas G, Hayashi J-i, Li C-Z. Volatilisation of alkali and alkaline earth metallic species during the pyrolysis of biomass: differences between sugar cane bagasse and cane trash. Bioresource technology. 2005;96(14):1570-1577.

211. Olsson JG, Pettersson JB, Padban N, Bjerle I. Alkali metal emission from filter ash and fluidized bed material from PFB gasification of biomass. Energy & fuels. 1998;12(3):626-630.

212. Zolin A, Jensen A, Jensen PA, Frandsen F, Dam-Johansen K. The influence of inorganic materials on the thermal deactivation of fuel chars. Energy & fuels. 2001;15(5):1110-1122.

213. Liaw SB, Wu H. A new method for direct determination of char yield during solid fuel pyrolysis in drop-tube furnace at high temperature and its comparison with ash tracer method. Energy & Fuels. 2018;33(2):1509-1517.

214. Davidsson K, Korsgren J, Pettersson JB, Jäglid U. The effects of fuel washing techniques on alkali release from biomass. Fuel. 2002;81(2):137-142.

215. Davidsson K, Stojkova B, Pettersson J. Alkali emission from birchwood particles during rapid pyrolysis. Energy & fuels. 2002;16(5):1033-1039.

216. Hirohata O, Wakabayashi T, Tasaka K, Fushimi C, Furusawa T, Kuchonthara P, et al. Release behavior of tar and alkali and alkaline earth metals during biomass steam gasification. Energy & fuels. 2008;22(6):4235-4239.

217. Xu W-t, Song Q, Zhao H-b, Zhuo J-k, Yao Q. Study on the capture of gaseous KCl by cellulose char. Energy & Fuels. 2018;33(1):362-368.

218. Wang L, Shen Y. Pyrolysis characteristics of cellulosic biomass in the presence of alkali and alkaline-earth-metal (AAEM) oxalates. Cellulose. 2021:1-11.

219. Arora JS, Ansari KB, Chew JW, Dauenhauer PJ, Mushrif SH. Unravelling the catalytic influence of naturally occurring salts on biomass pyrolysis chemistry using glucose as a model compound: a combined experimental and DFT study. Catalysis Science & Technology. 2019;9(13):3504-3524.

220. Wang K, Zhang J, Shanks BH, Brown RC. The deleterious effect of inorganic salts on hydrocarbon yields from catalytic pyrolysis of lignocellulosic biomass and its mitigation. Applied Energy. 2015;148:115-120.

221. Uslu A, Faaij AP, Bergman PC. Pre-treatment technologies, and their effect on international bioenergy supply chain logistics. Techno-economic evaluation of torrefaction, fast pyrolysis and pelletisation. Energy. 2008;33(8):1206-1223.

222. Bergman P. Combined torrefaction and pelletisation. The TOP process. 2005

223. Prins MJ, Ptasinski KJ, Janssen FJ. More efficient biomass gasification via torrefaction. Energy. 2006;31(15):3458-3470.

224. Zheng A, Zhao Z, Chang S, Huang Z, Wang X, He F, et al. Effect of torrefaction on structure and fast pyrolysis behavior of corncobs. Bioresource technology. 2013;128:370-377.

225. Boateng A, Mullen C. Fast pyrolysis of biomass thermally pretreated by torrefaction. Journal of Analytical and Applied Pyrolysis. 2013;100:95-102.

226. Tumuluru JS, Sokhansanj S, Wright CT, Hess JR, Boardman RD. A review on biomass torrefaction process and product properties. 2011

227. Bergman PC, Boersma A, Zwart R, Kiel J. Torrefaction for biomass co-firing in existing coal-fired power stations. Energy Research Centre of the Netherlands, ECN-C-05-013. 2005

228. Westover TL, Phanphanich M, Clark ML, Rowe SR, Egan SE, Zacher AH, et al. Impact of thermal pre-treatment on the fast pyrolysis conversion of southern pine. Biofuels. 2013;4(1):45-61.

229. Zheng A, Zhao Z, Chang S, Huang Z, He F, Li H. Effect of torrefaction temperature on product distribution from two-staged pyrolysis of biomass. Energy & Fuels. 2012;26(5):2968-2974.

230. Dalluge DL. Optimization of biomass fast pyrolysis for the production of monomers. 2013

231. Eseltine DE. Effect of using inert and non-inert gases on the thermal degradation and fuel properties of biomass in the torrefaction and pyrolysis region: Texas A & M University; 2012

232. Thanapal SS, Chen W, Annamalai K, Carlin N, Ansley RJ, Ranjan D. Carbon dioxide torrefaction of woody biomass. Energy & fuels. 2014;28(2):1147-1157.

233. Bach Q-V, Tran K-Q, Skreiberg Ø, Khalil RA. Effects of CO2 on wet torrefaction of biomass. Energy Procedia. 2014;61:1200-1203.

234. Bach Q-V, Tran K-Q, Skreiberg Ø. Accelerating wet torrefaction rate and ash removal by carbon dioxide addition. Fuel Processing Technology. 2015;140:297-303.

235. Saadon S, Uemura Y, Mansor N. Torrefaction in the presence of oxygen and carbon dioxide: the effect on yield of oil palm kernel shell. Procedia Chem. 2014;9:194-201.

236. Li M-F, Li X, Bian J, Xu J-K, Yang S, Sun R-C. Influence of temperature on bamboo torrefaction under carbon dioxide atmosphere. Industrial Crops and Products. 2015;76:149-157.

237. Li M-F, Chen L-X, Li X, Chen C-Z, Lai Y-C, Xiao X, et al. Evaluation of the structure and fuel properties of lignocelluloses through carbon dioxide torrefaction. Energy Conversion and Management. 2016;119:463-472.

238. Tran K-Q, Trinh TN, Bach Q-V. Development of a biomass torrefaction process integrated with oxy-fuel combustion. Bioresource technology. 2016;199:408-413.

239. Uemura Y, Sellappah V, Trinh TH, Hassan S, Tanoue K-i. Torrefaction of empty fruit bunches under biomass combustion gas atmosphere. Bioresource technology. 2017;243:107-117.

240. Sellappah V, Uemura Y, Hassan S, Sulaiman MH, Lam MK. Torrefaction of empty fruit bunch in the presence of combustion gas. Procedia engineering. 2016;148:750-757.

241. Ramos-Carmona S, Martínez JD, Pérez JF. Torrefaction of patula pine under air conditions: A chemical and structural characterization. Industrial Crops and Products. 2018;118:302-310.

242. Lu K-M, Lee W-J, Chen W-H, Liu S-H, Lin T-C. Torrefaction and low temperature carbonization of oil palm fiber and eucalyptus in nitrogen and air atmospheres. Bioresource technology. 2012;123:98-105.

243. Chen W-H, Zhuang Y-Q, Liu S-H, Juang T-T, Tsai C-M. Product characteristics from the torrefaction of oil palm fiber pellets in inert and oxidative atmospheres. Bioresource technology. 2016;199:367-374.

244. Chen W-H, Lu K-M, Liu S-H, Tsai C-M, Lee W-J, Lin T-C. Biomass torrefaction characteristics in inert and oxidative atmospheres at various superficial velocities. Bioresource technology. 2013;146:152-160.

245. Wannapeera J, Fungtammasan B, Worasuwannarak N. Effects of temperature and holding time during torrefaction on the pyrolysis behaviors of woody biomass. Journal of analytical and applied pyrolysis. 2011;92(1):99-105.

246. Chen Y, Yang H, Yang Q, Hao H, Zhu B, Chen H. Torrefaction of agriculture straws and its application on biomass pyrolysis poly-generation. Bioresource Technology. 2014;156:70-77.

247. Ru B, Wang S, Dai G, Zhang L. Effect of torrefaction on biomass physicochemical characteristics and the resulting pyrolysis behavior. Energy & Fuels. 2015;29(9):5865-5874.

248. Konsomboon S, Commandré J-M, Fukuda S. Torrefaction of various biomass feedstocks and its impact on the reduction of tar produced during pyrolysis. Energy & Fuels. 2019;33(4):3257-3266.

249. Uemura Y, Saadon S, Osman N, Mansor N, Tanoue K-i. Torrefaction of oil palm kernel shell in the presence of oxygen and carbon dioxide. Fuel. 2015;144:171-179.

250. Chen W-H, Lu K-M, Lee W-J, Liu S-H, Lin T-C. Non-oxidative and oxidative torrefaction characterization and SEM observations of fibrous and ligneous biomass. Applied Energy. 2014;114:104-113.

251. Beis S, Onay Ö, Koçkar Ö. Fixed-bed pyrolysis of safflower seed: influence of pyrolysis parameters on product yields and compositions. Renewable energy. 2002;26(1):21-32.

252. Pütün AE, Özbay N, Önal EP, Pütün E. Fixed-bed pyrolysis of cotton stalk for liquid and solid products. Fuel Processing Technology. 2005;86(11):1207-1219.

253. Horne PA, Williams PT. Influence of temperature on the products from the flash pyrolysis of biomass. Fuel. 1996;75(9):1051-1059.

254. Boateng AA, Daugaard DE, Goldberg NM, Hicks KB. Bench-scale fluidized-bed pyrolysis of switchgrass for bio-oil production. Industrial & Engineering Chemistry Research. 2007;46(7):1891-1897.

255. Peacocke G, Bridgwater A. Ablative plate pyrolysis of biomass for liquids. Biomass and Bioenergy. 1994;7(1-6):147-154.

256. Garcìa-Pèrez M, Chaala A, Roy C. Vacuum pyrolysis of sugarcane bagasse. Journal of analytical and applied pyrolysis. 2002;65(2):111-136.

257. Hoekstra E, Van Swaaij WP, Kersten SR, Hogendoorn KJ. Fast pyrolysis in a novel wire-mesh reactor: Decomposition of pine wood and model compounds. Chemical Engineering Journal. 2012;187:172-184.

258. Loison R. Pyrolyse rapide du charbon. 1964.

259. Hamilton LH, Ayling AB, Shibaoka M. A new experimental device for pyrolysing coal particles under controlled conditions over a wide range of heating rates. Fuel. 1979;58(12):873-876.

260. Niksa SJ, Russel WB, Saville DA. Captive sample reactor for kinetic studies of coal pyrolysis and hydropyrolysis on short time scales. Fuel. 1982;61(12):1207-1212.

261. Stangeby PC, Sears PL. Rapid pyrolysis and hydropyrolysis of Canadian coals. Fuel. 1981;60(2):131-135.

262. Sathe C, Hayashi J-I, Li C-Z. Release of volatiles from the pyrolysis of a Victorian lignite at elevated pressures. Fuel. 2002;81(9):1171-1178.

263. Sathe C, Hayashi J-i, Li C-Z, Chiba T. Release of alkali and alkaline earth metallic species during rapid pyrolysis of a Victorian brown coal at elevated pressures ☆. Fuel. 2003;82(12):1491-1497.

264. Zhou J, Gui B, Qiao Y, Zhang J, Wang W, Yao H, et al. Understanding the pyrolysis mechanism of polyvinylchloride (PVC) by characterizing the chars produced in a wire-mesh reactor. Fuel. 2016;166:526-532.

265. Zhou J, Qiao Y, Wang W, Leng E, Huang J, Yu Y, et al. Formation of styrene monomer, dimer and trimer in the primary volatiles produced from polystyrene pyrolysis in a wire-mesh reactor. Fuel. 2016;182:333-339.

266. Liaw SB, Yu Y, Wu H. Association of inorganic species release with sugar recovery during wood hydrothermal processing. Fuel. 2016;166:581-584.

267. Song B. Hydrothermal Processing of Biomass and Its Derived Sugar Compounds in Hot-Compressed Gamma-Valerolactone/Water Mixtures: Curtin University; 2018

268. Temminghoff EE, Houba VJ. Plant analysis procedures. 2004

269. Chen X. Pyrolysis and Combustion of Phosphorus containing Solid Fuels: Char Structure, Char Reactivity and Particulate Matter Emission: Curtin University; 2019

270. Garcia-Perez M, Wang S, Shen J, Rhodes M, Lee WJ, Li C-Z. Effects of temperature on the formation of lignin-derived oligomers during the fast pyrolysis of mallee woody biomass. Energy & Fuels. 2008;22(3):2022-2032.

271. Zhong C, Wei X. A comparative experimental study on the liquefaction of wood. Energy. 2004;29(11):1731-1741.

272. Ladanai S, Vinterbäck J. Global potential of sustainable biomass for energy; 2009 Report No.: 1654-9406.

273. Thielen A, Klus H, Muller L. Tobacco smoke: unraveling a controversial subject. Exp Toxicol Pathol. 2008;60(2-3):141-56. doi:10.1016/j.etp.2008.01.014

274. Li J, Pósfai M, Hobbs PV, Buseck PR. Individual aerosol particles from biomass burning in southern Africa: 2, Compositions and aging of inorganic particles. Journal of Geophysical Research: Atmospheres. 2003;108(D13):n/a-n/a. p. n/a. doi:10.1029/2002jd002310

275. Pósfai M, Simonics R, Li J, Hobbs PV, Buseck PR. Individual aerosol particles from biomass burning in southern Africa: 1. Compositions and size distributions of

carbonaceous particles. Journal of Geophysical Research: Atmospheres. 2003;108(D13):n/a-n/a. p. n/a. doi:10.1029/2002jd002291

276. Dauenhauer PJ, Colby JL, Balonek CM, Suszynski WJ, Schmidt LD. Reactive boiling of cellulose for integrated catalysis through an intermediate liquid. Green Chemistry. 2009;11(10) p. 1555. doi:10.1039/b915068b

277. Teixeira AR, Gantt R, Joseph KE, Maduskar S, Paulsen AD, Krumm C, et al. Spontaneous Aerosol Ejection: Origin of Inorganic Particles in Biomass Pyrolysis. ChemSusChem. 2016;9(11):1322-8. doi:10.1002/cssc.201600112

278. Teixeira AR, Mooney KG, Kruger JS, Williams CL, Suszynski WJ, Schmidt LD, et al. Aerosol generation by reactive boiling ejection of molten cellulose. Energy & Environmental Science. 2011;4(10) p. 4306. doi:10.1039/c1ee01876k

279. Brown AL, Dayton DC, Daily JW. A study of cellulose pyrolysis chemistry and global kinetics at high heating rates. Energy & Fuels. 2001;15(5):1286-1294.

280. Paulsen AD, Mettler MS, Dauenhauer PJ. The role of sample dimension and temperature in cellulose pyrolysis. Energy & Fuels. 2013;27(4):2126-2134.

281. Diebold JP. A unified, global model for the pyrolysis of cellulose. Biomass and Bioenergy. 1994;7(1-6):75-85.

282. Lewellen P, Peters W, Howard J Cellulose pyrolysis kinetics and char formation mechanism. Symposium (International) on Combustion; 1977 Elsevier. 1471-1480 p.

283. Kothari V, Antal Jr MJ. Numerical studies of the flash pyrolysis of cellulose. Fuel. 1985;64(11):1487-1494.

284. Yu Y, Liu D, Wu H. Characterization of water-soluble intermediates from slow pyrolysis of cellulose at low temperatures. Energy & fuels. 2012;26(12):7331-7339.

285. Boutin O, Ferrer M, Lédé J. Flash pyrolysis of cellulose pellets submitted to a concentrated radiation: experiments and modelling. Chemical Engineering Science. 2002;57(1):15-25.

286. Radlein DS, Grinshpun A, Piskorz J, Scott DS. On the presence of anhydro-oligosaccharides in the sirups from the fast pyrolysis of cellulose. Journal of Analytical and Applied Pyrolysis. 1987;12(1):39-49.

287. Shoji T, Kawamoto H, Saka S. Boiling point of levoglucosan and devolatilisation temperatures in cellulose pyrolysis measured at different heating area temperatures. Journal of Analytical and Applied Pyrolysis. 2014;109:185-195.

288. Bai X, Xue Y. Transport and Secondary Reactions of Depolymerized/Deconstructed Species. In: Fast Pyrolysis of Biomass; 2017. p. 57-77.

289. Wang Z. Effect of Pyrolysis Temperature on the Formation of Anhydrosugars During the Fast Pyrolysis of Cellulose in a Wire Mesh Reactor at Atmospheric Pressure. UNDERSTANDING CELLULOSE PRIMARY AND SECONDARY PYROLYSIS REACTIONS TO ENHANCE THE PRODUCTION OF ANHYDROSACCHARIDES AND TO BETTER PREDICT THE COMPOSITION OF CARBONACEOUS RESIDUES. 2013:80.

290. Brown RC, Wang K. Fast Pyrolysis of Biomass: Advances in Science and Technology. Royal Society of Chemistry; 2017.

291. Venkatakrishnan VK, Degenstein JC, Smeltz AD, Delgass WN, Agrawal R, Ribeiro FH. High-pressure fast-pyrolysis, fast-hydropyrolysis and catalytic hydrodeoxygenation of cellulose: production of liquid fuel from biomass. Green Chemistry. 2014;16(2):792-802.

292. Kuzhiyil N, Dalluge D, Bai X, Kim KH, Brown RC. Pyrolytic sugars from cellulosic biomass. ChemSusChem. 2012;5(11):2228-2236.

293. Sun Y, Lin L, Deng H, Li J, He B, Sun R, et al. Structural changes of bamboo cellulose in formic acid. BioResources. 2008;3(2):297-315.

294. Liu D, Yu Y, Long Y, Wu H. Effect of MgCl2 loading on the evolution of reaction intermediates during cellulose fast pyrolysis at 325° C. Proceedings of the Combustion Institute. 2015;35(2):2381-2388.

295. Hu B, Lu Q, Jiang X-y, Dong X-c, Cui M-s, Dong C-q, et al. Insight into the formation of anhydrosugars in glucose pyrolysis: a joint computational and experimental investigation. Energy & Fuels. 2017;31(8):8291-8299.

296. Ohara M, Takagaki A, Nishimura S, Ebitani K. Syntheses of 5-hydroxymethylfurfural and levoglucosan by selective dehydration of glucose using solid acid and base catalysts. Applied Catalysis A: General. 2010;383(1-2):149-155.

297. Mettler MS, Mushrif SH, Paulsen AD, Javadekar AD, Vlachos DG, Dauenhauer PJ. Revealing pyrolysis chemistry for biofuels production: Conversion of cellulose to furans and small oxygenates. Energy & Environmental Science. 2012;5(1):5414-5424.

298. Stefanidis G, Stankiewicz A. Alternative Energy Sources for Green Chemistry. Royal Society of Chemistry; 2016.

299. ChemSpider. 1,6-Anhydro-β-D-glucofuranose. Available from: http://www.chemspider.com/Chemical-Structure.20040261.html

300. Hayes DJ, Fitzpatrick S, Hayes MH, Ross JR. The biofine process–production of levulinic acid, furfural, and formic acid from lignocellulosic feedstocks. Biorefineries–Industrial Processes and Product. 2006;1:139-164.

301. Girisuta B. Levulinic acid from lignocellulosic biomass: University of Groningen; 2007

302. Geng J, Wang W-L, Yu Y-X, Chang J-M, Cai L-p, Shi SQ. Adding nickel formate in alkali lignin to increase contents of alkylphenols and aromatics during fast pyrolysis. Bioresource technology. 2017;227:1-6.

303. Niu Y, Tan H. Ash-related issues during biomass combustion: Alkali-induced slagging, silicate melt-induced slagging (ash fusion), agglomeration, corrosion, ash utilisation, and related countermeasures. Progress in Energy and Combustion Science. 2016;52:1-61.

304. Vamvuka D, Zografos D, Alevizos G. Control methods for mitigating biomass ash-related problems in fluidized beds. Bioresource technology. 2008;99(9):3534-3544.

305. Deng C, Liaw SB, Gao X, Wu H. Differences in soot produced from rapid pyrolysis of xylan, cellulose and lignin under pulverized-fuel conditions. Fuel. 2020;265:116991.

306. Van Lith SC, Jensen PA, Frandsen FJ, Glarborg P. Release to the gas phase of inorganic elements during wood combustion. Part 2: influence of fuel composition. Energy & Fuels. 2008;22(3):1598-1609.

307. Knudsen JN. Volatilization of inorganic matter during combustion of annual biomass: Technical University of Denmark; 2004

308. Knudsen JN, Jensen PA, Dam-Johansen K. Transformation and release to the gas phase of Cl, K, and S during combustion of annual biomass. Energy & Fuels. 2004;18(5):1385-1399.

309. Kong Z, Liaw SB, Gao X, Yu Y, Wu H. Leaching characteristics of inherent inorganic nutrients in biochars from the slow and fast pyrolysis of mallee biomass. Fuel. 2014;128:433-441.

310. Quyn DM, Wu H, Li C-Z. Volatilisation and catalytic effects of alkali and alkaline earth metallic species during the pyrolysis and gasification of Victorian brown coal. Part I. Volatilisation of Na and Cl from a set of NaCl-loaded samples. Fuel. 2002;81(2):143-149.

311. Wang S, Wang K, Liu Q, Gu Y, Luo Z, Cen K, et al. Comparison of the pyrolysis behavior of lignins from different tree species. Biotechnology Advances. 2009;27(5):562-567.

312. Shen Q, Zhang T, Zhu M-F. A comparison of the surface properties of lignin and sulfonated lignins by FTIR spectroscopy and wicking technique. Colloids and Surfaces A: Physicochemical and Engineering Aspects. 2008;320(1-3):57-60.

313. Derkacheva O, Sukhov D Investigation of lignins by FTIR spectroscopy. Macromolecular Symposia; 2008 Wiley Online Library. 61-68 p.

314. Li R, Chen Q, Zhang H. Detailed investigation on sodium (Na) species release and transformation mechanism during pyrolysis and char gasification of high-Na Zhundong coal. Energy & Fuels. 2017;31(6):5902-5912.

315. Li J, Pósfai M, Hobbs PV, Buseck PR. Individual aerosol particles from biomass burning in southern Africa: 2, Compositions and aging of inorganic particles. Journal of Geophysical Research: Atmospheres. 2003;108(D13)

316. Johansen JM, Jakobsen JG, Frandsen FJ, Glarborg P. Release of K, Cl, and S during pyrolysis and combustion of high-chlorine biomass. Energy & Fuels. 2011;25(11):4961-4971.

317. Chen D, Mei J, Li H, Li Y, Lu M, Ma T, et al. Combined pre-treatment with torrefaction and washing using torrefaction liquid products to yield upgraded biomass and pyrolysis products. Bioresource technology. 2017;228:62-68.

318. Jiang S, Hu X, Shao X, Song Y, Xia D, Li C-Z. Effects of thermal pre-treatment and ex-situ grinding on the pyrolysis of mallee wood cylinders. Fuel Processing Technology. 2017;159:211-221.

319. Yang Z, Sarkar M, Kumar A, Tumuluru JS, Huhnke RL. Effects of torrefaction and densification on switchgrass pyrolysis products. Bioresource technology. 2014;174:266-273.

320. Ma Z, Wang J, Li C, Yang Y, Liu X, Zhao C, et al. New sight on the lignin torrefaction pre-treatment: Relevance between the evolution of chemical structure and the properties of torrefied gaseous, liquid, and solid products. Bioresource technology. 2019;288:121528.

321. Wen J-L, Sun S-L, Yuan T-Q, Xu F, Sun R-C. Understanding the chemical and structural transformations of lignin macromolecule during torrefaction. Applied Energy. 2014;121:1-9.

322. Dai G, Zou Q, Wang S, Zhao Y, Zhu L, Huang Q. Effect of torrefaction on the structure and pyrolysis behavior of lignin. Energy & Fuels. 2018;32(4):4160-4166.

323. Mahadevan R, Adhikari S, Shakya R, Wang K, Dayton DC, Li M, et al. Effect of torrefaction temperature on lignin macromolecule and product distribution from

HZSM-5 catalytic pyrolysis. Journal of Analytical and Applied Pyrolysis. 2016;122:95-105.

324. Lee J, Oh J-I, Ok YS, Kwon EE. Study on susceptibility of CO2-assisted pyrolysis of various biomass to CO2. Energy. 2017;137:510-517.

325. Donohoe BS, Decker SR, Tucker MP, Himmel ME, Vinzant TB. Visualizing lignin coalescence and migration through maize cell walls following thermochemical pre-treatment. Biotechnology and bioengineering. 2008;101(5):913-925.

326. Casas A, Alonso MV, Oliet M, Rojo E, Rodríguez F. FTIR analysis of lignin regenerated from Pinus radiata and Eucalyptus globulus woods dissolved in imidazolium ‐ based ionic liquids. Journal of Chemical Technology & Biotechnology. 2012;87(4):472-480.

327. Yan T, Xu Y, Yu C. The isolation and characterization of lignin of kenaf fiber. Journal of Applied Polymer Science. 2009;114(3):1896-1901.

328. Traoré M, Kaal J, Cortizas AM. Application of FTIR spectroscopy to the characterization of archeological wood. Spectrochimica Acta Part A: Molecular and Biomolecular Spectroscopy. 2016;153:63-70.

329. Zhuang J, Li M, Pu Y, Ragauskas AJ, Yoo CG. Observation of Potential Contaminants in Processed Biomass Using Fourier Transform Infrared Spectroscopy. Applied Sciences. 2020;10(12):4345.

330. Horikawa Y, Hirano S, Mihashi A, Kobayashi Y, Zhai S, Sugiyama J. Prediction of lignin contents from infrared spectroscopy: chemical digestion and lignin/biomass ratios of cryptomeria japonica. Applied biochemistry and biotechnology. 2019;188(4):1066-1076.

331. Senneca O, Cerciello F, Russo C, Wütscher A, Muhler M, Apicella B. Thermal treatment of lignin, cellulose and hemicellulose in nitrogen and carbon dioxide. Fuel. 2020;271:117656.

332. Senneca O, Cerciello F, Heuer S, Ammendola P. Slow pyrolysis of walnut shells in nitrogen and carbon dioxide. Fuel. 2018;225:419-425.

Every reasonable effort has been made to acknowledge the owners of copyright material. I would be pleased to hear from any copyright owner who has been omitted or incorrectly acknowledged.

APPENDIX 1: Copyright Permission Statements

Chapter 5, reprinted with permission from (Jinxiu Cao, Sui Boon Liaw, Yu Long, Yun Yu, and Hongwei Wu. Formation of reaction intermediates and primary volatiles during acid-catalysed fast pyrolysis of cellulose in a wire-mesh reactor, Proceedings of the Combustion Institute, 2021, 38, (3), 4301-4308. Copyright (2020) The Combustion Institute. Published by Elsevier Inc.

APPENDIX 2: Attribution Tables

[1] **Jinxiu Cao**, Yun Yu, and Hongwei Wu. Contributions of thermal ejection and evaporation to the formation of primary volatiles during cellulose fast pyrolysis.

Authors and full affiliations:

Authors	**Conception and design**	**Experiments conduction & data acquisition**	**Data processing & analysis**	**Interpretation & discussion**	**Manuscript writing, revision and finalisation**	**Final Approval**
Yun Yu	×		×	×	×	
I acknowledge that these represent my contribution to the above research output. Sign:						
Hongwei Wu	×		×	×	×	×
I acknowledge that these represent my contribution to the above research output. Sign:						

[2] **Jinxiu Cao**, Sui Boon Liaw, Yu Long, Yun Yu, and Hongwei Wu. Formation of reaction intermediates and primary volatiles during acid-catalysed fast pyrolysis of cellulose in a wire-mesh reactor. Proceedings of the Combustion Institute, 2021, 38, (3), 4301-4308.

Authors and full affiliations:

Authors	**Conception and design**	**Experiments conduction & data acquisition**	**Data processing & analysis**	**Interpretation & discussion**	**Manuscript writing, revision and finalisation**	**Final Approval**
Sui Boon Liaw	×			×		
I acknowledge that these represent my contribution to the above research output. Sign:						
Yu Long	×			×		
I acknowledge that these represent my contribution to the above research output. Sign:						
Yun Yu	×		×	×	×	
I acknowledge that these represent my contribution to the above research output. Sign:						
Hongwei Wu	×		×	×	×	×
I acknowledge that these represent my contribution to the above research output. Sign:						

[3] **Jinxiu Cao**, Yun Yu, and Hongwei Wu. The release and transformation of organic and inorganic sodium during the fast pyrolysis of sodium impregnated lignin.

Authors and full affiliations:

Authors	**Conception and design**	**Experiments conduction & data acquisition**	**Data processing & analysis**	**Interpretation & discussion**	**Manuscript writing, revision and finalisation**	**Final Approval**
Yun Yu	×		×	×	×	
I acknowledge that these represent my contribution to the above research output. Sign:						
Hongwei Wu	×		×	×	×	×
I acknowledge that these represent my contribution to the above research output. Sign:						

[4] **Jinxiu Cao**, Yun Yu, and Hongwei Wu. Effect of carbon dioxide torrefaction on the fast pyrolysis of lignin in a wire-mesh reactor.

Authors and full affiliations:

Authors	**Conception and design**	**Experiments conduction & data acquisition**	**Data processing & analysis**	**Interpretation & discussion**	**Manuscript writing, revision and finalisation**	**Final Approval**
Yun Yu	×		×	×	×	
I acknowledge that these represent my contribution to the above research output. Sign:						
Hongwei Wu	×		×	×	×	×
I acknowledge that these represent my contribution to the above research output. Sign:						